Universidade de Aveiro Departamento de Engenharia Cerâmica e do Vidro
2007

Jean Carlos da Conceição Lorenzzi

Boron nitride thin films deposited by magnetron sputtering on Si_3N_4

Filmes finos de nitreto de boro depositados por pulverização catódica em Si_3N_4

Universidade de Aveiro Departamento de Engenharia Cerâmica e do Vidro
2007

Jean Carlos da Conceição Lorenzzi

Boron nitride thin films deposited by magnetron sputtering on Si_3N_4

Filmes finos de nitreto de boro depositados por pulverização catódica em Si_3N_4

Dissertação apresentada à Universidade de Aveiro para cumprimento dos requisitos necessários à obtenção do grau de Mestre em Engenharia e Ciência dos Materiais, realizada sob a orientação científica do Dr. Rui Ramos Ferreira e Silva, Professor Associado do Departamento de Engenharia Cerâmica e do Vidro da Universidade de Aveiro .e do PhD. Jens H. Andreasen, Professor Associado do Departamento de Egenharia Mecânica da Universidade de Aalborg – Dinamarca.

It doesn’t matter how beautiful your theory is,
It doesn’t matter how smart you are.
If it doesn’t agree with experiment, it’s wrong.

Richard P. Feynman

o júri

presidente

Prof. Dr. Vitor Brás Sequeira Amaral
Professor associado da Universidade de Aveiro

Prof. Dr. José Manuel de Oliveira Castro Castanho
Professor auxiliar da Faculdade de Ciências e Tecnologia da Universidade de Coimbra

Prof. Dr. Rui Ramos Ferreira e Silva
Professor associado da Universidade de Aveiro

Acknowledgments

Agradecimentos

There are many people that must be acknowledged for their technical and moral support that led to the completion of this work. I wish to express my sincere appreciation to everyone who contributed to this study.

First, I would like to express my gratitude to my supervisors PhD. Professor Rui Ramos Ferreira e Silva for giving me an opportunity to work under his guidance and also for assigning me to this very interesting project.

Then, I would like to thank Assoc. Professor PhD. Jens H. Andreasen, my Co-supervisor, for his guidance during the EMMS mobility in Aalborg-Denmark.

A special acknowledgement goes to PhD. Mercedes Vila, who has always put aside her own projects to help me when I needed assistance. Her vast experience and creativity helped me greatly along the way, and it was essential to the completion of this thesis.

Special thanks to PhD. Filipe Oliveira for his strong support and advices, especially during those moments when my brain was out of order.

I would also like to acknowledge the technical assistance from PhD. Professor Armando Lourenço for sharing the experience in thin films by R.F. magnetron sputtering and also for his invaluable help during those long depositions.

I would also like to express my thanks to Dr. Carlos Miguel Cardeal Enes Granadeiro, Ricardo João Borges Pinto for their help during the FTIR characterisation, Dra. Rosário Soares for her strong support during the XRD measurements and Prof. Dr. Albano Cavaleiro for his support during the mechanical characterisation.

To my fellow colleagues, António José Fernandes, Diogo Mata, MSc. Ermelinda Salgueiredo, Micaela Sousa, MSc. Filipa Neves, MSc. Flávia Almeida, Eng. Paulo Duarte, PhD. Margarida Amaral, at the Diamond Group of Ceramic and Glass Engineering Department, thanks for being there and providing support when I needed.

I would also like to thank my EMMS colleagues Eng. Júlio César Longo, Eng. Fábio Bertocco, Gil Gonçalves, Eng. Marcos Ghislandi, for their friendship and help, and also for many inspiring discussions.

The financial support of the Erasmus Mundus Programme is gratingly acknowledged.

And last, but not least, my Family Inês Wollinger da Conceição, Vilson José Lorenzzi, Elzira Wollinger da Conceição, João Maria da Conceição, Ana Carla da Conceição Lorenzzi and Estelle Mairesse who supported me during all this time and helped me overcome to my problems.

Sincerely
Jean Carlos da Conceição Lorenzzi
Aveiro, September 2007

Palavras-chave

Filmes de nitreto de boro, Si_3N_4, Magnetron sputtering, FTIR, Nanodureza e tensões residuais

Resumo

O Nitreto de boro é um material polimorfo, sendo as fases hexagonal (h-BN) e cúbicas (c-BN) as predominantes. A fase hexagonal do nitreto de boro apresenta uma estrutura em camadas sp^2, semelhante a grafite, enquanto que a fase cúbica do nitreto de boro tem forte ligações sp^3, como o diamante. O h-BN apresenta boas propriedades dieléctricas, é um material refractário, resistente a corrosão, é conhecido por ser um lubrificante sólido que tem aplicações na protecção de moldes de injecção e em outros processos mecânicos de elevadas temperaturas ou lubrificação em ambientes de elevada humidade. Contudo, o h-BN é extremamente macio. Em contraste, o c-BN apresenta excelentes propriedades térmicas, eléctricas e ópticas, sendo ainda um dos materiais conhecidos com dureza mais elevada (70 GPa). Além disso, c-BN apresenta propriedades superiores em relação ao diamante quando aplicado em ferramentas de corte na maquinagem de materiais ferrosos, devido a sua alta estabilidade química a altas temperaturas durante a maquinagem. Essa combinação de propriedades faz dele um forte candidato no campo das ferramentas de corte e em dipositivos electrónicos. No presente trabalho, filmes finos de nitreto de boro foram depositados por DC e RF magnetron sputtering, utilizando alvos de B_4C e h-BN prensados a quente, numa atmosfera de deposição contituída por misturas de Ar e N_2. Os filmes finos de BN foram depositados simultâneamente em dois tipos de substratos: cerâmicos de Si_3N_4 com diferentes acabamentos superficiais e em discos de Si(100). A influência dos parâmetros de deposição, tais como a temperatura do substrato, composição da atmosfera de deposição na espessura dos filmes, taxa de deposição, cristalinidade, tensão residual, fases presentes e dureza, foram sistematicamente investigados usando técnicas como, SEM, XRD, FT-IR e nanodureza. O h-BN foi a principal fase observada nas análises dos espectros de FT-IR e nos difractogramas de XRD. O estado de tensão dos filmes finos de BN films é estremamente afectado pela temperatura do substrato, composição do gás de trabalho e pelo acabamento superficial dos substratos. O estudo da influência da temperatura mostraram que a taxa de deposição aumenta com o aumento da temperatura do substrato. Tensões residuais elevadas ocorrem para altas concentrações de árgon e para substratos polidos em suspensão de diamante 15 μm. Nos espectros de FT-IR, a forma das bandas de vibração variam de uma forma alargada para uma configuração estreita, correspondendo a uma menor desordem da fase hexagonal do BN, devido a variação da composição da atmosfera de deposição. Os valores de dureza obtidos estão numa faixa que vai desde os valores do h-BN macio (6 GPa) até valores próximos dos limites encontrados para filmes contendo a fase cúbica (16 GPa), acima de 40%.

Keywords

BN thin films; Si_3N_4 substrate; magnetron sputtering; FTIR, Nanohardness and films stress.

Abstract

Boron nitride is a polymorphic material, the hexagonal (h-BN) and the cubic (c-BN) being its main crystalline structure. The hexagonal boron nitride has a layered sp2-bonded structure, similar to graphite, while the cubic boron nitride has a hard sp3-bonded diamond-like structure. h-BN presents good dielectric properties, refractoriness, corrosion-resistant characteristics, low friction and low wear rate, and it is a well-known solid lubricant which has wide applications in metal-forming dies and other metal working processes at high temperatures or lubrication in high relative humidity environments. However, h-BN is mechanically soft. In contrast, c-BN presents excellent thermal, electrical and optical properties, with a hardness up to 70 GPa. Moreover, c-BN is superior to diamond as cutting tool for ferrous materials due to its high thermal chemical stability during machining. In the present work, thin films of boron nitride have been deposited by D.C. and R.F. magnetron sputtering from hot-pressed B4C and h-BN targets, using mixtures of Ar and N_2, as working gases. The BN thin films were deposited simultaneously on two different substrates: Si3N4 ceramics with different surface finishing and Si(100) wafers. The influence of parameters such as substrate temperature and working gas composition ratio, on film thickness, deposition rate, cristallinity, residual stress, phase composition and hardness, were systematically investigated using techniques like SEM, XRD, FT-IR and nanohardness. h-BN was the main observed phase. The stress-state of the thin BN films is largely affected by the substrate temperature, working gas composition and the substrate surface finishing. The substrate temperature studies show that the deposition rate increases with an increasing of the substrate temperature. Large high residual stresses are developed for higher argon ratios and for substrate finishing with 15 μm diamond paste. In the FT-IR spectra, the shape of the vibration band changes from broad to narrow, corresponding to a less disorder h-BN phase, due to the working gas composition. The hardness values obtained are typical in the range of a soft h-BN (6 GPa) to values approaching the limit of the range reported for films containing a fraction of cubic phase (16 GPa) up to 40%.

Contents

Chapter 1 - Introduction ………………………………………………………….……… 1

Chapter 2 - Literature review ……………………………………………………..….... 4

2.1. Silicon nitride ……………………………………………………………… 4

2.2. Boron nitride (BN) …………………………………………………….… 9

2.3. Sputtering technique ……………………………………….…...……. 11

2.4. Boron nitride thin films ……………………………...……………..… 18

Chapter 3 - Experimental methods and characterisation techniques … 21

3.1. Silicon nitride substrates (Si_3N_4) …………………………...…….... 21

3.1.1. Production of silicon nitride substrates ………………………… 21

3.1.2. Characterisation of silicon nitride substrates ………….…....… 23

3.2. BN thin films ……………………….……………………….….…… 25

3.2.1. Production and characterisation of the targets …….……...… 25

3.2.2. Coating deposition ………………………………………………. 26

3.2.2.1. DC magnetron sputtering ……………………………. 26

3.2.2.2. RF magnetron sputtering …………………...….…. 28

3.2.3. Coating characterisation methods ……………….….…….. 31

Chapter 4 – Results and Discussion …………………………..……….. 32

4.1. Silicon nitride substrates (Si_3N_4) ……………………….……..….... 32

4.2. Boron nitride thin films ……..…………………………………...… 37

4.2.1. Targets characterisation ………………………………….. 37

4.2.2. DC magnetron sputtering ………………………………….…… 39

4.2.3. RF magnetron sputtering ……………………………….… 41

4.2.3.1. Substrate temperature studies …..………………… 42

4.2.3.2. Working gas composition studies ………………..… 50

Chapter 5 – Conclusions ……………………………………………………..……. 58

Chapter 6 – Recommendation of future work …………...……………….. 60

Bibliography …………………...…………………………………………………….. 61

List of Figures

Fig. 1.1 - Illustration of new challenges related to thin films materials and devices [4] ………………. **1**

Fig. 2.1 - Crystal structures of trigonal α-Si_3N_4 (space group P31c and with lattice parameter a=0.7818 and c= 0.559) and hexagonal β-Si_3N_4 (space group $P6_3/m$ and with lattice parameter a=0.7595 and c= 0.29023), emphasizing the corner-sharing SiN_4 tetrahedra [16] ………………………………………………………………………………………………. **5**

Fig. 2.2 - Typical microstructure of a liquid-phase sintered Si_3N_4 ceramics; (a) schematic and (b) SEM micrograph [17], where: 1- Si_3N_4 matrix grains, 2-crystalline secondary phase, 3-amorphous phase at triple junctions and grain boundaries …………………………………… **7**

Fig. 2.3 - Structures of sp^3-bonded and sp^2-bonded phases for BN with their respective stacking sequences [39] ……………………………………………………………………………….. **9**

Fig. 2.4 - Schematic representation of a crystal structure of c-BN [39] ………………………………… **11**

Fig. 2.5 - Schematic diagram of a sputtering deposition [49] ……………………………………………. **12**

Fig. 2.6 - Depiction of energetic particle bombardment effects on surfaces and growing films [50] … **13**

Fig. 2.7 - Schematic diagram of deposition on an on-axis mounted substrate [54] …………………… **15**

Fig. 2.8 - Schematic deposition chamber and off-axis RF magnetron sputtering technique [55] ……. **17**

Fig. 3.1 - (a) graphite resistance heated furnace used to sinter the substrates, (b) uniaxial pressing mould, and (c) view of Si_3N_4 substrates after sintering ……………………………………….. **22**

Fig. 3.2 - Schematic diagram of the sintering cycle of silicon nitride (Si_3N_4) substrates ……………… **23**

Fig. 3.3 - Flow chart for the preparation of Si_3N_4 substrates …………………………………………….. **23**

Fig. 3.4 - (a) SEM of a Vickers indentation defining indent and median crack parameters "a" and "c", respectively; (b) view of the cracks around a Vickers indentation ……………………… **25**

Fig. 3.5 - (a) Schematic diagram of HP cycle of the BN targets and (b) HP targets produced ………. **26**

Fig. 3.6 - Different views of the experimental set-up for the D.C. magnetron sputtering deposition from Physical Department at Aveiro University ………………………………………………. **27**

Fig. 3.7 - Different views of RF magnetron sputtering equipment from Physics Department of Aveiro University ……………………………………………………………………………………… **28**

Fig. 3.8 - Schematic diagram of the BN thin film deposition system …………………………………… **29**

Fig. 4.1 - (a-b) Scanning Electron micrographs of the sintered Si_3N_4 ceramics without surface etching ……………………………………………………………………………………………… **33**

Fig. 4.2 - SEM micrograph of Si_3N_4 after etching in (a) H_3PO_4 and (b) etched by CF_4 plasma ……… **33**

Fig. 4.3 - (a-b) SEM micrograph of the fracture surface of the Si_3N_4 ceramic after etching in H_3PO_4. **34**

Fig. 4.4 - X-ray Diffraction pattern of the powders mixture and the sintered Si_3N_4 using CuKα radiation ……………………………………………………………………………………………. **34**

Fig. 4.5 - The FTIR absorption spectra for Si_3N_4 substrates …………………………………………….. **35**

Fig. 4.6 - Scanning electron micrograph of Si_3N_4 indentation; (a) SEM of indentation, imprint (b) SEM of an indentation crack **36**
Fig. 4.7 - X-ray Diffraction pattern of h-BN hot-pressed target, using CuKα radiation. Intensity axis is in log (10) scale **37**
Fig. 4.8 - X-ray Diffraction pattern of B_4C hot-pressed target, using CuKα radiation. Intensity axis is in log (10) scale **38**
Fig. 4.9 - Fourier Transform Infrared (FTIR) absorption spectrum of h-BN hot-pressed target **38**
Fig. 4.10 - Fourier Transform Infrared (FTIR) absorption spectrum of B_4C hot-pressed target **39**
Fig. 4.11 - FTIR absorption spectra for BN films deposited by D.C. Magnetron sputtering under different conditions **40**
Fig. 4.12 - SEM micrographs of the films deposited by DC sputtering at different conditions **41**
Fig. 4.13 - FT-IR absorption spectra in transmittance mode of BN films deposited on Si_3N_4 substrates (surface finishing 6μm) under different substrate temperatures **43**
Fig. 4.14 - FT-IR absorption spectra in transmittance mode of BN films deposited on Si_3N_4 substrates (surface finishing 15μm) under different substrate temperatures **43**
Fig. 4.15 - Stress and peak position of the BN films deposited on Si_3N_4 substrates (surface finishing of 6 μm and 15 μm) under different substrate temperatures **44**
Fig. 4.16 - FT-IR absorption spectra in transmittance mode of BN films deposited on Si(100) substrates under different substrate temperatures **45**
Fig. 4.17 - Glancing-angle X-ray Diffraction patterns of the BN film on Si(100) wafer substrates deposited at different substrate temperatures **45**
Fig. 4.18 - SEM micrographs of the surface of BN films on Si_3N_4 (surface finishing of 6 μm) substrates deposited at different substrate temperatures **47**
Fig. 4.19 - SEM cross-sectional images of BN layer system on Si_3N_4 (surface finishing of 6 μm) substrates deposited at different substrate temperatures **48**
Fig. 4.20 - Dependence of the thickness and deposition rate of BN thin films with substrate temperature (Ts) **49**
Fig. 4.21 - Hardness and errors associate with the measurement as function of substrate temperature **50**
Fig. 4.22 - FT-IR absorption spectra in transmittance mode of BN films deposited on Si_3N_4 substrates (surface finishing of 6 μm) at 400ºC, using different working gas composition Ar/N_2 (%vol.) **51**
Fig. 4.23 - FT-IR absorption spectra in transmittance mode of BN films deposited on Si_3N_4 substrates (surface finishing of 15μm) at 400ºC, using different working gas composition Ar/N_2 (%vol.) **51**
Fig. 4.24 - Stress and peak position of the BN films deposited on Si_3N_4 substrates (surface finishing of 6 μm and 15 μm) under working atmospheres ratio (Ar/N_2) ....
Fig. 4.25 - FT-IR absorption spectra in transmittance mode of BN films deposited on Si(100) substrates at 400ºC, using different working gas composition Ar/N_2 (%vol.) **52**
Fig. 4.26 - Glancing-angle (2º) X-ray diffraction patterns of the BN film on Si(100) wafer substrates deposited at 400ºC, using different ratios of Ar/N_2 (%vol.) **53**
Fig. 4.27 - SEM micrographs of the surface of BN films on Si_3N_4 (surface finishing of 6 μm) substrates deposited at 400ºC using gas mixtures of Ar/N_2 (%vol.) as working gas **54**

Fig. 4.28 - SEM cross-sectional images of BN layer system on Si_3N_4 (surface finishing of 6 μm) substrates deposited at 400ºC using gas mixtures of Ar/N_2 (%vol.) as working gas ………. **55**

Fig. 4.29 - Dependence of the thickness and deposition rate of BN thin films with the N_2 working gas content ………………………………………………………………………………………… **56**

Fig. 4.30 - Hardness and errors associate with the measurement as function of working gas composition ……………………………………………………………………………………… **57**

List of Tables

Table 2.1 - Typical properties (at room temperature) for hot-pressed and pressureless sintered silicon nitrides [17] …… **7**

Table 2.2 - Properties of BN Materials [40-47] …… **10**

Table 2.3 - Comparison of physical properties of single-crystalline diamond and c-BN [45-47] …… **11**

Table 3.1 - Composition and characteristics of the raw materials used to the produce Si_3N_4 substrates …… **21**

Table 3.2 - Deposition parameters for D.C sputtering using B_4C target. (**Ssf** - substrate surface finishing, **DC** - power applied to the target, **Bias** - bias applied to the substrate; **Ar/N_2** - gas composition, **P_t** - total pressure during deposition, , **D**-distance target-substrate, **t-** deposition time) …… **27**

Table 3.3 - Deposition parameters for BN thin film deposition by RF sputtering using h-BN as target: (**sb** – Kind of substrate, **Ssf** – substrate surface finishing, **RF** -power applied to the target, **P_t** - total pressure during deposition, **Ar/N_2** – working gas composition, **D** - distance target-substrate, **t** - deposition time, **T** - substrate temperature) …… **30**

Table 4.1 - Physical properties of silicon nitride used as substrates …… **32**

Table 4.2 - Phase content and mechanical properties of silicon nitride substrates …… **36**

Table 4.3 - Identification of the X-ray reflection planes, taken from Fig. 4.17, of the BN coating deposited on Si(100), substrate temperature studies …… **46**

Table 4.4 - The physical and mechanical properties of BN thin films prepared by R.F magnetron sputtering using different substrate temperatures …… **49**

Table 4.5 - Identification of the X-ray reflection planes, taken from Fig. 4. 26, of the BN coating deposited on Si(100), during the working gas (Ar/N_2) ratio study …… **54**

Table 4.6 - The physical and mechanical properties of BN thin films prepared by R.F magnetron sputtering using different working gas ratio (Ar/N_2) …… **56**

List of Abbreviations

PVD	*Physical Vapour Deposition*
CVD	*Chemical Vapour Deposition*
RF	*Radio frequency*
DC	*Direct current*
BN	*Boron nitride*
c-BN	*Cubic boron nitride*
h-BN	*Hexagonal boron nitride*
w-BN	*Wurtzitic boron nitride*
r-BN	*Rhombohedral boron nitride*
t-BN	*Turbostratic boron nitride*
Si_3N_4	*Silicon nitride*
B_4C	*Boron carbide*
HP	*Hot pressing*
HIP	*Hot isostatic pressing*
HT/HP	*High temperature high pressure*
GPS	*Gas pressure sintering*
LPS	*Liquid phase sintering*
IBAD	*Ion-beam assisted deposition*
PLD	*Pulsed laser deposition*
XRD	*X-ray Diffraction*
SEM	*Scanning Electron Microscopy*
FT-IR	*Fourier transform Infrared*
K_{IC}	*Fracture Toughness* ($MPa.m^{1/2}$)
Hv	*Vickers Hardness (GPa)*
E	*Young's modulus (GPa)*
TO	*Transverse optical*
RT	*Room temperature*

Chapter 1

Introduction

The importance of synthesis of new coatings for the industry has resulted in a great increase of innovative thin film processing technologies. Presently, this progress goes hand-in-hand with the explosion of scientific and technological advances in microelectronics, optics and nanotechnology [1].

Thin films are essential in a significant number of components like, for example, thermal barrier coatings and wear protections, enhancing their service life by protecting materials against mechanical, thermal and atmospheric influences [2, 3]. Currently, the rapidly changing needs for thin film coated materials and devices are generating new opportunities for the development of new solutions. Fig. 1.1 shows the elements that undergo the Thin Film Science.

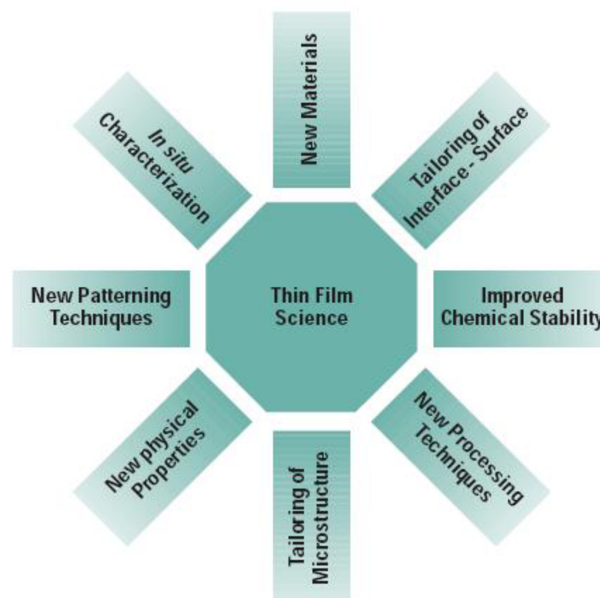

Fig. 1.1 – Illustration of new challenges related to thin films materials and devices [4].

It is very well known that cubic boron nitride (c-BN) is one of the hardest materials. It is a promising candidate as hard coating for cutting tools due to its extreme properties, similar to those of diamond in terms of hardness, thermal conductivity and optical transparency. But it has two advantages in comparison with diamond: i) c-BN is chemically inert in oxygen

atmospheres, even more stable against oxidation up high temperature than diamond; ii) boron and nitrogen atoms do not diffuse into ferrous [5] substrate materials under thermal loading, contrarily to carbon in diamond. Therefore, c-BN seems to be better suited for wear protection films on steel substrates [6].

These properties make c-BN a potential candidate for many thin film applications not only, as wear protecting layers on tools, but also as transparent protecting films on optical components or as heat dissipating films in electronics and laser diode technology. However, a disadvantage of c-BN is their cost and processing complexity.

In many cutting and forming operations, coated tools are indispensable for industrial production. Hard coatings for wear reduction, like TiN, TiCN, CrN and TiAlN or dry lubricant coatings like MoS_2 are well established [7]. One consequence of increasing the productivity and product quality is the need to increase the tool performance. Particularly, the trend to operate under dry conditions, high speed cutting, cutting of hard materials, and machining of lightweight materials is still a challenge for the development of new tools and coatings.

The synthesis of c-BN can be performed in different ways, classically in bulk form at high temperature and high pressure (HT/HP), but to obtain thin films, PVD and CVD are the most common. Magnetron sputtering is a PVD method involving the removal of material from a solid cathode, while the substrate is placed in a low-pressure chamber between two electrodes assisted by a magnetron. It is commonly used for thin film deposition at room temperature.

In many cases, magnetron sputtered films now outperform films deposited by other PVD processes, and can perform the same functionality as much thicker films produced by other surface coating techniques. Consequently, magnetron sputtering has now a significant impact in application areas including hard, wear resistant coatings, low friction coatings, corrosion resistant coatings, decorative coatings and coatings with specific optical or electrical properties [8].

The commonly used magnetron sputtering techniques are: (i) Radio Frequency (RF) sputtering by applying a RF signal to the electrode (target) it can be used for both conductor and insulator targets; (ii) Direct current (DC) sputtering by applying a DC voltage to the electrode it can only be used with conducting targets and (iii) Reactive sputtering where a reactive gas is used with a inert gas during the deposition.

The deposition of boron nitride films by DC and RF magnetron sputtering envisaging enhanced wear resistance of industrial components namely, cutting tools, was thus the aim of the present work. This technique presents a great interest for industrial applications, due to its low work temperature and up scaling potential.

The BN thin films, partially comprising the c-BN phase, were produced in the Ceramic and Glass Engineering Department and in the Physics Department of Aveiro University.

Primary studies were performed using DC magnetron sputtering using B_4C as target, but this technique was put aside because of some equipment restrictions. For this reason, RF magnetron sputtering was performed from a hot-pressed h-BN disc target.

The deposition processes were carried out in two different vacuum chambers (for DC and for RF magnetron sputtering), with mixtures of Ar and N_2 as working gases. Several parameters were altered during film depositions in order to optimise the BN growth.

BN thin films (thickness between 180-500 nm) were grown on Si(100) wafers and silicon nitride (Si_3N_4) substrates, simultaneously. The use of silicon nitride as a substrate is related to its superior properties - high fracture toughness and mechanical strength, thermal shock resistance, good creep behaviour - and potential high interface compatibility with BN, similar to that with the diamond [9]. The Si_3N_4 ceramic substrates discs with a diameter of 10 mm were prepared by the powder technology at Aveiro University in the Ceramic and Glass Engineering Department. The Si(100) wafers were used as substrate in order to provide a support during the characterisation.

The characterisation of the Si_3N_4 substrates and the BN films was made at the Institute of Mechanical Engineering in Aalborg University, Denmark and also at Aveiro University. Several techniques were used in order to characterise the substrates and coatings, namely: Fourier Transform Infrared (FT-IR), X-ray diffraction (XRD) using the glancing incidence angle configuration, Scanning Electron Microscopy (SEM) and nanohardness.

Chapter 2

Literature Review

The purpose of this chapter is to resume the most important theoretical concepts for interpretation of the experimental data on silicon nitride substrates processing and BN coating growth and properties. The chapter is divided into four parts. In the first and second ones, some background about silicon nitride and boron nitride compounds is presented. The third part reports the main concepts of Physical Vapour Deposition (PVD) chosen as coating technique in this work. The last section is an overview on literature concerning BN thin films.

2.1. Silicon nitride

Silicon nitride (Si_3N_4) was developed in the 1960s and 1970s in a search for fully dense, high strength and high toughness materials [10]. A prime driver for its development was to replace metals with ceramics in advanced turbine and reciprocating engines to give higher operating temperatures and efficiencies. Although the ultimate goal of a ceramic engine has never been achieved, silicon nitride ceramics have been used in a number of industrial applications, such as engine components, bearings and cutting tools for machining cast irons and nickel-based alloys [11, 12].

Silicon nitride is a polymorphic material, presenting three crystallographic modifications designated as the α, β and γ phases. While the α and β modifications can be produced under normal nitrogen pressure and have great importance in the production of advanced ceramics, the recently discovered γ-Si_3N_4 can be formed only at extremely high pressures [13] and has no practical use yet.

In a simple chemical picture, chemical bonding in α- and β- Si_3N_4 are due to the overlap of the sp^3 hybrid orbitals of silicon atoms with the sp^2 hybrid orbitals of the nitrogen atoms. Each nitrogen atom has a remaining p atomic orbital which is nonbonding and that is occupied by a single pair of electrons [13, 14].

The basic unit of Si_3N_4 is the SiN_4 tetrahedron. A silicon atom is located at the centre of a tetrahedron, with four nitrogen atoms at each corner. The SiN_4 tetrahedra are joined by sharing corners in such a manner that each nitrogen is common to three tetrahedra. Thus nitrogen has three silicon atoms as neighbours [15]. The structural difference between α- and

β- Si_3N_4 can be explained by different arrangements of Si-N layers, as it can be seen in Fig. 2.1. The basic units are linked together to form puckered six-membered rings which surround large holes. These basal planes form the building blocks for the structures of α and β- Si_3N_4.

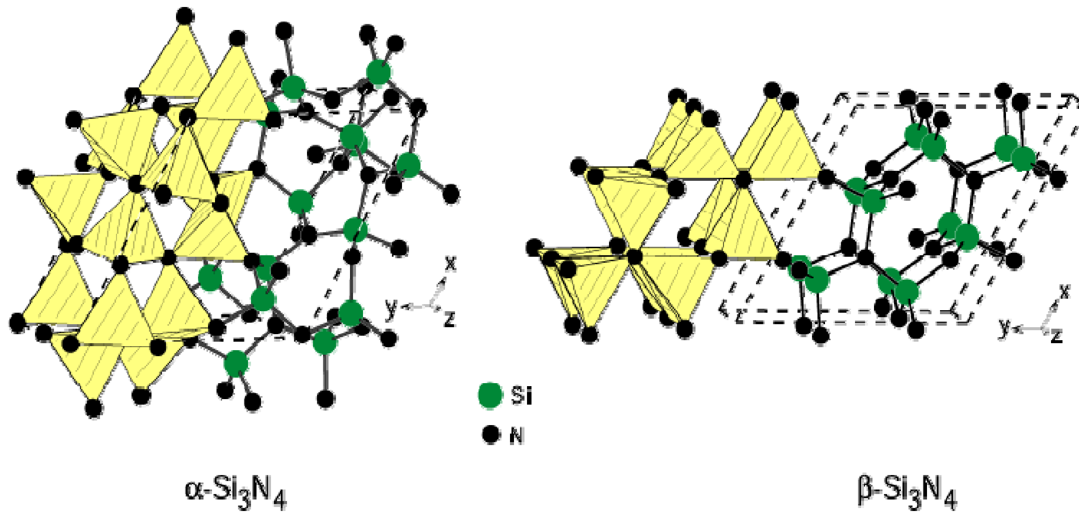

Fig. 2.1 - Crystal structures of trigonal α-Si_3N_4 (space group P31c and with lattice parameter a=0.7818 and c= 0.559) and hexagonal β-Si_3N_4 (space group $P6_3/m$ and with lattice parameter a=0.7595 and c= 0.29023), emphasizing the corner-sharing SiN_4 tetrahedra [16].

The α- Si_3N_4 structure is formed by stacking the basal planes in the ABCDABCD... order, and β- Si_3N_4 is constructed of basal planes stacked in the ABAB... sequence [17]. The AB layer is the same in α- Si_3N_4 and β- Si_3N_4, and the CD layer in α- Si_3N_4 is related to the AB layer of β- Si_3N_4 by a c-glide plane. Regarding the unit cell dimensions, α- and β- Si_3N_4 structures are related by Aα ≈ Bβ.

The β- Si_3N_4 structure exhibits channels parallel to the c-axis which are about 0.15 nm in diameter enabling higher diffusion coefficients of ions when compared to the α-structure. These channels are changed into voids with seven nearest neighbouring nitrogen atoms in α-Si_3N_4. The α- and β-forms have trigonal and hexagonal symmetry, respectively.

The high degree of covalent bonding makes it very difficult to produce pure dense Si_3N_4 ceramics by solid state sintering. The main reason for this relies on the fact that the diffusion of silicon and nitrogen in the volume or at the grain boundaries of Si_3N_4 is extremely slow [18]. The densification of Si_3N_4 is thus conducted via the presence of a liquid phase with the help of oxide additives

At the sintering temperatures, typically in the range 1550 – 1750 ºC, the oxide additives react with the silica present on the Si_3N_4 powder particles, forming an oxynitride liquid phase which acts as mass transport medium [19]. However, at high temperatures Si_3N_4 starts to dissociate [20].

Many studies have been reported on Si_3N_4 ceramics with Y_2O_3 and Al_2O_3 as sintering additives because of their excellent sinterability and mechanical properties, such as bending

strength and fracture toughness. It is generally recognised that the kind and amount of sintering additives, as well as raw materials and sintering conditions, greatly affect the microstructure after sintering [21,22]. As a consequence, many different sintering techniques have been developed.

One common densification method is the nitridation of silicon compacts, leading to Reaction-Bonded silicon nitride materials. By this method, complex shapes can be produced using various ceramic forming methods (slip casting, injection moulding, die pressing, isostatic pressing) with low costs. However, the process leads to a material of limited density (about 70-88%) resulting in poor mechanical properties. Because of the residual porosity the strength of the reaction bonding silicon nitride materials is relatively low. Furthermore, the pore structure goes ahead to high oxidation rates and to small erosion resistance [23, 24]. Thus, low densities and pore structure limit the range of possible applications of the reaction bonding silicon nitride materials.

Hot-pressing (HP) of pure silicon nitride powder at high temperatures does not result in full density and also leads to the production of porous materials with properties similar to those of the reaction bonding silicon nitride [25]. In spite of this, the first dense Si_3N_4 ceramic was that accomplished by uniaxial hot pressing Si_3N_4 powders containing MgO as sintering additive [26]. Such kind of hot-pressed Si_3N_4 ceramics is a high strength material, which can be used at temperatures up to 1000°C without a decrease in strength. Because of high cost and difficulties to machine the components, hot-pressing, today, has limited use for the production of simple shaped parts and low quantities.

Another method used to produce dense Si_3N_4 material is by applying an isostatic pressure (>100 MPa) instead of uniaxial pressure, i.e. hot-isostatic pressing (HIP). During this process a high gas pressure is applied to consolidate a powder compact or to remove the residual porosity from pre-sintered bodies. The uniform manner of applying the high pressure results in fully isotropic material properties. The possibility to use much higher pressures than in uniaxial hot-pressing leads to an enhancement in the densification of the products. Thus, fully dense ceramic parts can be produced from powders of lower sintering activity and with smaller amounts of additives when compared with uniaxial hot pressing. Resulting materials combine excellent mechanical and thermo-mechanical properties, but the cost of the process is relatively high.

Another sintering method for high-strength Si_3N_4 ceramics is the gas pressure sintering (GPS), under 10 MPa. This method allows sintering of the complex-shaped parts with medium cost. However, the most economical method to sinter Si_3N_4 powder compacts with additives at atmospheric pressure and temperature around 1700°-1800°C, is pressureless sintering (PS).

In this study, the silicon nitride substrates were consolidate using PS technique. The resulting microstructure of dense Si_3N_4 consists mainly of β-Si_3N_4 grains and a mostly

amorphous grain-boundary phase in the form of thin layers or at triple junctions, Fig. 2.2a. During cooling or after heat treatment, crystalline secondary phases may arise in the intergranular transient (Fig. 2.2). This intergranular phase strongly affects the mechanical properties, especially at high temperatures. The thickness of the grain boundary film depends either on the types of additives as on the amount of liquid phase.

A typical feature of sintered Si_3N_4 ceramics is the morphology of the Si_3N_4 grains (Fig 2.2b). Residual α-grains are equiaxial while the β-phase exhibits an elongated grain structure with an aspect ratio (ratio between length and thickness) usually in the range of 5 to 10 [27]. The microstructural development is controlled mainly by the Si_3N_4 starting powders, the additives used and the sintering parameters.

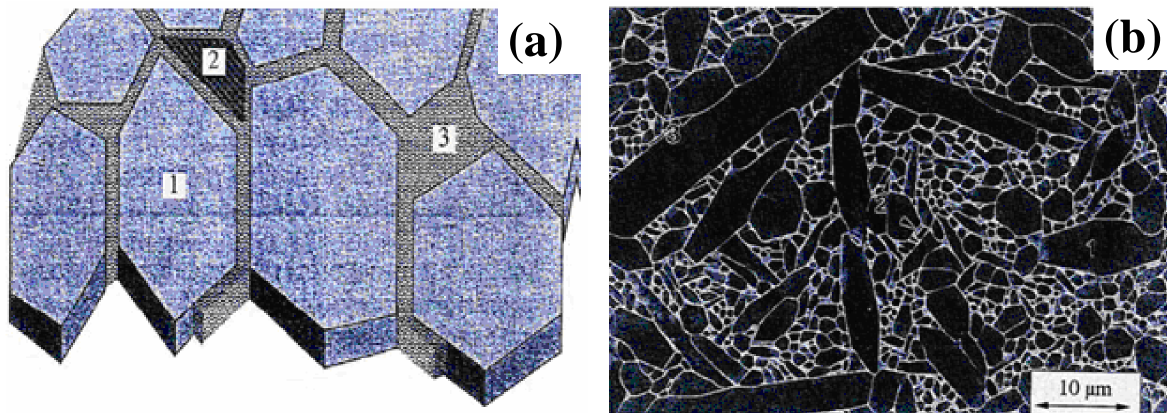

Fig. 2.2 - Typical microstructure of a liquid-phase sintered Si_3N_4 ceramics; (a) schematic and (b) SEM micrograph [17], where: 1- Si_3N_4 matrix grains, 2-crystalline secondary phase, 3-amorphous phase at triple junctions and grain boundaries.

Typical data for the properties of hot-pressed and pressureless sintered Si_3N_4 are presented in Table 2.1.

Table 2.1- Typical properties (at room temperature) for hot-pressed and pressureless sintered silicon nitrides [17].

Property	Hot pressed Si_3N_4	Pressureless sintered Si_3N_4
Density(g/cm^3)	>3.20	3.20
Thermal conductivity (W/mK)	29.3	15.5
Flexural strength (MPa)	1200	800
Compressive strength (MPa)	4500	4000
Thermal expansion (10^{-6}/K)	3.2	3.4
Young's modulus (GPa)	320	280
Toughness-K_{IC} (MPa.m$^{1/2}$)	8.3	5.4
Hardness (GPa)	18	16

It can be inferred from the given data, (Table 2.1) that Si_3N_4 possesses high strength, good thermal-shock resistance due to the low coefficient of thermal expansion. Moreover, it

has a high resistance to oxidation when compared to other high-temperature structural materials [28].

The mechanical properties of Si_3N_4 ceramics depend on the presence of pores, cracks and inclusions. Among these factors, porosity has been demonstrated to have a pronounced effect on mechanical strength. Fracture toughness differs mainly with variations in the microstructure. The grain shape and size along with the phase composition of the grain-boundary phase have a strong influence. High fracture toughness of Si_3N_4 based ceramics could be explained on the basis of similar toughening mechanisms as in whisker reinforced composite materials (grain bridging, pull-out, crack deflection, and crack branching [29]). However, these toughening mechanisms are only active when the dominant fracture mode is intergranular.

The ratio between transgranular and intergranular fracture depends on the strength of both intergranular phase and Si_3N_4 grains. A material with higher toughness has a weaker grain boundary. On the other side, the strength of the grain-boundary phase is connected with the local residual stresses [30]. When the thermal expansion coefficient of the grain-boundary phase is higher than that of the Si_3N_4 grains, the grain-boundary phase is under tensile stress and the fraction of intergranular fracture is higher. As a consequence, the fracture toughness increases. In contrast, ceramics with a grain boundary phase under compression have low fracture toughness because of a higher amount of transgranular fracture [31].

Thermal conductivity is another interesting property of Si_3N_4 which combined with the excellent mechanical properties makes it a serious candidate for high-performance substrates under thermo dynamical loading [32].

2.2. Boron nitride (BN)

The elements boron and nitrogen, both neighbours to carbon in the Periodic Table, form 1:1 compounds, which are microstructural and isoelectronic to the polymorphs of carbon. The hexagonal modification of boron nitride (h-BN) has a layered sp^2-bonded structure similar to graphite (Fig. 2.3a) and it is sometimes called “white graphite” [33]. Hexagonal BN was prepared for the first time in the mid-19th century [34, 35]. It remained a laboratory curiosity for more than hundred years, until hot-pressed h-BN shapes were firstly made in 1957 [36]. Hexagonal boron nitride is the only BN phase found in nature. The cubic modification (c-BN) is a hard sp^3-bonded diamond-like phase with a cubic zinc-blende structure (Fig. 2.3d). In 1957, cubic BN was first grown in bulk crystalline form by using a high pressure and high temperature method [37]. In 1970, c-BN thin films deposited by a physical vapour deposition (PVD) were presented. Hexagonal and cubic BN are the only two stable phases of boron nitride.

The stacking sequences in h-BN and c-BN can vary, producing also metastable sp^2- and sp^3-bonded poly-types. By rearranging the basal planes of sp^2-bonded BN in a staggered arrangement, rhombohedral BN (r-BN) is obtained (Fig. 2.3b). The metastable sp^3-bonded modification of boron nitride is wurtzitic BN (w-BN, Fig. 2.3.c).

As with graphitic carbon, sp^2-bonded boron nitride is often found in a disordered, turbostratic form (t-BN). This is the most commonly observed form of sp^2-bonded material in boron nitride thin films. For a turbostratic structure, the two-dimensional in-plane order of quasi-hexagonal basal planes is largely retained, but these planes are stacked in a random sequence and with random rotation around the c-axis [38]. Thin films of boron nitride may also be formed without a distinct crystallographic order and without any distinctly identified phase. The films are then defined as amorphous boron nitride (a-BN).

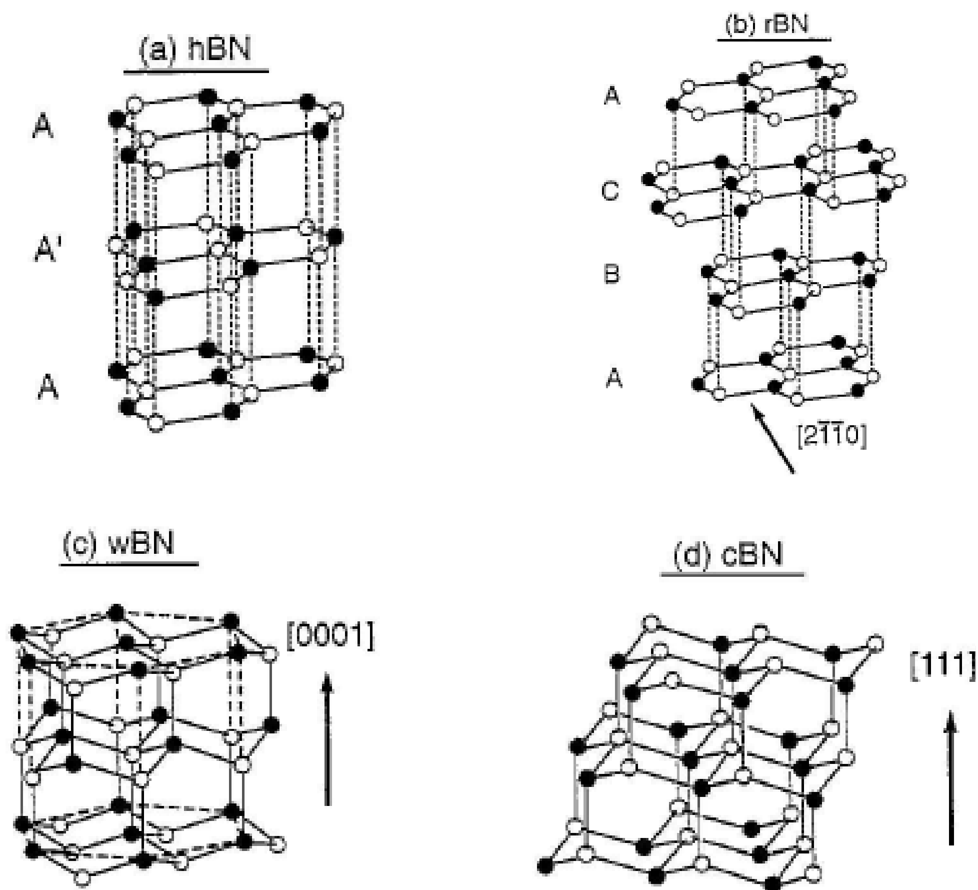

Fig. 2.3 - Structures of sp^3-bonded and sp^2-bonded phases for BN with their respective stacking sequences [39].

Hexagonal boron nitride is widely used because of its combination of properties, e.g., low density, high temperature stability, chemical inertness, stability in air up to 1000°C, stability to thermal shock, easy workability of hot-pressed shapes, excellent electrical insulating character, very high thermal conductivity [33,39]. Bulk h-BN can therefore be used as a solid lubricant and as a ceramic insulating material in high temperature environments. It

can also be employed as a crucible for melting glass and metals, and as a neutron absorber and shield for nuclear reactors. A comprehensive list of physical properties of the most important phases of BN can be found in several material handbooks, and a short list of data is compiled in Table 2.2.

Table 2.2 - Properties of BN Materials [40-47].

Property	c-BN	h-BN	a-BN
Space group	cubF43m (216)	$P6_3mc$ (186)	
Crystal structure	cubic	hexagonal zinc blende	amorphous
Lattice constant (Å)	a = 3.6158	a = 2.50475 c = 6.6482	
Density (g/cm^3)	3.48	2.2	1.74
Hardness (GPa)	40–60	1-6	2-6
Band gap activation energy (eV)	0.19–0.23	0.05–0.41	
Thermal conductivity (W.cm^{-1}K^{-1})	2–9	0.68	0.36
Oxidation stability (ºC)	1200	-	-
Elastic modulus (GPa)	850	30-100	-
Linear thermal expansion (10^{-6} K^{-1})	4.8 (700 K)	3.8	-

The cubic boron nitride (c-BN) form was first produced in 1957 by Robert H. Wentorf, a physical chemist for the General Electric Company [37], just two years after the first artificial diamonds were synthesized [42]. In analogy to the fabrication of diamond crystals, c-BN was produced from hexagonal boron nitride submitted to high pressure and high-temperature (HP/HT) conditions.

The interest in c-BN has increased tremendously since the late 1980's, which is directly related to the fact that c-BN thin films can be routinely synthesized by a large variety of physical and chemical vapour deposition techniques.

The crystal structure of c-BN can be seen in the Fig. 2.4 [43] and consists in two unit cells of the cubic structure that are shown at the right-hand side. In the middle, the structure is projected along one of the threefold axes (cube diagonal). At the left-hand side, the tetrahedral environments around one kind of atoms are emphasized. Boron and nitrogen atoms occupy equivalent positions; hence the structure may be thought to be composed of NB4/4 as well as BN4/4 tetrahedra.

After diamond, it is one of the hardest materials known, with roughly 50-70 GPa Vickers hardness. However, c-BN exhibits a much better chemical inertness and thermal stability. Diamond readily reacts with iron, cobalt, and nickel at temperatures above 1000ºC or is subject to oxidation at temperature higher than 800ºC, which results in a disintegration of the diamond surface into gaseous CO_2. In contrast, c-BN is chemically inert against iron group metals for temperatures of up to 1800ºC [43], and its high stability against oxidation is a

consequence of the formation of liquid or solid B_2O_3, which protects the surface against further oxidation [44].

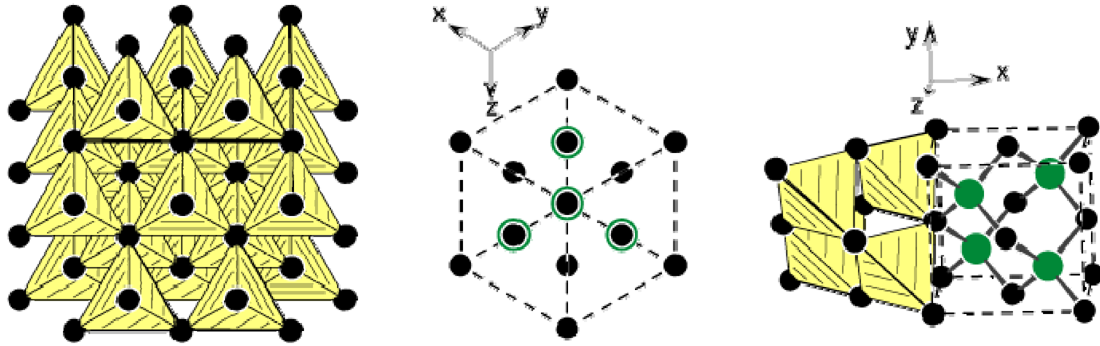

Fig. 2.4 - Schematic representation of a crystal structure of c-BN [39].

Cubic boron nitride also has the potential to outclass diamond concerning electronic applications. It not only has a high band-gap and the second highest room temperature thermal conductivity after diamond, but, in contrast to diamond, it can be easily doped to obtain both n- and p-type conductivities [45, 46]. However, large scale industrial applications are still not possible, mainly because the c-BN crystals exhibit a rather high defect density and impurity concentration. A comparison between c-BN and diamond is given in Table 2.3.

Table 2.3 - Comparison of physical properties of single-crystalline diamond and c-BN [45-47]

Properties	Diamond	c-BN
Structure	CubFd3m	CubF43m (216)
Lattice constant (Å)	3.567	3.615
Interatomic distance (Å)	1.545	1.565
Atomic density (g/cm^3)	$1.77x10^{23}$	$1.68x10^{23}$
Density (g/cm^3)	3.51	3.48
Hardness (GPa)	100	75
Elastic modulus (GPa)	1140	850
Thermal conductivity at RT (W/cm.K)	20-22	2-13
Thermal expansion coefficient ($10^{-6}K^{-1}$)	0.8	4.8
Melting point (K)	4027	3246
Oxidation stability (ºC)	600	1200
Band gap (eV)	5.45	6.4

2.3. Sputtering technique

Sputtering is a PVD technique that involves the removal of material from a solid cathode, while the substrate is placed in a low-pressure chamber between two electrodes assisted by a magnetron. It is commonly used for thin film deposition at room temperature.

Sputtering is the phenomena of momentum transfer from an incident energetic projectile to a solid target resulting in the ejection of surface atoms or molecules. In the sputter deposition process, the target (a source of coating material) and the substrate are placed in the vacuum chamber and evacuated to a pressure typically in the range of10^{-4} to 10^{-7} mbar [48].

A schematic diagram of the sputter coating process is shown in Fig. 2.5. Sputtering laboratory sources are usually magnetrons that use strong electric and magnetic fields to entrap electrons close to the surface of the magnetron, which is known as the target. They are connected to a negative voltage supply, and the substrate generally faces the target. A glow discharge is initiated after an inert gas (usually argon) is introduced into the evacuated chamber.

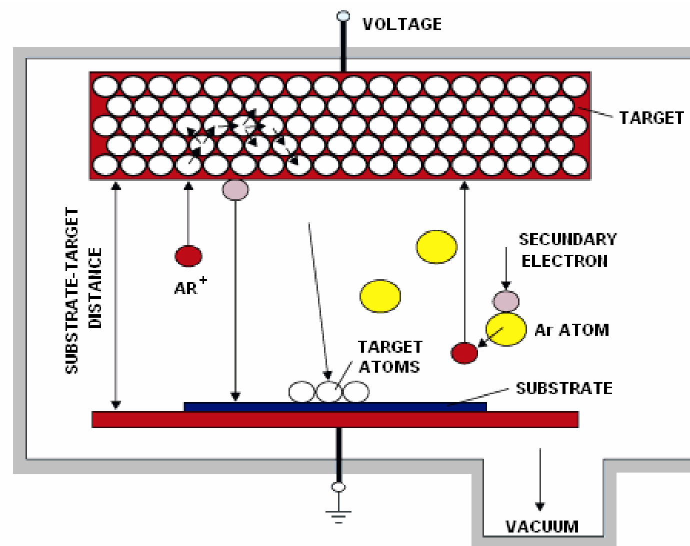

Fig. 2.5 - Schematic diagram of a sputtering deposition [49].

Non-metallic targets are generally prepared by hot-pressing of the powders. The metal and non-metals targets tend to have purities of 99.99% or higher. In addition, less than the theoretical densities are achieved during powder processing. These metallurgical realities are sometimes reflected in emission of particulates, release of trapped gases, non-uniform target erosion, and deposited films of inferior quality. Targets are available in a variety of shapes (e.g., disks, plates, etc.) and sizes. Prior to use, they must be bonded to a cooled backing plate to avoid thermal cracking and thermal degradation. Metal-filled epoxy cements of high thermal conductivity are employed for this purpose.

The number of atoms ejected from the surface per incident ion is called the sputter yield and is an important measure of the efficiency of the sputtering process. Besides, the sputter yield depends on the energy of the incident ions, the masses of the ions and target atoms, and the binding energy of the atoms in the solid [50].

Critical to the analysis and design of sputtering processes is an understanding of what happens when ions collide with surfaces [50]. Some of the interactions that occur are schematically shown in Fig. 2.6.

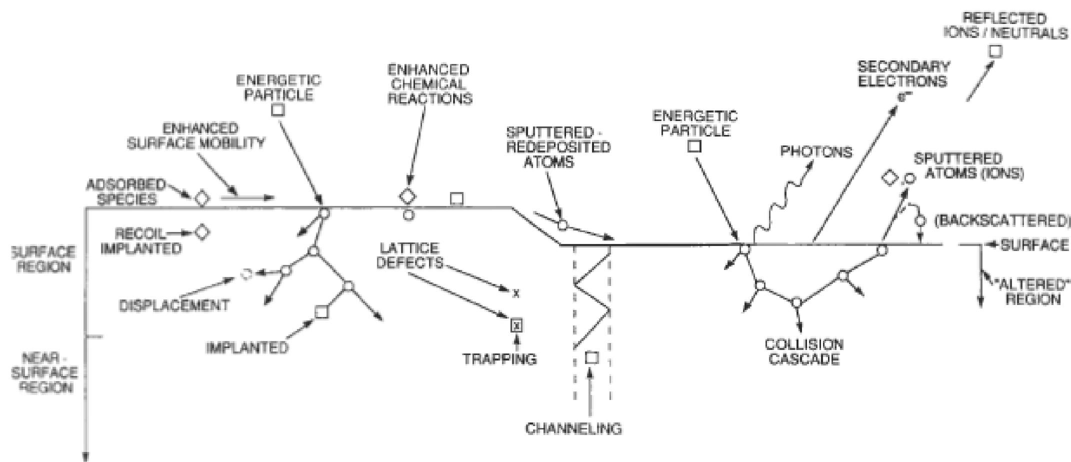

Fig. 2.6 - Depiction of energetic particle bombardment effects on surfaces and growing films [50].

Each interaction depends on the type of ion (mass, charge), the nature of the surface atoms involved, and, importantly, on the ion energy. Several of these interactions have been capitalised in widely used thin-film processing, deposition, and characterisation techniques [51].

Reactive Sputtering

Sputtering is an atomistic process and most of the atoms emitted from a target, regardless of whether it is an elemental or compound/alloy cathode, are emitted as atoms rather than molecules or clusters. Chemical reactions of these atoms moving from the cathode to the sample are rare, but it is completely possible that the freshly-deposited atom on a film surface chemically reacts with gas atoms that impinge on the surface to form a compound film. In other words, reactive sputtering can be explained as being the film deposition of compounds on substrates by sputtering from targets in the presence of a reactive gas, usually mixed with the inert working gas (invariably Ar).

There are two approaches to reactive deposition, one where the cathode is a metal plate, and the other where the cathode is composed by the material to be deposited, for instance, a nitride or an oxide. The most common compounds reactively sputtered (and the reactive gases employed) are briefly listed [52]:

- Oxides (oxygen) - Al_2O_3, In_2O_3, SnO_2, SO_2, Ta_2O_5;
- Nitrides (nitrogen, ammonia) – BN, TaN, TiN, AlN, Si_3N_4;
- Carbides (methane, acetylene, propane) - TiC, WC, SiC;
- Sulfides (H_2S) - CdS, CuS, ZnS;
- Oxycarbides and oxynitrides of Ti, Ta, Al, and Si.

The choice of whether to employ compound targets and sputter directly or sputter reactively is not always clear. If reactive sputtering is selected, then there is the option of using simple dc diode, RF, or magnetron configurations. Many considerations must be done before making these choices, such as [52]:

- Target purity - It is easier to manufacture high-purity metal targets than to make high-purity compound targets. Since hot pressed and sintered compound powders cannot be consolidated to theoretical bulk densities, the incorporation of gases, porosity, and impurities is inevitable. Film purity using elemental targets is high, particularly because high-purity reactive gases are commercially available.
- Deposition rates - Sputter rates of metals drop dramatically when compounds are formed on the targets. Decreases in deposition rate well in excess of 50% occur because of the lower sputter yield of the compounds relative to metals. The effect is very much dependent on the reactive gas pressure. Conditioning of the target in pure Ar is required to restore the pure metal surface and desired deposition rates. When high deposition rates are needed, the reactive sputtering mode of choice is either dc or RF magnetron.
- Stoichiometry and properties - Considerable variation in the composition and properties of reactively sputtered films is possible, depending on the operating conditions.

Magnetron Sputtering

The term “magnetron” was originally applied to describe tubes used to generate microwave power for radar applications. It is still used for this purpose, and the builder or owner of a microwave plasma system will use a “magnetron” power source to run the plasma. The same general magnetron effect found in these tubes can be somehow altered to make an extremely efficient sputtering cathode. These cathodes operate in a diode mode, either in RF or DC, but are rarely, if ever, called diodes. Magnetron sputtering sources are the current workhorse of the sputter deposition field, used in perhaps 95% of all sputtering applications.

The first paper on the magnetron as a sputtering device was reported in the 1960s [53]. Since then, magnetrons have suffered a continuous development in various industrial fields, especially microelectronic and surface processing, and are widely used for thin film deposition.

A magnetron uses a static magnetic field configured at the cathode location. The magnetic field is located parallel to the cathode surface. Secondary electrons which are emitted from the cathode due to ion bombardment are constrained by this magnetic field (B) to move in a direction perpendicular to both the electric field (E) (normal to the surface) and the magnetic field. This is known as an E×B (E cross B) drift, which is also the basis for the

Hall Effect. This drift causes electrons to move parallel to the cathode surface in a 90 degrees direction away from the magnetic field. If the magnetic field is set up correctly, this E×B drift can be arranged to close on itself, forming a current loop of drifting secondary electrons. A schematic diagram of the sputter coating process is shown in Fig. 2.7 [54].

Because of the higher efficiency of this ionization mechanism, the process can by operated at pressures around 1.5 mbar with high current densities at low voltages, thus providing high sputtering rates. There are several configurations of magnetron (e.g. cylindrical and planar) sputter sources.

The cylindrical magnetron is a very useful technique to prepare uniform coatings over large areas, since long cathodes are employed in these techniques. Furthermore, the cylindrical-hollow magnetron technique is effective for coating complex-shaped objects. The cylindrical-post magnetron can be used to substantially decrease the substrate bombardment by energetic particles, hence minimising the heat of the substrate. Metallic films and dielectric films can be deposited with high deposition rates using planar magnetron sputtering, when compared to diode sputtering [50].

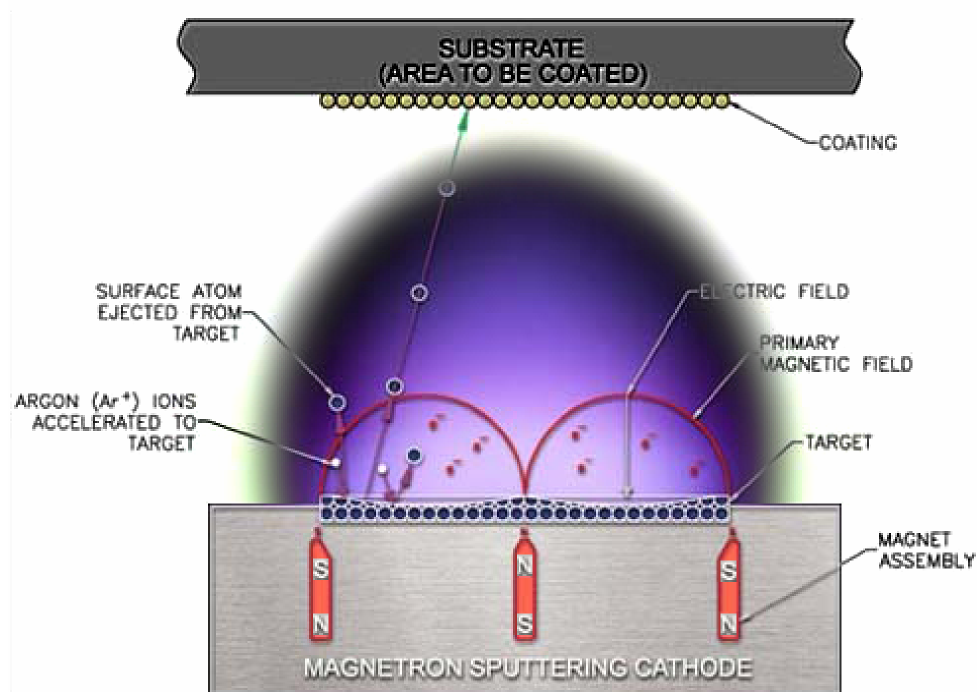

Fig. 2.7 - Schematic diagram of deposition on an on-axis mounted substrate [54].

The sputtering process is limited by the low deposition rates, low ionisation efficiencies in the plasma. These limitations have been overcome by the development of magnetron sputtering and, more recently, of unbalanced magnetron sputtering. Magnetrons make use of the fact that a magnetic field configured parallel to the target surface can constrain the secondary electrons motion to the vicinity of the target. The magnets are arranged in such a way that one pole is positioned at the central axis of the target and the

second pole is formed by a ring of magnets around the outer edge of the target. Trapping the electrons in this way substantially increases the probability of an ionising electron-atom collision to occur. The increased ionisation efficiency of a magnetron results in a dense plasma in the target region. This, in turn, leads to an increased ion bombardment of the target, giving higher sputtering rates and, therefore, higher deposition rates at the substrate.

DC Sputtering

As mention before, sputtering is a complicated process with several operation parameters being correlated. In a simple DC sputtering system the target serves as the source material to be deposited. In DC sputtering a negative potential up to some hundred volts is applied to the target. As a result, the Ar^+ ions are accelerated towards the target setting material free and also they produce secondary electrons. Argon is the most commonly used sputtering gas which serves as the medium where a glow discharge is initiated and sustained. Microscopically, argon ions in the discharge strike the target plate and eject neutral target atoms through energetic collisions [48]. These atoms enter and pass through the discharge region and they are eventually deposited on the substrate as growing film. The DC sputtering is restricted to conducting materials like metals or doped semiconductors.

At low pressures, the cathode sheath is wide and ions are produced far from the target; their chances of being lost to the walls are great. The mean-free electron path between collisions is large, and electrons collected by the anode are not replenished by ion-impact-induced cathode secondary emission. Therefore, ionization efficiencies are low, and self-sustained discharges cannot be maintained below approximately 15 mbar [49]. As the pressure is increased at a fixed voltage, the electron mean-free path is decreased, more ions are generated and larger currents flow. But if the pressure is too high, the sputtered atoms undergo increased collisional scattering and are not efficiently deposited. In general, the deposition rate is proportional to the power consumed or to the square of the current density, and inversely dependent on the electrode spacing.

RF Sputtering

The radio frequency (RF) magnetron sputtering technique, schematically shown in Fig. 2.8, consists in a target, which is a plate of a stoichiometric mixture of the material to grow, and a substrate located on a grounded sample holder positioned perpendicular to the target.

The glow discharge is initiated by applying power to the target in a controlled gas atmosphere and is constituted by partially ionized gas of ions, electrons and neutral species. The ejected material diffuses until it reaches and nucleates on the substrate. The duration of this process controls the thin film thickness [52].

The development of the RF sputter deposition technique made it possible to deposit films from non-conducting sputtering targets which cannot be sputtered by the DC methods due to the charge accumulation on the target surface.

Most ions are almost immobile, compared to electrons which can follow the temporal variations in the applied potential typical RF frequencies used for sputtering (5–30 MHz). When the electrode is coupled to an RF generator, a negative voltage is developed on the electrode due to the difference in mobility between electrons and ions [52]. Since the insulating target electrode constitutes a capacitor in the electrical circuit, there should be no DC component, so that the current can flow. Therefore, the voltage on the electrode surface is required to be self-biased negatively to compensate the difference in mobility of electrons and ions, and to satisfy the condition of net zero current (averaged over each cycle).

The magnitude of the resulting negative bias is almost the same as the zero-to-peak voltage of the RF signal. The period in which the electrode acts as an anode is very short and the electrode mostly acts as a cathode during the RF cycle.

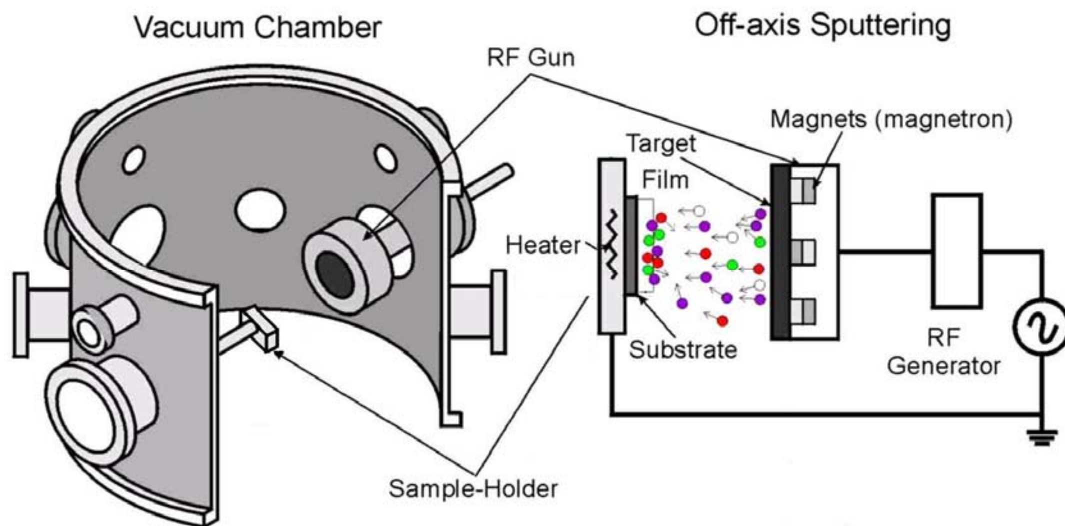

Fig. 2.8 – Schematic deposition chamber and off-axis RF magnetron sputtering technique [55].

Therefore, one can expect the target to be sputtered as in the DC case. A significant number of ions are not accumulated on the target surface, while the electrode acts as a cathode due to the high frequency employed in RF sputtering (normally 13.56 or 27,12MHz). The deposition can be performed at considerably lower pressures, such as 10^{-2} to 10^{-6} mbar in RF sputtering, when compared to the planar DC discharge, since the electrons oscillating at high frequencies can obtain sufficient energy to cause ionizing collisions, thus reducing the number of electrons lost (without making collisions) [56]. RF sputtering is widely used to deposit several types of conducting, semiconducting, as well as insulating coatings despite the complexity of the RF power source.

2.4. Boron nitride thin films

Boron nitride thin films have a significant technological potential in electronics, namely h-BN is applied as semiconductors as a protective coating, as a gate insulator in a metal-insulator-semiconductor field-effect transistor (MISFET), as a diffusion source, and as a thin film varistor or voltage limiter. Cubic boron nitride films can also be used as transparent substrates for X-ray lithography masks, and as protective coatings [40, 57].

In addition, the development of c-BN coating for cutting tools, combining the advantages of a c-BN coating and of the cutting material, becomes of great importance for many branches of metalworking industry, particularly in those cases where the reactivity of diamond makes this unsuitable.

The synthesis of c-BN thin films under low pressure and temperature was firstly reported by Sokolowski *et al.* [58] in 1979. Great efforts have been made to grow c-BN thin films from a gaseous phase. From early 90s, deposition methods at low pressure and temperature start appearing from different laboratories for the preparation of c-BN films. The processes adopted by these researchers include c-BN prepared by physical vapour deposition (PVD) and chemical vapour deposition (CVD). The most usual CVD methods are plasma-assisted chemical vapour deposition [59, 60], inductively coupled plasma (ICP) CVD, electron cyclotron resonance (ECR) plasma assisted CVD and microwave plasma enhanced CVD [61, 62]. PVD methods, such as ion-assisted e-beam evaporation [63, 64], ion-assisted pulsed laser deposition [65, 66], and DC and RF magnetron sputtering are used in the deposition of c-BN films [67, 68].

Matsumoto and Zhang [69] reported the production of c-BN by plasma-jet CVD and microwave plasma CVD using Ar-N_2-BF_3-H_2 gas. The obvious characteristic advantages of the plasma jet CVD are the involvement of fluorine ions and the high gas pressure of approximately 6.67 10^{-2} mbar [69], when compared to other PVD-like plasma-assisted CVD processes. The energy of ions hitting the surface of the film must be strongly reduced due to the scattering processes in the gas phase.

Processes like CVD plasma-assisted employ a high density plasma source and a low processing gas pressure under high vacuum conditions. The substrate is usually biased at several hundreds eV to extract the ions from the plasma. The plasma can be generated using a variety of source materials, e.g. plasma-assisted chemical vapour deposition (PACVD) methods use gaseous B-containing species such as diborane or borazine as plasma sources. In PVD-like processes the material is frequently provided by sputtering a B, BN or B_4C target, either by using radio frequency (RF) or direct current (DC). Direct current sputtering is only possible with conducting targets like B_4C, but it is usually accompanied by a higher growth rate than RF sputtering. The latter, though, does work with insulating targets like h-BN or pure B. This technique has been extended and modified in the past, e.g. applying a negative bias voltage to the sample has been shown to enhance the onset of c-BN nucleation [39]. In addition, the use of magnetic fields can increase the ion flux, thus allowing a higher deposition

rate, and both unbalanced magnetron sputter sources as well as conventional magnetron sources combined with external magnets or coils have been used to extend the plasma.

In ion-assisted processes, boron-containing species are provided by either electron beam evaporation (ion beam assisted deposition, IBAD), laser ablation (pulsed laser deposition, PLD) or ion beam sputtering (IBS) of a solid h-BN or B target. Boron atoms and/or BN molecules are then deposited with thermal energies onto the substrate. Simultaneously, the growing film is bombarded with nitrogen and noble gas ions with typical energies of several hundreds eV. The growth process is therefore rather complex and different effects such as condensation and thermal desorption, implantation of ions, recoil implantation of atoms deposited on the surface and re-sputtering have to be considered. Additionally, the interpretation of the obtained data within the existing c-BN growth models is difficult, because the substrate is not only irradiated with ions (which have well-defined energies) but also with neutral atoms, molecules and clusters. These problems do not exist for a specific type of PVD method, namely the Mass- Separated Ion Beam Deposition (MSIBD). In contrast to all other PVD techniques, thin films are prepared solely by deposition of alternating cycles of energetic B^+ and N^+ ions under ultra-high vacuum (UHV) conditions [70]. In this case, the deposition parameters, like ion energy, ion flux ratio of different ion species and the substrate temperature are well-defined and independently controllable. In contrast with IBAD, both nitrogen and boron are deposited as singly charged energetic ions and no noble gas or other ions, nor neutral atoms or molecules, are involved in an appropriate ion source. The ions are accelerated to a high energy in order to create an intense beam and to be magnetically mass separated. The amount of deposited ions can be accurately determined by measuring the ion charge. This relatively simple deposition process makes MSIBD the ideal tool to study the influence of the deposition parameters on the c-BN growth. However, its deposition rate is only in the order of several tenths nm/h, which makes an industrial application almost impossible.

Cubic boron nitride films synthesised by RF magnetron sputtering present a well-succeeded deposition. Several models were proposed to explain the growth process of such a metastable material. Reinke *et al*. [71] suggested a growth model which is based on the fact that sputter yield of c-BN was found to be lower than that of h-BN, and that c-BN deposition takes place just under the sputter region. However, this model cannot explain the growth of h-BN at high ion current densities reported by several workers [72]. RF bias sputtering has also been tried by Mieno and Yoshida [73] and Bewilogua *et al*. [74] in which a bias is applied to the substrate in order to enhance ion bombardment. In RF bias sputtering, interference dephasing between the RF power sources for target and substrate electrodes occurs. This may result in distraction of the energy distribution of charged particles and may modulate film deposition assisted by ions/or electrons [75]. Even though the ion-assisted methods worked well for the above groups, there are several researchers who reported the existence of a non cubic BN phase adjacent to the substrate followed by deposition of c-BN [76-77]. Thus, a better understanding of the deposition process is necessary for improving the

c-BN growth. Specifically, there are still significant problems regarding intrinsic stress and adhesion to the substrate for c-BN films deposited by different techniques. The most advantageous technology route is yet to emerge for the fruitful exploitation of this technologically import ant material.

A common feature to all PVD methods for c-BN thin film synthesis is the requirement of low energy ion bombardment of the growing film, which leads to the opinion that ion–solid interaction is directly or indirectly responsible for the formation of the cubic boron nitride phase. This is reflected in various growth models based on subplantation [78,79], stress induced c-BN phase formation [80,81], and thermal spike induced c-BN growth. Based on an extensive set of experimental data, which was for example compiled by Mirkarimi *et al.* [39] and recently Kulisch *et al.* [82], it was possible to establish experimental parameter regimes for c-BN growth.

Some parameters were identified to be decisive for the phase formed during PVD of boron nitride thin films [83]: *ion energy* – it is related with the power applied; *ion mass* – it is linked with the mixture of gas or pressure of gas during the deposition that can control the stoichiometry of films which are sputtered from a target; *substrate bias* – DC or R.F applied in the substrate which has the effect of accelerating electrons or ions towards the substrate or keeping them away; *target-substrate distance, deposition pressure* - pressure controls, how many collisions occur for the particles on their way from the target to the substrate and *substrate temperature* can have a strong impact on the growth behaviour with respect to crystallinity or density of the samples. These parameters are, however, not independent of each other. This parameter is suitable to predict the necessary deposition parameters to establish c-BN growth for a number of different growth techniques. However, the momentum transfer criterion may not be valid at low ion energies [39].

Chapter 3

Experimental methods and characterisation techniques

In this chapter, the experimental setup is presented. It has been divided into two parts. The first one refers to the production and characterisation of the silicon nitride substrates. The second part deals with the DC and RF magnetron sputtering deposition and physical characterisation techniques of the boron nitride thin films.

3.1. Silicon nitride substrates (Si_3N_4)

3.1.1. Production of silicon nitride substrates

The starting powders used to prepare the substrates of silicon nitride were: α-Si_3N_4 (H.C. Starck grade M11), with a β-Si_3N_4 content lower than 4 wt.(%); Y_2O_3 (H.C. Starck grade C), with a minimum purity of 99.95% and Al_2O_3 (ALCOA CT 3000 SG), with a purity of 99.6%. Y_2O_3 and Al_2O_3 act as sintering additives in this system. Table 3.1 gives some of the properties of these raw materials and their relative proportion used in the powder mixture.

Table 3.1 – Composition and characteristics of the raw materials used to the produce Si_3N_4 substrates.

Material	Composition wt (%)	Particle size (μm)	specific surface area ($m^2.g^{-1}$)	Density ($g.cm^{-3}$)
α-Si_3N_4	89.30	0.6	12 - 15	3.19
Y_2O_3	7.00	0.9	10 - 16	5.03
Al_2O_3	3.70	0.7	6.5 - 8.5	3.99
Mixture (α-Si_3N_4+Y_2O_3+Al_2O_3)	100	0.6	13-15	3.33

The powders were mixed in a planetary mill with isopropylic alcohol, as dispersion agent, for 8 h at 150 rpm, using an agate jar container with silicon nitride balls as milling media. Weighting of the milling media and the container before and after milling showed no contamination by the ball nor by the container to be negligible.

The powders mixture was dried in an oven in order to eliminate all the solvent. After that, the powder was sieved through a 100 μm mesh sieve, and thereafter, the powder was uniaxially pressed into discs with ϕ=15 mm, at 40 MPa during 1min. Then, the samples were isostatically compacted under a pressure of 200 MPa during 5 min.

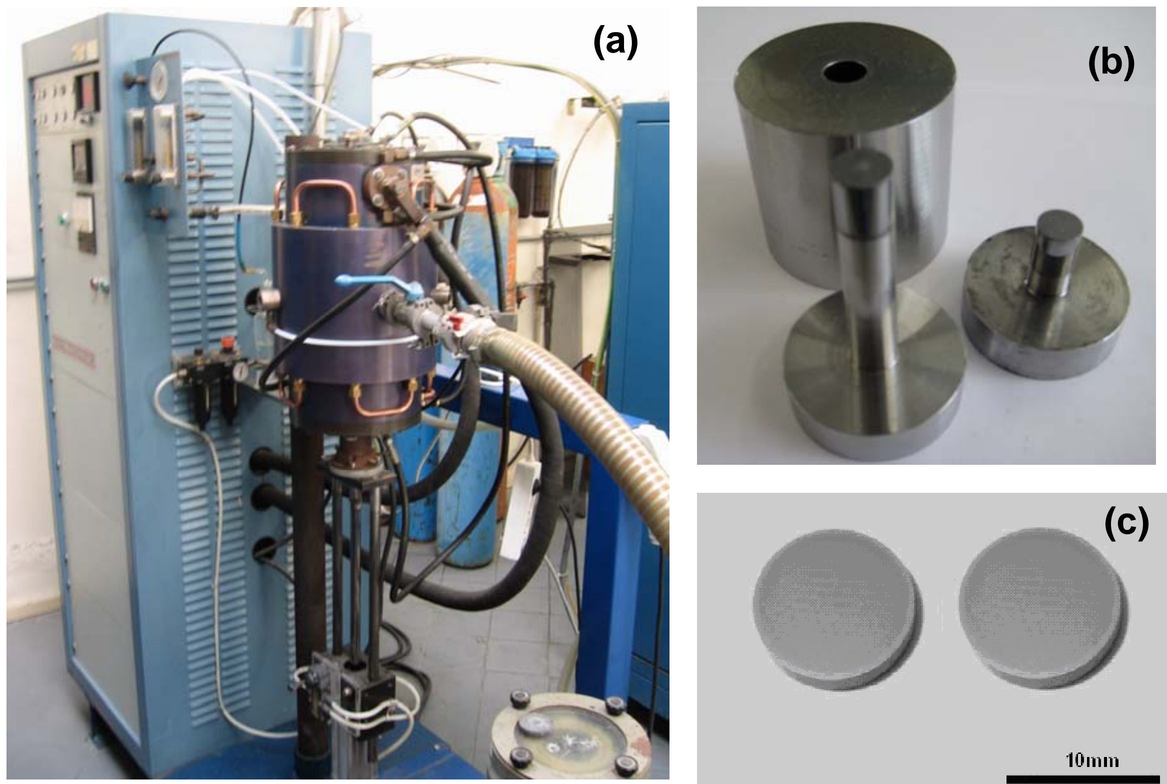

Fig. 3.1 – (a) graphite resistance heated furnace used to sinter the substrates, (b) uniaxial pressing mould, and (c) view of Si_3N_4 substrates after sintering.

Pressureless sintering was performed in a graphite resistance heated furnace (Thermal Technology INC, Fig. 3.1a) with the samples placed into a graphite crucible involved by a powder bed (70 wt% powder mixture and 30wt.% BN), to avoid the mass losses during the sintering process.

The heating rate used was 10ºC.min^{-1}, until 1750ºC, in a nitrogen atmosphere of 1.8 MPa. The sintering dwell time was 2 h long. After sintering, the samples were cooled inside the furnace at a rate of 10 ºC·min^{-1}. The entire sintering cycle can be seen in Fig. 3.2. The procedures used for the preparation of the Si_3N_4 ceramic substrates are outlined in the flow diagram of Fig. 3.3.

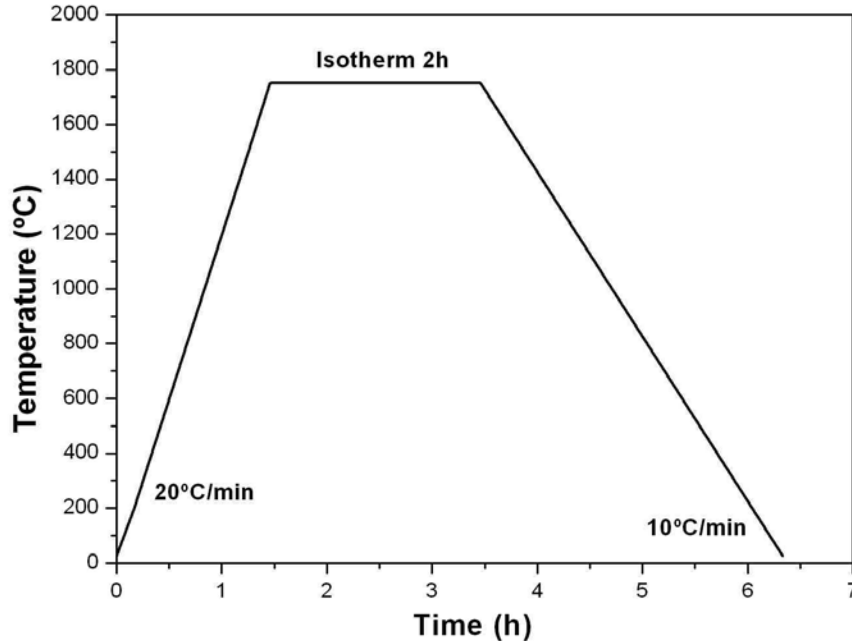

Fig. 3.2 – Schematic diagram of the sintering cycle of silicon nitride (Si_3N_4) substrates.

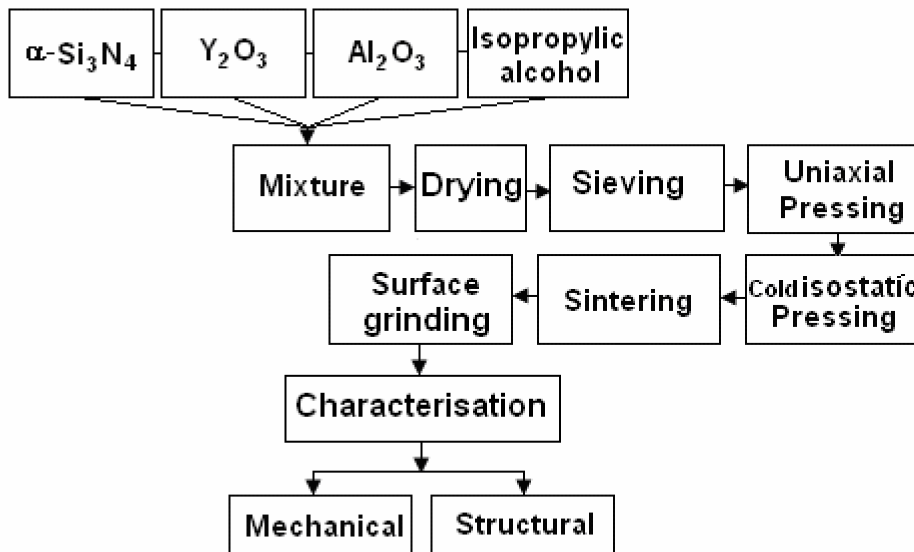

Fig. 3.3 - Flow chart for the preparation of Si_3N_4 substrates.

3.1.2. Characterisation of silicon nitride substrates

The surfaces of the Si_3N_4 samples were ground and polished with 15 μm diamond suspension (DIAMIT industrial Diamond). The ceramic samples were ultrasonically cleaned in acetone and dried at 100ºC to measure density by the immersion method. After that, the samples were polished with diamond suspension in sequence: 6 μm, 1 μm and 1/4 μm (DIAMIT industrial Diamond). After the polishing, it was necessary to etch the Si_3N_4 specimens in order to reveal the grain boundaries and other microstructural details during the scanning electron microscopy (SEM) observation. It was used two different etching

procedures. In a first one, a solution containing concentrated phosphoric acid (H_3PO_4 85%) was used at 250ºC for 5 min. Alternatively, CF_4 plasma etching (EMITECH K1050x) was carried out at 100 W for 2 min. Here, a radio frequency generator emits high-frequency electromagnetic oscillations, thus producing highly active fluorine radicals inside the reaction chamber.

The polished surfaces chemically etched with H_3PO_4 85%, as well as the fractured surfaces of Si_3N_4 specimens, were examined by SEM (LEO 1550 with Gemini Column), and equipped with an energy-dispersive spectrometer (EDS, RONTEC). In order to obtain the best contrast between different phases, the micrographs were recorded in back-scattering electron mode (BSE) for polished surfaces. In addition, the polished surfaces etched with CF_4 plasma were observed in a different SEM apparatus (Hitach 4100S).

The crystalline phases in the sintered bodies and in the initial powder mixture were analysed by X-ray Diffraction analysis (XRD, Rigaku, radiation Cu.Kα). The α–Si_3N_4 and β–Si_3N_4 phase contents in the sintered samples were determined from the XRD intensities of (201) and (210) reflections of α-Si_3N_4 and (101) and (210) reflections of β-Si_3N_4. This relationship was proposed by Suzuki and Kanno [96], and it can be calculated from the following equations (3.1) and (3.2),

$$\alpha(\%) = \frac{\{I_\alpha(210) + I_\alpha(201)\}}{\{I_\alpha(210) + I_\alpha(201) + I_\beta(101) + I_\beta(210)\}} x100 \tag{3.1}$$

$$\beta(\%) = 100 - \alpha(\%) \tag{3.2}$$

where $I_{\alpha(h\ k\ l)}$ and $I_{\beta(h\ k\ l)}$ are the peak intensities of *(hkl)* reflections of α-Si_3N_4 and β-Si_3N_4, respectively.

Attenuated Total Reflectance Fourier Transform Infrared Spectroscopy (FTIR-ATR) is a technique used for analysis of the surface of materials. It is also suitable for characterisation of materials which are either too thick or too strong absorbing to be analysed by transmission spectroscopy. For the bulk material or thick film, no sample preparation is required for ATR analysis. In ATR-IR spectroscopy, the infrared radiation is passed through an infrared transmitting crystal with a high refractive index, allowing the radiation to reflect within the ATR element several times. The phase identification of the sintered samples was carried out in a Mattson 7000 spectrophotometer spectroscopy, equipped with deuterium triglycine sulphate detector, at a resolution of 2 cm^{-1}, in the range of 400-4000 cm^{-1}.

Hardness and fracture toughness of the Si_3N_4 specimens were measured using a Vickers diamond pyramid indenter (G Officine Galileo, MicroScan OM) by applying a load of 9.8 N and a loading time of 10 s; the hardness was evaluated from 10 indentations. Fig. 3.4a shows an indentation impression on the Si_3N_4 substrate. The Vickers hardness was calculated using equation (3.3) and also with support of picture like those of Fig. 3.4.

$$H_V = 0.1891 \frac{F}{(2a)^2} .(10^{-9}).[GPa] \tag{3.3}$$

Where: HV is the Vickers hardness in N/m^2, F is the applied load in N and 2a^2 is the average value of the projected indentation diagonals in m.

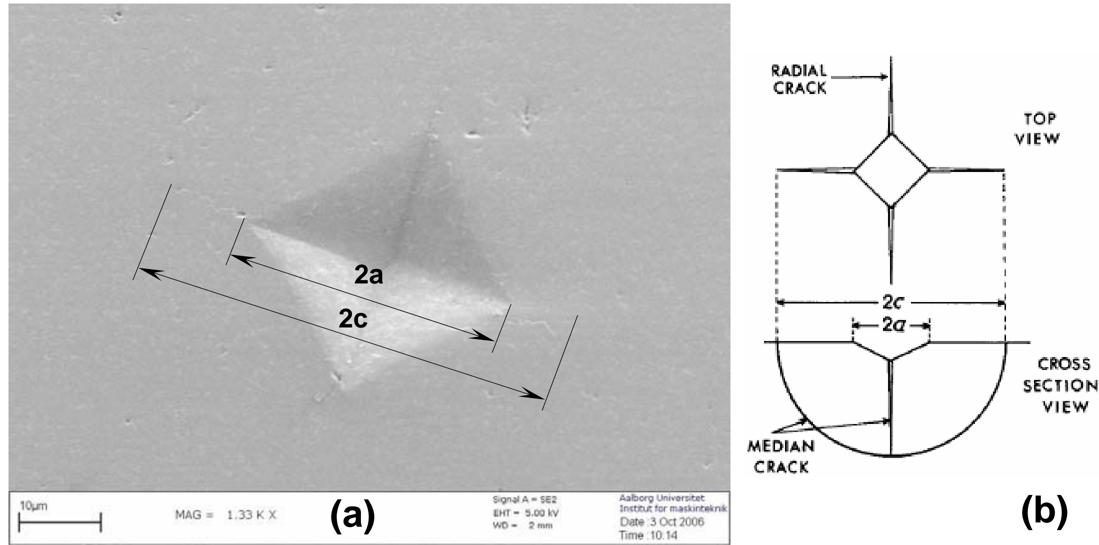

Fig. 3.4 - (a) SEM of a Vickers indentation defining indent and median crack parameters "a" and "c", respectively; (b) view of the cracks around a Vickers indentation.

The fracture toughness of the sintered samples was calculated by the Anstis *et al.* [85] equation (3.5). The indentation cracks measured in specimens were observed by SEM (LEO 1550 with Gemini column). These measurements were used to calculate the fracture toughness of the substrate according to the equation below (3.4).

$$K_{IC} = 0.0156 \left(\frac{E}{H_V} \right)^{1/2} . \left(\frac{P}{c^{3/2}} \right) \tag{3.4}$$

Where: *KIc* (MPa.m$^{1/2}$) is the fracture toughness, *E* (GPa) is the Young's modulus, *Hv* (GPa) is the hardness, *P* (N) is the peak applied load, c (m) is the length of the radial cracks minus the half diagonal size (Fig. 3.4b).

3.2. BN thin films

3.2.1. Production and characterisation of the targets

The targets of h-BN and B_4C were processed by Hot Pressing (HP) sintering from raw powders (h-BN and B_4C from H.C. Stark, Germany) without sintering additives. The HP process was carried out in an industrial apparatus (Termolab) located at Durit -Empresa Portuguesa do Tungsténio S.A. The powders were hot pressed at 1750°C for 2 hours under a

30 MPa of uniaxial compressive stress in N_2 atmosphere. The load was applied when the temperature was approximately 1100ºC and it was held during the whole dwell time. The pressure applied to the targets was only removed when the temperature achieved 1600ºC during the cooling stage. The hot pressing cycle can be seen in the schematic diagram of Fig. 3.5a while the Fig. 3.5b shows the hot pressed targets. Sintered discs were obtained with a ϕ= 50 and ϕ= 76 mm and a thickness of 3 mm for h-BN and B_4C, respectively.

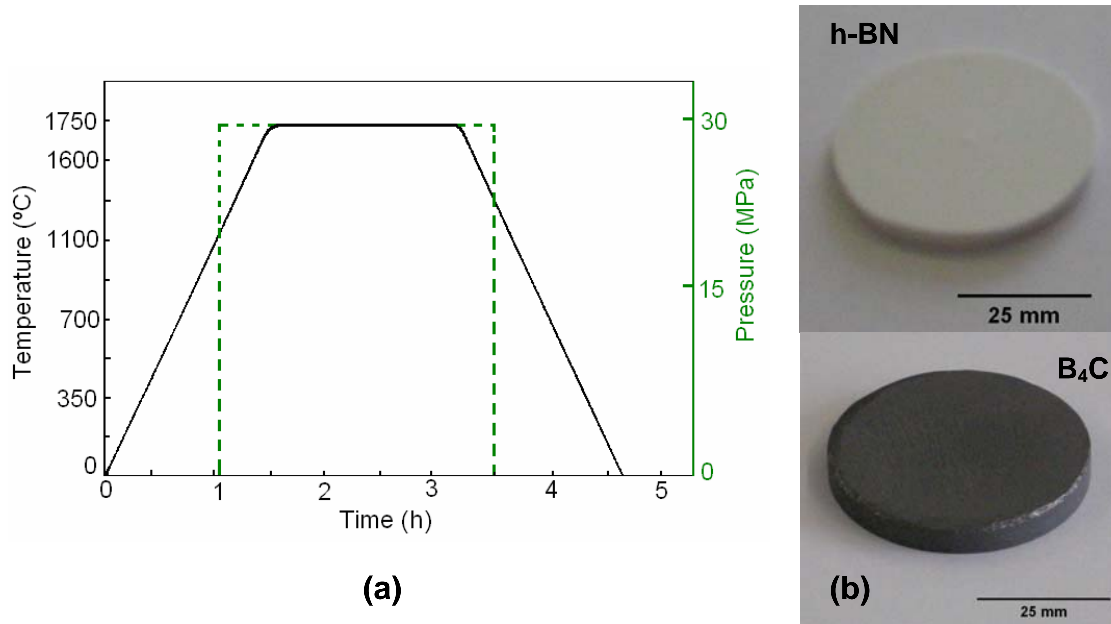

Fig. 3.5 – (a) Schematic diagram of HP cycle of the BN targets and (b) HP targets produced.

X-ray diffraction analysis (XRD, Rigaku, radiation Cu.Kα) and Fourier Transform Infrared FT-IR (Mattson 7000 spectrophotometer) spectroscopy were performed in the targets in order to verify the quality of the target preparation, the crystalline structure and the phase composition of the targets.

3.2.2. Coating deposition

3.2.2.1. DC magnetron sputtering

The experiments for DC magnetron sputtering BN deposition were performed on a CRIOLAB PC 30.1 apparatus (Fig. 3.6) at the Physics Department of Aveiro University. The vacuum chamber has cylinder geometry with a 50 cm of diameter, resulting in volume of 65 L. The base pressure of $5x10^{-6}$ mbar is achieved by using rotary (VARIAN) and a turbomolecular pump (Alcatel ATP 400). Boron carbide (B_4C) was used as an electrically conducting target with a ϕ= 76 mm and thickness of 3 mm. The sputter device worked in a planar magnetron arrangement.

Fig. 3.6 – Different views of the experimental set-up for the D.C. magnetron sputtering deposition from Physical Department at Aveiro University.

Silicon nitride samples with different surface finishing (15 and 6 μm) were fixed onto a sample holder which was located in front of the target. Prior to its introduction into the deposition system, the Si_3N_4 substrates were cleaned with acetone, ethanol and deionised water in this sequence. The distance between the substrate and the target surface was kept at 90 mm for all depositions. Ar and N_2 were used as sputter gases controlled by a mass flow system.

Before deposition, the deposition chamber was initially pumped down to less than $5x10^{-6}$ mbar. Then, a purified Ar gas was introduced. Afterwards, the target was sequentially pre-sputtered (sputtered-cleaned) in an argon discharge for 30 minutes.

The controlled parameters for BN deposition by D.C sputtering using B_4C as target material are given in Table 3.2. The sample BN-4 was negatively biased with an RF power supply (Huttinger PFG 300RF).

Table 3.2 – Deposition parameters for D.C sputtering using B_4C target. (**Ssf** - substrate surface finishing, **DC** - power applied to the target, **Bias** - bias applied to the substrate; **Ar/N_2** - gas composition, **P_t** - total pressure during deposition, , **D**-distance target-substrate, **t**-deposition time).

Sample	*Ssf (μm)*	*DC (W)*	*Bias (V)*	*Ar/N_2 (%)*	*P_t (mbar)*	*D (mm)*	*t (min)*
BN – 1	15 μm	120 W	-	50/50	$6x10^{-3}$	90	60
BN – 2	15 μm	120 W	-	20/80	$6x10^{-3}$	90	60
BN – 3	15 μm	120 W	-	80/20	$6x10^{-3}$	90	60
BN – 4	15 μm	120 W	- 100 V	50/50	$6x10^{-3}$	90	60
BN – 5	15 μm	120 W	-	50/50	$6x10^{-3}$	90	120

3.2.2.2. RF magnetron sputtering

The R.F magnetron sputtering depositions were performed in two different apparatus. Basically, both equipment machine are equivalent, they present the same magnetron model of 50 mm diameter and the same RF power generator (13.56 MHz). The main differences between them are the shape of the deposition chamber, the possibility to apply a bias and also the option to heat up the substrates. The most complex equipment is the RF magnetron sputtering from Physics Department of Aveiro University (Fig. 3.7), which is here described. The RF magnetron sputtering 13.56MHz (home made with CRIOLAB collaboration) is shown in Fig. 3.7 (a-e). The deposition system consists of a planar two-inch magnetron (Ion X2 9020.2) powered by a Huttinger PFG 300RF generator through an impedance box unit. The chamber (CARBURN MDC MFC INC. USA) has a spherical shape and is certificated to support until 10^{-11} mbar of pressure.

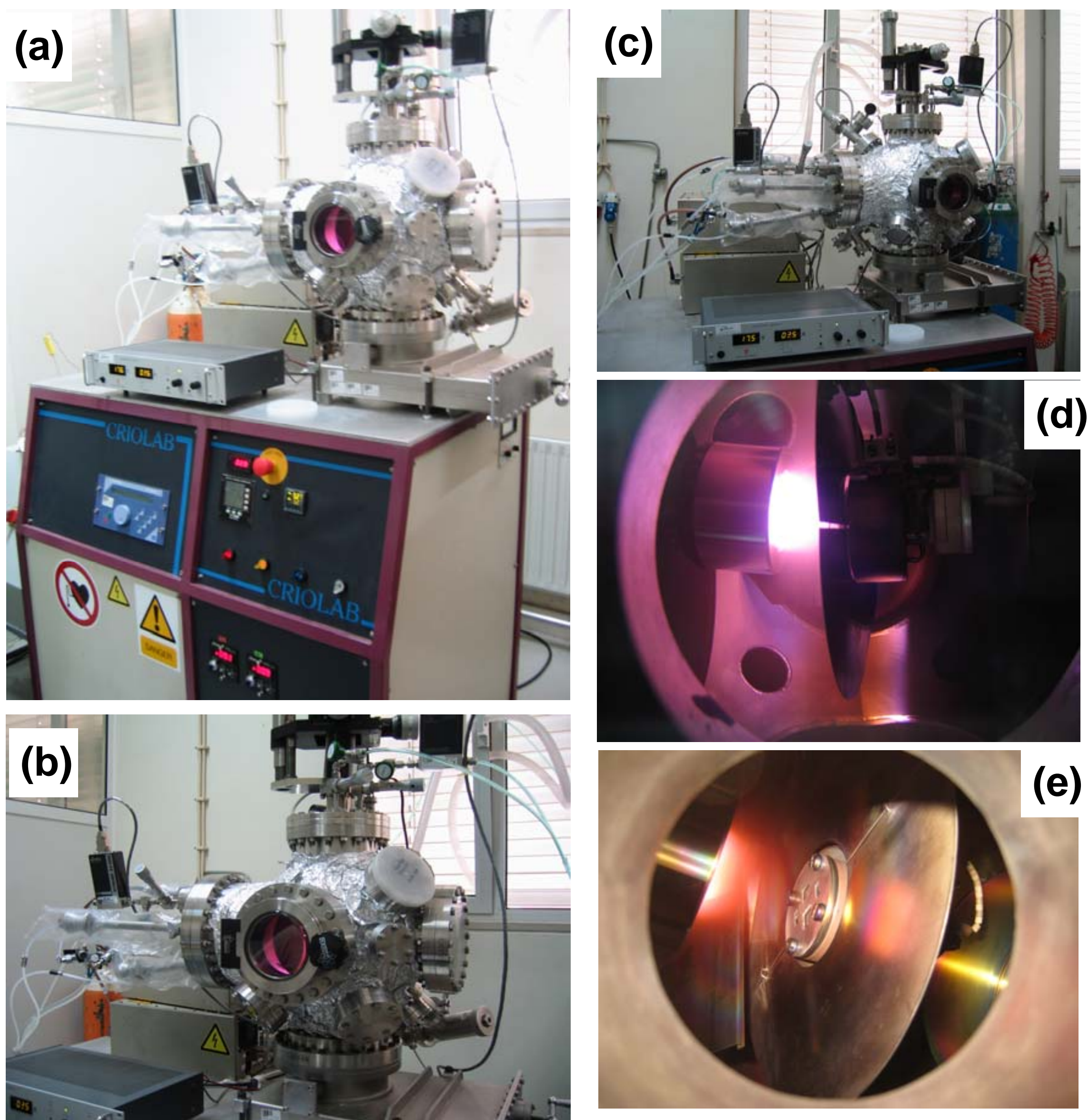

Fig. 3.7 – Different views of RF magnetron sputtering equipment from Physics Department of Aveiro University.

The experimental set-up for the RF magnetron sputtering deposition is shown schematically in Fig. 3.8. A pressed h-BN disc with a diameter 50 mm and 3 mm thickness was used as target. The target was mechanically clamped to the magnetron and water cooled.

In these depositions, Si_3N_4 samples with different surface finishing (polished with 6 and 15μm diamond suspension) and Si(100) wafers (Silicon Quest Int'l.) were used as substrates. The surface roughness of the Si_3N_4 samples used as substrates was measured before deposition with a perfilometer (Perthometer M1-Marh device) leading to Ra= 0.082 μm and Ra=0.012 μm for the finishing sample preparations of 15 μm and 6μm Si_3N_4, respectively.

The specimens were afterwards cleaned in an ultrasonic bath with two different organic solvents (alcohol and acetone) and deionised water. The substrates were fixed onto a holder which was resistively heated (SM 2020D Delta Elektronica) and held at floating potential.

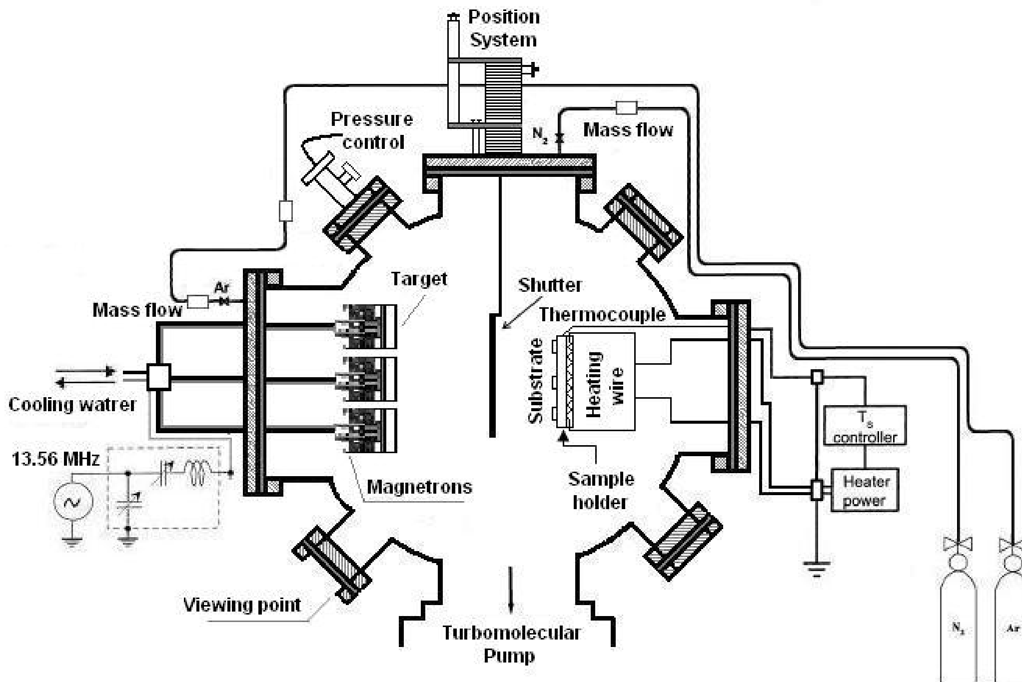

Fig. 3.8 - Schematic diagram of the BN thin film deposition system.

During deposition, the substrate temperature was measured by a thermocouple and controlled by a Eurotherm 2216e controller. The substrate holder was mounted oppositely to the target, in a horizontal configuration, and the distance between the substrate and target surface was always kept constant at 50 mm.

Before deposition, the chamber was pumped down to less than $2x10^{-7}$ mbar, using a vacuum system consisting of a rotary pump (VARIAN DS 302) plus a turbomolecular pump (LEYBOLD VACUUM).

After that, the target was pre-sputtered (cleaning step) in an Ar^+ discharge at 41 W RF power for 30 minutes, approximately. Then, a mixture composed by Ar and N_2 was

introduced into the chamber to be used as discharge working gas. The composition of the working gas mixture was controlled by two independent mass flow controllers (MKS Type 246). The total deposition pressure was approximately $5x10^{-3}$ mbar, and the deposition time was kept constant at 210 min. The BN films were deposited at fixed values of RF input power applied to the target of 41 W.

The most important parameters for the deposition of BN by RF sputtering using a h-BN target are given in Table 3.3.

Table 3.3 – Deposition parameters for BN thin film deposition by RF sputtering using h-BN as target: (**Sb** – Kind of substrate, **Ssf** – substrate surface finishing, **RF** -power applied to the target, P_t - total pressure during deposition, **Ar/N$_2$** – working gas composition, **D** - distance target-substrate, **t** - deposition time, **T** - substrate temperature).

Sample	*Sb*	*Ssf* (*μm*)	*RF power* (*W*)	P_t (*mbar*)	*Ar/N$_2$* Vol *(%)*	D (mm)	t (min)	T_s (ºC)
BN-6a	Si_3N_4	6μm	41	$5x10^{-3}$	90/10	50	210	500
BN-6b	Si_3N_4	15μm	41	$5x10^{-3}$	90/10	50	210	500
BN-6c	Si(100)	mirror	41	$5x10^{-3}$	90/10	50	210	500
BN-7a	Si_3N_4	6μm	41	$5x10^{-3}$	90/10	50	210	400
BN-7b	Si_3N_4	15μm	41	$5x10^{-3}$	90/10	50	210	400
BN-7c	Si(100)	mirror	41	$5x10^{-3}$	90/10	50	210	400
BN-8a	Si_3N_4	6μm	41	$5x10^{-3}$	90/10	50	210	300
BN-8b	Si_3N_4	15μm	41	$5x10^{-3}$	90/10	50	210	300
BN-8c	Si(100)	mirror	41	$5x10^{-3}$	90/10	50	210	300
BN-9a	Si_3N_4	6μm	41	$5x10^{-3}$	90/10	50	210	150
BN-9b	Si_3N_4	15μm	41	$5x10^{-3}$	90/10	50	210	150
BN-9c	Si(100)	mirror	41	$5x10^{-3}$	90/10	50	210	150
BN-10a	Si_3N_4	6μm	41	$5x10^{-3}$	90/10	50	210	RT
BN-10b	Si_3N_4	15μm	41	$5x10^{-3}$	90/10	50	210	RT
BN-10c	Si(100)	mirror	41	$5x10^{-3}$	90/10	50	210	RT
BN-11a	Si_3N_4	6μm	41	$5x10^{-3}$	100/0	50	210	400
BN-11b	Si_3N_4	15μm	41	$5x10^{-3}$	100/0	50	210	400
BN-11c	Si(100)	mirror	41	$5x10^{-3}$	100/0	50	210	400
BN-12a	Si_3N_4	6μm	41	$5x10^{-3}$	70/30	50	210	400
BN-12b	Si_3N_4	15μm	41	$5x10^{-3}$	70/30	50	210	400
BN-12c	Si(100)	mirror	41	$5x10^{-3}$	70/30	50	210	400
BN-13a	Si_3N_4	6μm	41	$5x10^{-3}$	50/50	50	210	400
BN-13b	Si_3N_4	15μm	41	$5x10^{-3}$	50/50	50	210	400
BN-13c	Si(100)	mirror	41	$5x10^{-3}$	50/50	50	210	400

3.2.3. Coating characterisation methods

The characterisation of BN films is non-trivial and requires the use of several complementary techniques. This is mainly related to the fact that c-BN thin films are usually nanocrystalline, highly-defective and embedded between two sp^2-bonded layers [39].

The BN films were also characterised by Fourier transformed infrared spectroscopy (FT-IR) in the absorption mode (Mattson 7000 spectrophotometer, using ATR) in order to identify the composition of the BN phases. It is the most common way to characterise the presence of BN phases. It offers the advantage of being very fast and non-destructive, and it can be done both in reflection and transmission geometries. For h-BN, the two IR-active phonons have TO frequencies around 780 cm^{-1} and 1380 cm^{-1}. These correspond to out-of-plane bending of the B-N-B bond between the basal planes and B-N in-plane stretching vibrational modes of the hexagonal lattice, respectively. The absorption band at 1030 cm^{-1} is due to the transverse optical (TO) mode of c-BN [86].

Crystal structure and the crystallinity were determined by X-ray Diffraction (XRD, Rigaku) using the glancing incidence angle (2º) configuration. The incident X-ray angle was set at 5° and the diffraction pattern was taken by continuous mode with a step width of 0.05°.

The thickness and surface morphology of the films were mainly characterised in cross-section by Scanning Electron Microscopy (SEM - Hitach 4100S).

Due to the low thickness of the BN films, nanohardness measurements have been performed in the samples. It was used an equipment from Fisher Instruments (Fischerscope H100) to measure the hardness. It was used a nominal load of 1mN. Previously, it were applied different loads and they did not present any nanoindentation size effect, in the range of 1mN to 10mN. Measurement of the indentation depth was achieved with a capacitance displacement gauge of 2-nm accuracy. Measurement of the film hardness requires consideration of only the most shallow indentation depths, ideally those indents less than 10% of the film thickness. The hardness values are an average of 20 indentations.

Chapter 4

Results and Discussion

The main results of this project are presented and discussed in this section. This chapter is divided in two parts. In the first part, the results of the silicon nitride characterisation are presented, namely the microstructural and mechanical features. The second part deals with the results of the BN thin films coatings on silicon nitride ceramic substrates and silicon wafers.

4.1. Silicon nitride substrates (Si_3N_4)

Table 4.1 shows the results of quantitative phase composition, density and weight loss of the Si_3N_4 sintered samples. The specimens were almost completely densified and very small weight losses occurred during sintering.

Table 4.1 – Physical properties of silicon nitride used as substrates.

System Substrate	***Phases by XRD***	***Density ($g.cm^{-3}$) SD***	***Relative density (%) SD***	***Weight loss (%) SD***
Si_3N_4 - Y_2O_3 - Al_2O_3	β-Si_3N_4, α-Si_3N_4, Y_2SiAlO_5N	3.19 ± 0.11	99.6 ± 0.2	-0.11 ± 0.09

Fig. 4.1a and 4.1b show the surface of the samples without etching. These micrographs allow observing the Si_3N_4 matrix with the intact intergranular phase, as the later is completely attacked or dissolved by the subsequent etching procedure. The EDS analysis of the intergranular glassy phase (bright area) confirmed the presence of Si and Y.

According to Honma *et al.* [21], it was possible to detect that there is a relationship between the behaviour of the sintering additives and the formation of microstructure during sintering. Three phenomena take place sequentially: (1) Reactions between sintering additives and SiO_2, which exists on the surface of the Si_3N_4 powder, and among the sintering aids system. The densification proceeds non-uniformly. (2) Formation of a homogeneous glassy phase at grain boundaries and transformation of α-Si_3N_4 to β-Si_3N_4. The densification

proceeds rapidly. (3) Transformation of α-Si_3N_4 to β-Si_3N_4, formation and growth of prismatic grains and final densification occurring at the same time. Yttrium exists dissolved at grain boundaries and some part of Al dissolves into β-Si_3N_4.

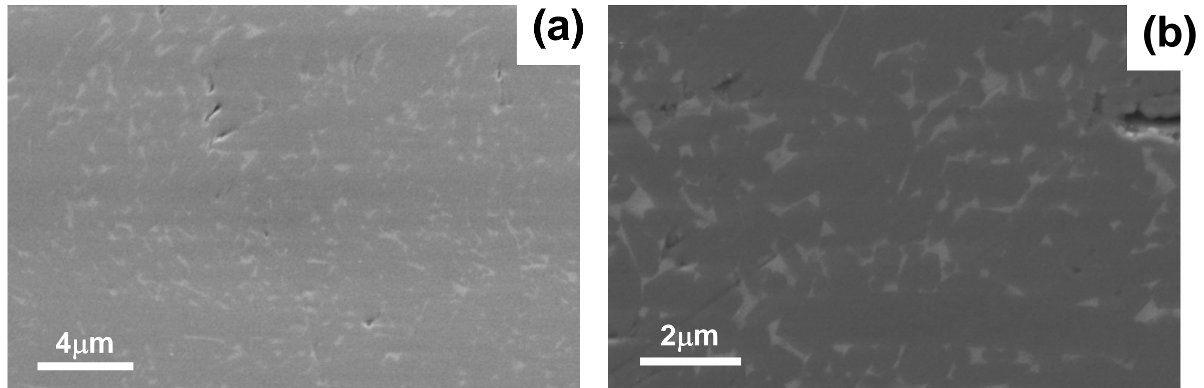

Fig. 4.1 - (a-b) Scanning Electron micrographs of the sintered Si_3N_4 ceramics without surface etching.

Fig. 4.2 shows the microstructure of the Si_3N_4 ceramics etched by a solution containing concentrated acid H_3PO_4 (Fig. 4.2a) and etched by CF_4 plasma (Fig. 4.2b). It can be observed the typical microstructure of a sintered Si_3N_4 ceramic, revealing hexagonal elongated β-Si_3N_4 grains.

It is possible to observe from Fig 4.2a that the intergranular phase between the Si_3N_4 grains (second phase) was dissolved by H_3PO_4 chemical attack. In contrast, in Fig. 4.2b, where the etching was performed by CF_4 plasma, the microstructure reveals a preserved intergranular phase.

The elongated grain morphology is a consequence of the phase transformation of α →β-Si_3N_4 during the solution-precipitation process of liquid phase sintering. As the sintering time increases, grain growth occurs by coalescence processes due to the different chemical potentials between smaller and larger Si_3N_4 grains. According to Smith *et al.* and Takata *et al.* [87, 88] the densification is enhanced by decreasing the viscosity and liquefaction temperature of the glassy phase.

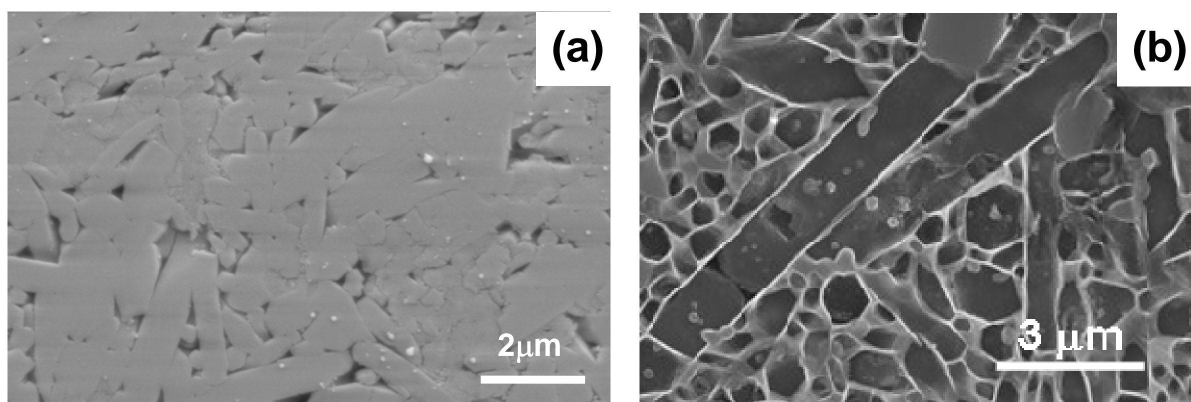

Fig. 4.2 – SEM micrograph of Si_3N_4 after etching in (a) H_3PO_4 and (b) etched by CF_4 plasma.

The typical fracture surfaces of Si_3N_4 ceramic are shown in the Fig. 4.3. It is possible to observe the elongated grain of Si_3N_4 being surrounded by small rounded grains of Si_3N_4 and also the type of fracture mechanism that is a mixture of transgranular and intergranular.

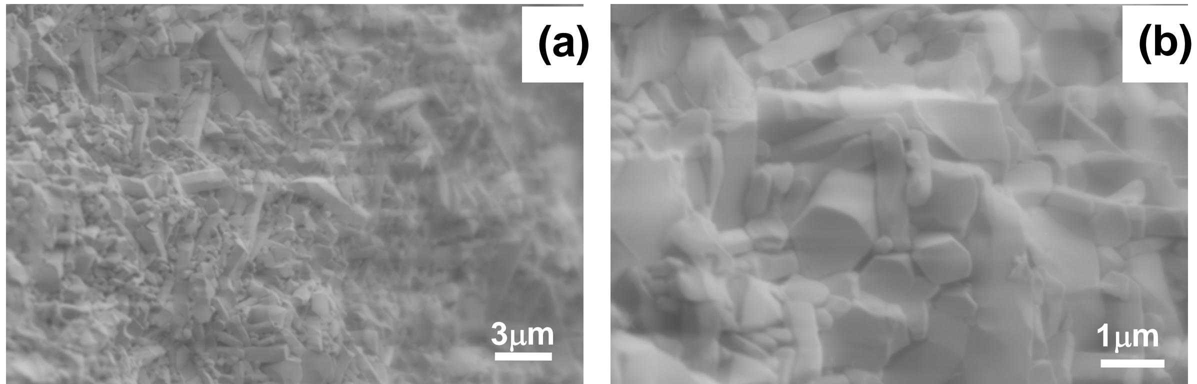

Fig. 4.3 – (a-b) SEM micrograph of the fracture surface of the Si_3N_4 ceramic after etching in H_3PO_4.

The X-ray diffraction (XRD) pattern of the raw powders (Fig. 4.4) indicates that the powder mixture is composed by Al_2O_3, Y_2O_3 and α-Si_3N_4. It is evident a very small amount of β-Si_3N_4. Contrarily, the X-ray diffraction pattern of the sintered bond of Si_3N_4 from Fig. 4.4 shows the prevalence of β–Si_3N_4, with only a small trace of α–Si_3N_4, which implies that an almost a complete α–β transformation occurred during the sintering process. These results can be confirmed by applying the equations (3.1) and (3.2), being presented in the Table 4.2. A second phase was identified as Y_2SiALO_5N, which was apparently formed by the reaction of the oxides additives with Si_3N_4. However, only a few traces are evident, denoting the glassy nature of the intergranular phase.

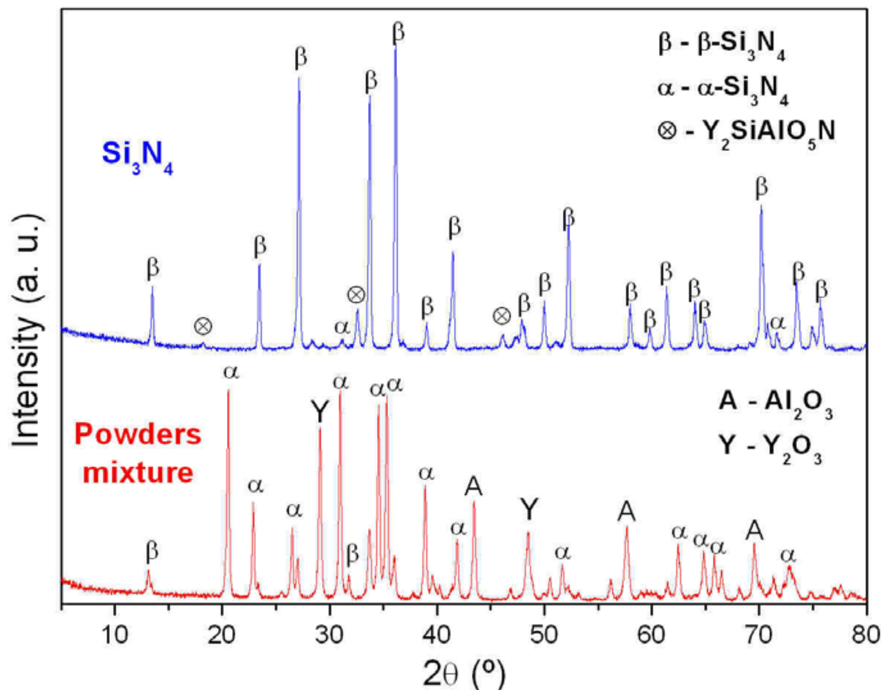

Fig. 4.4 - X-ray Diffraction pattern of the powders mixture and the sintered Si_3N_4 using CuKα radiation.

The qualitative chemical information of the bonds present in the Si_3N_4 substrates were obtained by using Fourier transforms infrared (FT-IR) spectroscopy measurements. Fig. 4.5 shows the infrared absorption spectra taken in the 400–3100 cm^{-1} range of the Si_3N_4 substrate.

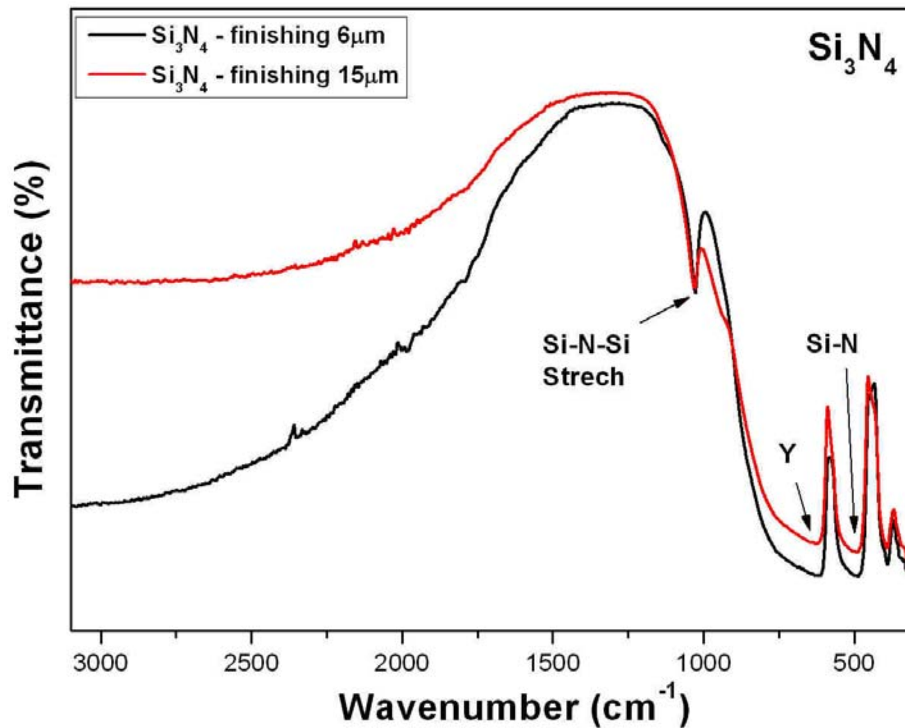

Fig. 4.5 - The FTIR absorption spectra for Si_3N_4 substrates.

The vibrational frequencies, in Fig. 4.5, that are associated with Si–N-Si and Si–N bonding groups have received a significant amount of attention [89]. The absorption bands located at 490 cm^{-1} and 604 cm^{-1} are associated with Si-N and yttrium oxide, respectively.

The absorption band assigned at 1031 cm^{-1} is associated with the Si–N–Si stretching mode. This Si–N-Si bond gives rise to very strong band below 1031 cm^{-1} and, because of the increasing absorption by multiple reflections, is completely absorbed in this region of the spectrum. A very weak absorption band also appears at 1786 cm^{-1}, that can be attributed to the N-H bending mode. Alumina, which has a broad band at 798 cm^{-1} (not present) and presents 3.3 wt% of the mixture, cannot be seen and has no substantial effect to the spectra of substrate.

Fig. 4.6a gives an example of an indentation-fractured specimen of Si_3N_4 ceramic substrate.

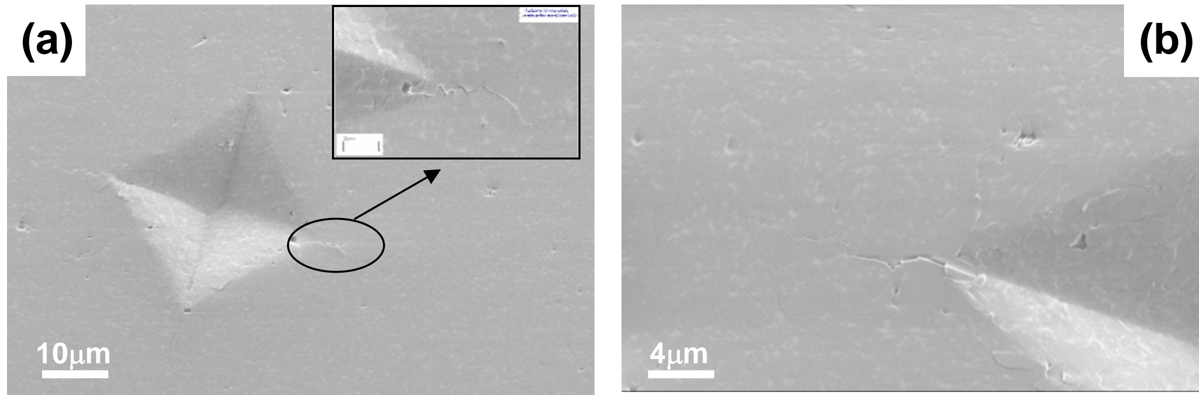

Fig. 4.6 - Scanning electron micrograph of Si_3N_4 indentation; (a) SEM of indentation, imprint (b) SEM of an indentation crack.

The measured values of hardness, fracture toughness and density of the Si_3N_4 substrates are given in Table 4.2. The Young's modulus used to calculate the fracture toughness was measured by Belmonte *et al.* [90] on similar specimens.

Table 4.2 – Phase content and mechanical properties of silicon nitride substrates.

Substrate	α and β Phase content		Hardness Hv (GPa)	Fracture Toughness K_{IC} (MPa.m$^{1/2}$)	Young's modulus E (GPa)
	α (%)	β (%)			
Si_3N_4	2.35	97.65	15.5 ± 0.5	5.8 ± 0.2	300

The Si_3N_4 hardness of depends on the phase composition. A composition with a high value of α– Si_3N_4, which is not transformed during the sintering stage, has a high hardness like solid solution α– Si_3N_4 (Up to 20 GPa). Usually, the value for β– Si_3N_4 is approximately 16 GPa [91].

According to Wachtmann [92] the fracture toughness varies for the Si_3N_4 ceramics in a wide range, from 3 to 12 MPa.m$^{1/2}$. This is, in one hand, connected with variations in the microstructure and, in the other hand, by different methods of determination giving slightly different values. Two main microstructural factors influence the fracture toughness: grain shape and size, and the composition of the intergranular phase. The present value of about 6 MPa.m$^{1/2}$ is the result of the medium aspect ratio β-Si_3N_4 grains and relatively weak intergranular glassy phase.

In summary, the good mechanical properties of Si_3N_4 are attributed to the α → β phase transformation during the sintering process. This transformation changes the equiaxial α into an idiomorphic β rod-like grain, which is directly responsible for the high fracture toughness behaviour observed in this kind of material.

4.2. Boron nitride thin films

4.2.1. Targets characterisation

As mention before, two different targets were produced, one electrically conductor (B_4C) and one electrically insulator (h-BN) for the DC and RF magnetron sputtering techniques, respectively.

The densities measured after sintering by hot-pressing for B_4C and h-BN were 2.11 and 1.86 g/cm^3, respectively. These densities represent 84 and 85% of the theoretical densities of B_4C and h-BN (2.51g/cm^3 and 2.20 g/cm^3).

Fig. 4.7 and Fig. 4.8 show the X-ray diffraction patterns of the h-BN and B_4C targets. The former phases for h-BN, shown in Fig. 4.7, presents an intense peak at 2θ=26.78º corresponding to the (200) crystal plane and several smaller peaks at 41.60º (100), 43.86º (101), 50.17º (102), 55.18º (004), 59.57º (103), 71.41º (104) and at 75.91º (2-10). All these peaks are corresponding to the hexagonal phase of boron nitride (h-BN) [93, 94].

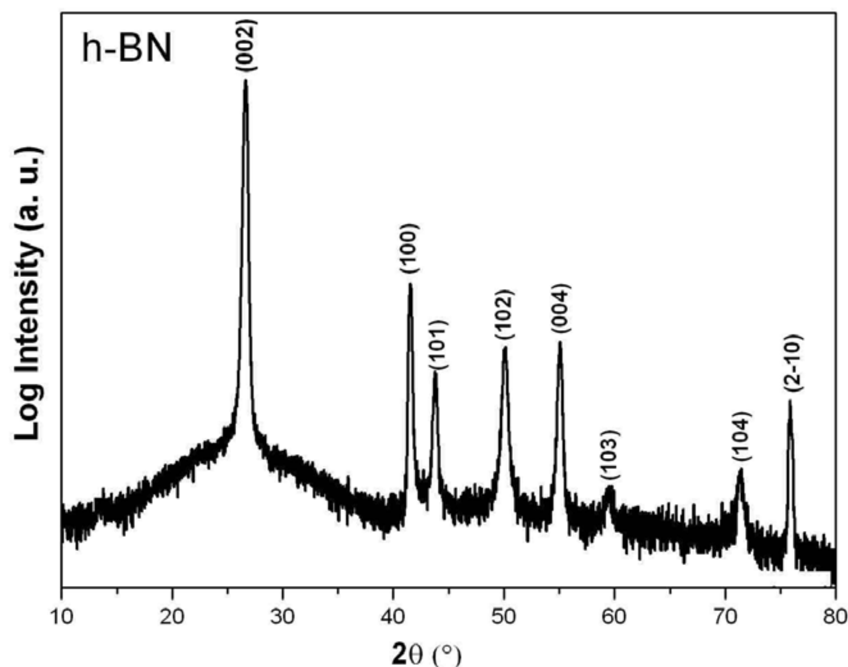

Fig. 4.7 – X-ray Diffraction pattern of h-BN hot-pressed target, using CuKα radiation. Intensity axis is in log (10) scale.

Boron carbide target (B_4C) has rhombohedral crystal structure. The main peak from its XRD pattern, in Fig. 4.8, is located at 2θ=37.68º and corresponds to the (021) crystal plane. Other peaks that are assigned to different crystal planes from boron carbide are present. On the other hand, three other peaks were observed at 2θ=26.34º, 2θ=41.61º and 2θ=44.43º. All these peaks correspond to reflection planes of graphite [95, 96]. This graphite is due to the contamination from the hot pressing mould during the target preparation. The

peak at 2θ=26.34º, that correspond to the (002) (hkl), which is the strongest in the XRD pattern for graphite, represents the perpendicular direction (c-axis) to the graphite hexagonal plane.

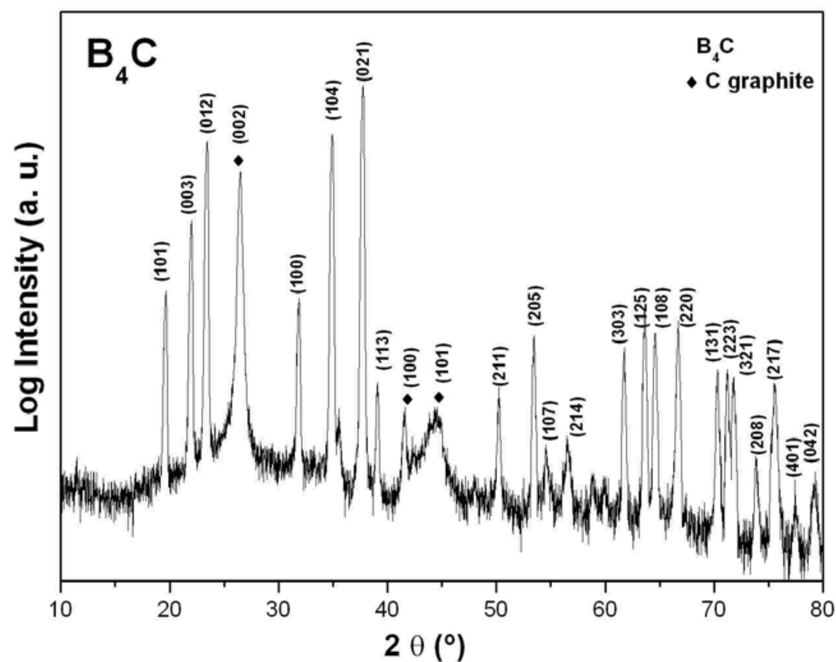

Fig. 4.8 – X-ray Diffraction pattern of B_4C hot-pressed target, using CuKα radiation. Intensity axis is in log (10) scale.

Figure 4.9 shows the FT-IR spectrum of the h-BN target. It can be seen in the target spectra the presence of two bands. These bands are located at ~770 cm^{-1} (A_{2u} mode) and ~1383 cm^{-1} (E_{1u} mode), [86] which correspond to h-BN vibrational resulting from the out-of plane B–N–B bending vibration and in-plane B–N stretching mode, respectively.

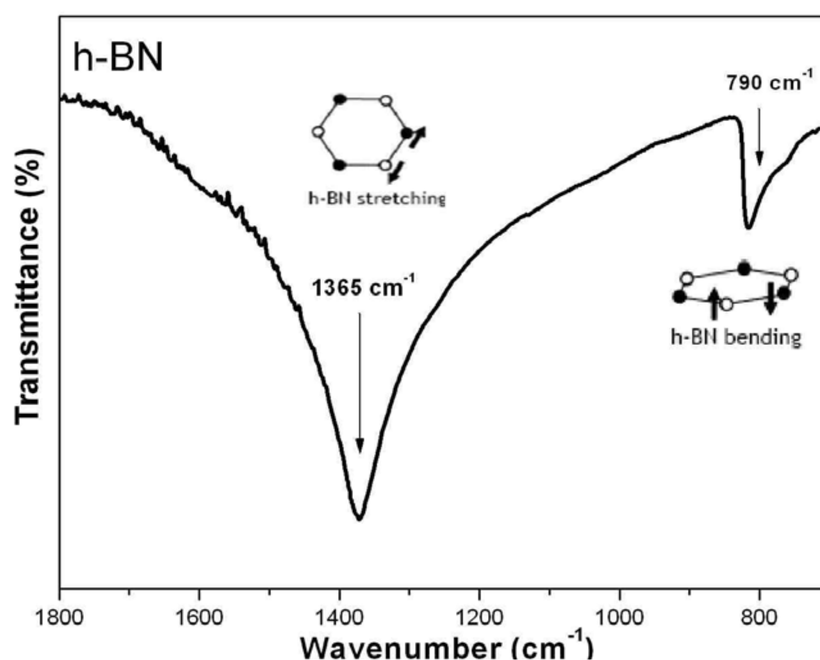

Fig. 4.9 – Fourier Transform Infrared (FTIR) absorption spectrum of h-BN hot-pressed target.

Fig. 4.10 shows FT-IR spectrum obtained from B_4C target produced by hot-pressing sintering. Experimentally, the spectrum taken from the B_4C target presents three IR bands that are identified in the 700 to 1000 cm^{-1} range, which correspond to the B_4C vibration. Moreover, the spectrum shows an absorption band at 1085 cm^{-1}, resulting from the B–C stretching bonds [97]. The broad peak at 1380 cm^{-1} is most likely due to the boron icosahedra, which have extremely high oscillator strength because of their large size and tight binding [98]. The vibration mode at 1530 cm^{-1} has been attributed to the anti-symmetric stretching of B–C bonds in the linear chain that interconnects the icosahedra [99, 100].

These results, from XRD and FT-IR analysis, ensure the high quality of the target preparation, both of h-BN and B_4C ceramics.

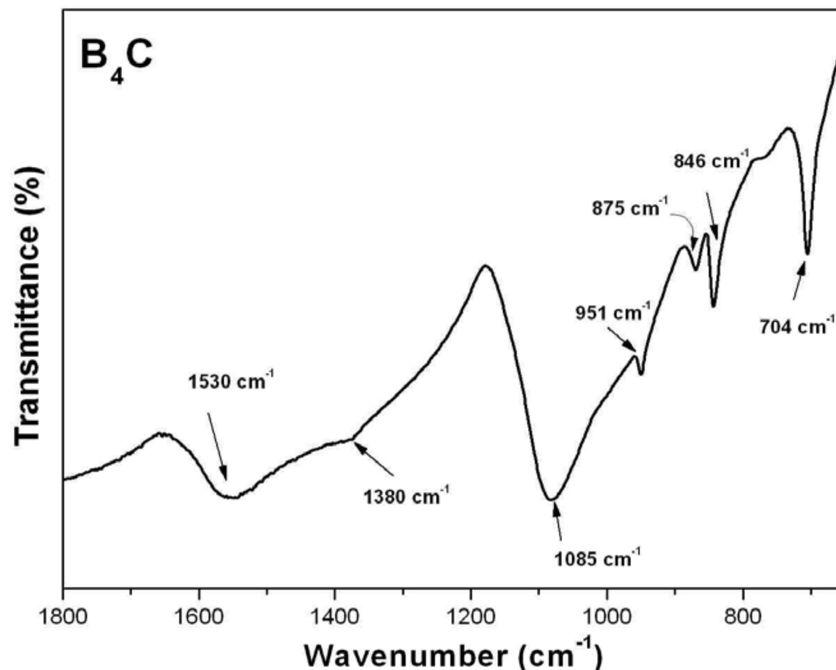

Fig. 4.10 – Fourier Transform Infrared (FTIR) absorption spectrum of B_4C hot-pressed target.

4.2.2. D.C magnetron sputtering deposition

Fig. 4.11 shows the FT-IR absorption spectra obtained from BN films deposited by DC magnetron sputtering under different conditions. It is clearly observed that the coated substrates have the same bands than the uncoated substrate. This evidence proves that very few BN phase was formed during the deposition. It was only observed the absorption band located at 1031 cm^{-1} that is associated with the Si–N–Si stretching mode. The absorption band near 830 cm^{-1} corresponds to the stretching vibration of the Si-N bond [20].

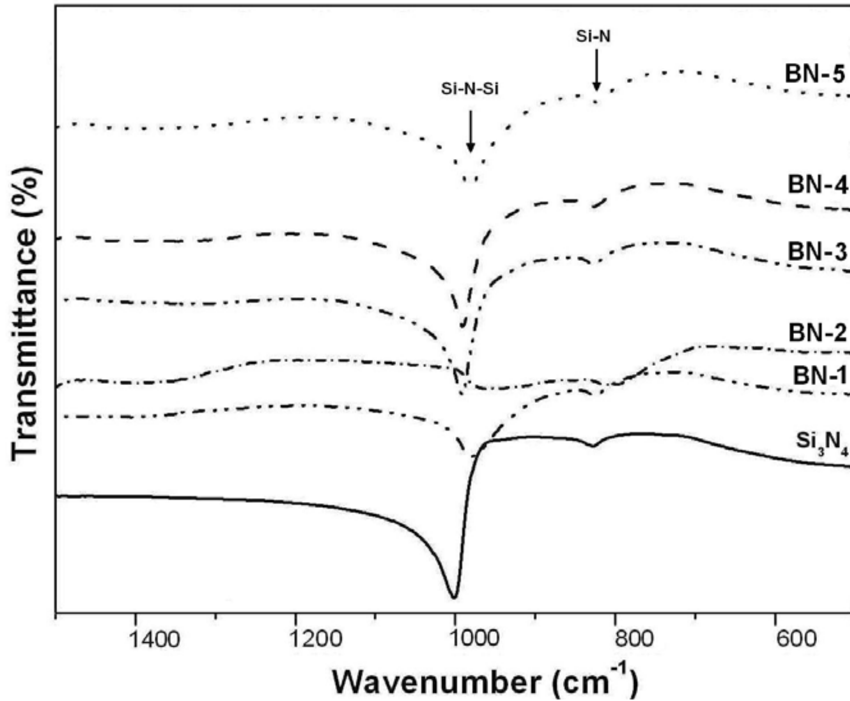

Fig. 4.11 – FTIR absorption spectra for BN films deposited by DC Magnetron sputtering under different conditions.

The surface morphologies of Si_3N_4 submitted to different deposition conditions have been investigated by SEM, as seen in Fig. 4.12. SEM image labelling, on the right side, give information about the deposition conditions: initial surface finishing (diamond grit); working gas composition, ratio of N_2/Ar (% vol.); deposition time; DC power applied and substrate bias voltage, if it is the case.

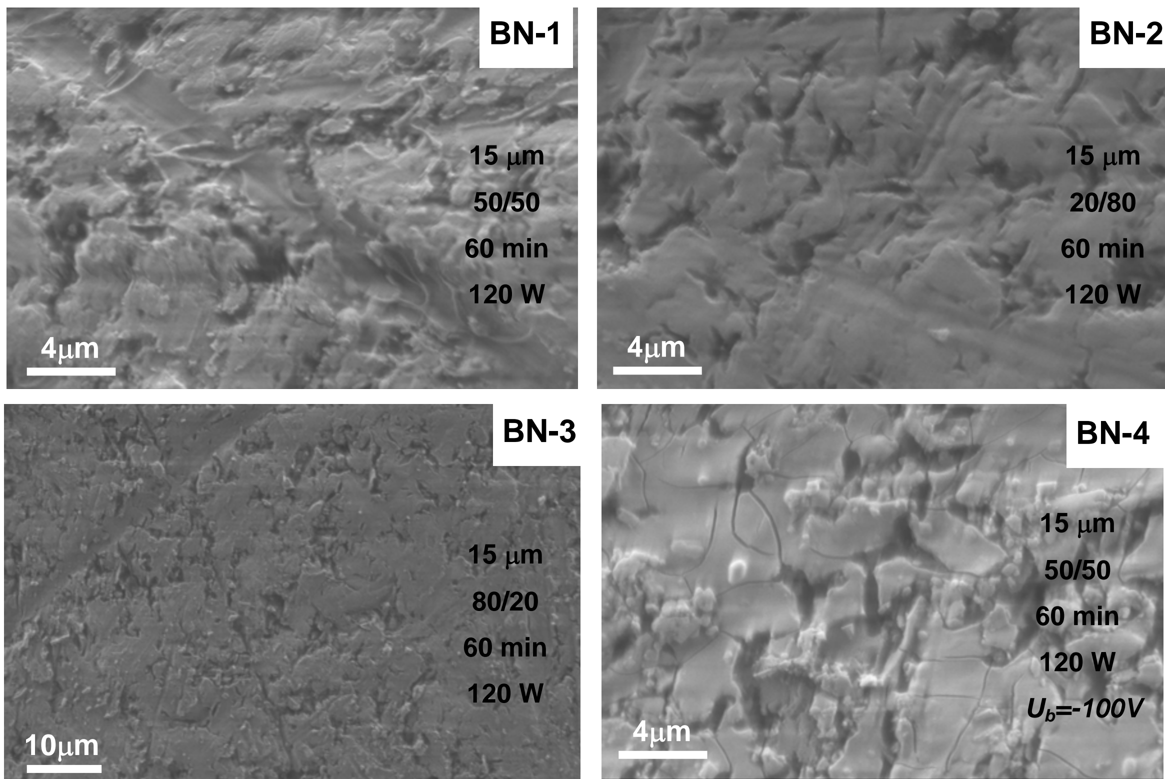

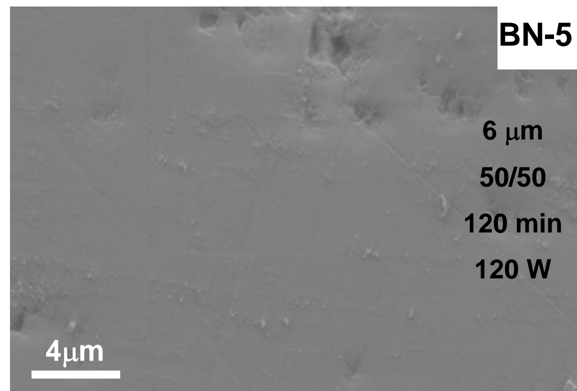

Fig. 4.12 – SEM micrographs of the films deposited by DC sputtering at different conditions.

From the observation of the samples BN-1 and BN-3, where the only processing difference between them is the N_2/Ar gas ratio, it is possible to say that the samples do not present significant microstructural differences. In all the cases the surface morphology replicates the surface finishing of the Si_3N_4 ceramic substrates.

Sample BN-4 was the only one in which a negative *bias* was used in the substrate and it presents a surface morphology similar to a cracked film. Yet using FT-IR as a support tool, not signal of the BN films was detected. As stated before, BN-5 was prepared using the same parameters as specimen BN-1, but with different initial surface finishing and deposition time. The surface roughness of the substrate used to prepare sample BN-5 polished at 6 μm was Ra= 0.012 μm. Again, the microstructural morphology is the result of the surface finishing (polishing).

Taking the set of results from DC magnetron sputtering, this technique was abandoned, and the work proceeded with RF magnetron sputtering deposition.

4.2.3. R.F magnetron sputtering deposition

In this part of the work, two sets of depositions experiments were performed in order to study the influence of the parameters on the BN thin film:

i. by varying the substrate temperature (Ts), while keeping the other parameters, the working gas composition, gas pressure, distance between target-substrate and RF target bias voltage constant;

ii. by varying the working gas composition, while the gas pressure, substrate temperature (Ts), distance between target-substrate and RF target bias were kept constant;

4.2.3.1. Substrate temperature studies

By peak identification of FT-IR spectroscopy is possible to detect the nature of the bonding between the nearest atoms and see any presence of BN phase. In special, peaks of c-BN are clearly distinguished of those of the h-BN.

With the purpose of studying the phase changes as a function of temperature, the acquired FT-IR spectra for samples deposited under different substrate temperatures ranging between RT and 500 ºC are presented in Fig. 4.13, Fig. 4.14 and Fig. 4.16.

Fig. 4.13 presents a set of samples grown over substrates with a 6 μm surface finishing. The hexagonal BN (h-BN) phase or the turbostratic (t-BN) phase with sp^2 bonding, exhibit characteristic peaks at 1350 cm^{-1} and 1500 cm^{-1} [101, 102]. As it is shown in Fig 4.13, there is this broad band composed by those two peaks in which the minimum is shifted as a function of temperature.

As it has been reported, these shifts are usually related to residual stresses which distort the crystal unit cell, producing variations of the peak energy of IR absorption bands. According to Fritz *et al.* [103] the variability of position of BN peaks are due to the film stress and mixture of metastable phases. But it should be pointed out that stoichiometry effects also play and important role in peak shifting. It has also been reported that the broadening of the peaks is due to the increase of disorder [113].

There is also a phase that is reported at 1610 cm^{-1} [39, 101, 102, 104] characteristic of the longitudinal (LO) optical modes h-BN which appear at 1595 cm^{-1} in the present samples. In addition, a FT-IR absorption band appears at 940 cm^{-1}. It is suggested by the literature that this absorption band can be assigned to E-BN [102, 105, 106]. According to Batzanov *et al.* [107] explosion boron nitride (E-BN) is a mixture of graphite-like h-BN and amorphous BN (mixing of sp^2 and sp^3 bonding). This phase is more accentuated in the substrate with surface finishing of 15 μm (Fig. 4.14).

In order to decide the nature of these peak shifts, and if they were related to stress, a similar trend should be observed the same behaviour on the c-BN associated vibration mode in the range of 1000-1100 cm^{-1} [113]. However this peak range is coincident with one of the Si_3N_4 substrate signals and is impossible to evaluate. The Si_3N_4 substrate in the FT-IR spectra shows a high signal at 1030 cm^{-1}, covering the signal of a possible c-BN band.

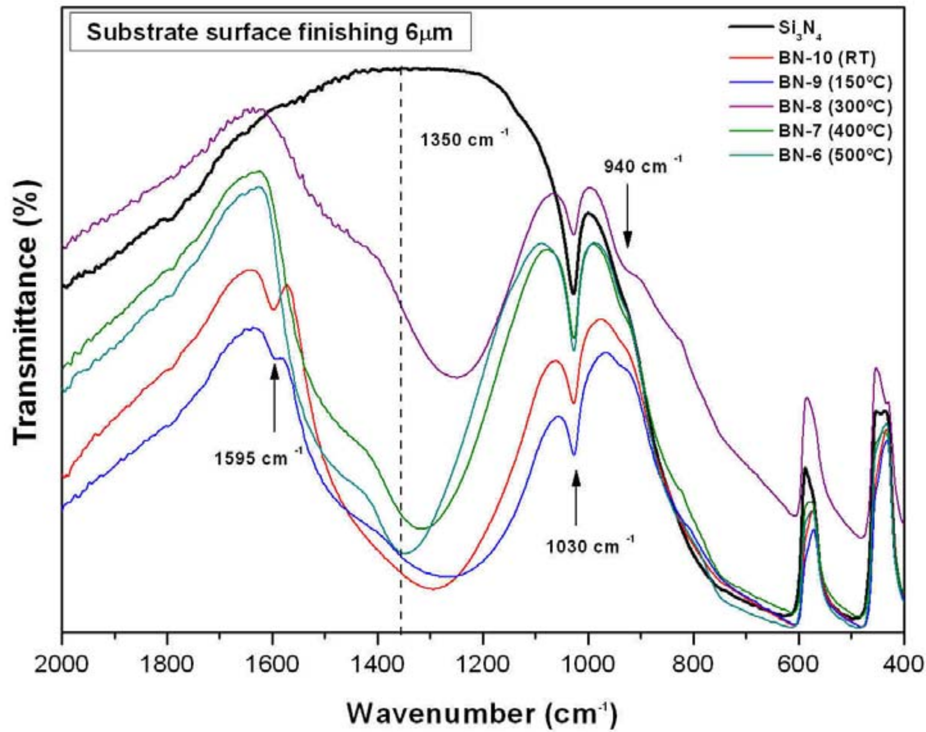

Fig. 4.13 – FT-IR absorption spectra in transmittance mode of BN films deposited on Si_3N_4 substrates (surface finishing 6μm) under different substrate temperatures.

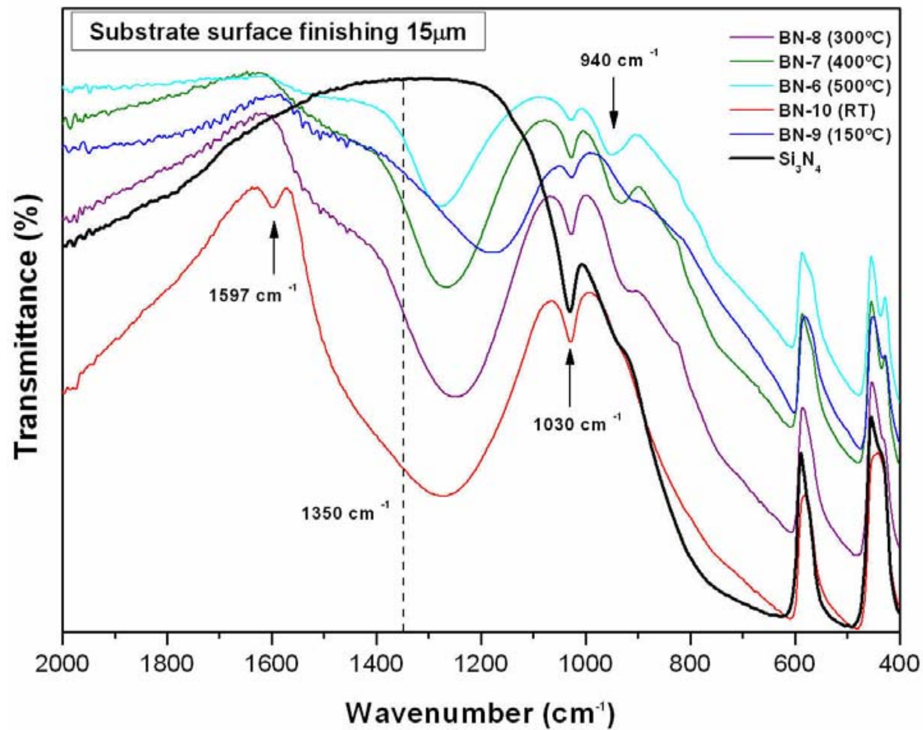

Fig. 4.14 – FT-IR absorption spectra in transmittance mode of BN films deposited on Si_3N_4 substrates (surface finishing 15μm) under different substrate temperatures.

Nevertheless, from Fig. 4.14, which are the spectra of the same films, but deposited over a 15 μm surface finished substrates, it can be observed that the mean peak position at 1350 cm^{-1} for the same films (same composition) are more shifted with respect to the ones

grown over 6 μm substrates. In this case, an introduction of residual stress is clearly demonstrated as a function of the surface finishing.

Thereby, the compressive stress can be estimated from the peak shift of the LO phonon mode of h-BN (v_0=1350 cm^{-1}) [108, 109]:

$$v_0 = v_{L0} + 3.45\frac{cm^{-1}}{GPa}.\sigma_{comp.} \tag{4.1}$$

As it can be seen in Fig. 4.15, the peak shifts for 15 μm surface finishing and possible related stress, are higher than for the 6 μm surface finished ones. The values of stress reported for other researcher corresponding to a compressive stress about 10-40 GPa [109-110], which correspond to those one measured in the present samples.

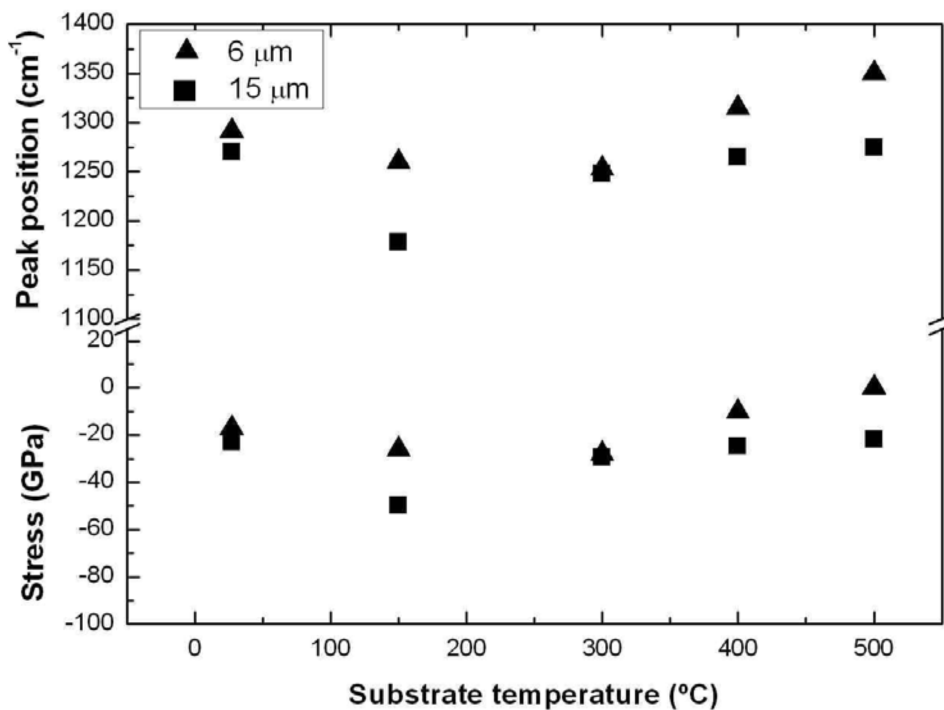

Fig. 4.15 – Stress and peak position of the BN films deposited on Si_3N_4 substrates (surface finishing of 6 μm and 15 μm) under different substrate temperatures.

As an attempt of facilitate film analysis, films were grown simultaneously over Si(100) substrates. FT-IR spectra are shown in Fig. 4.16, and as it can be seen, the same bands appear in the range of 1000-1100 cm^{-1} and still, c-BN contribution is not able to see due to the Silicon substrate contributions in the same range. In the Si(100) substrate the coincidence band appear at 1100 cm^{-1}.

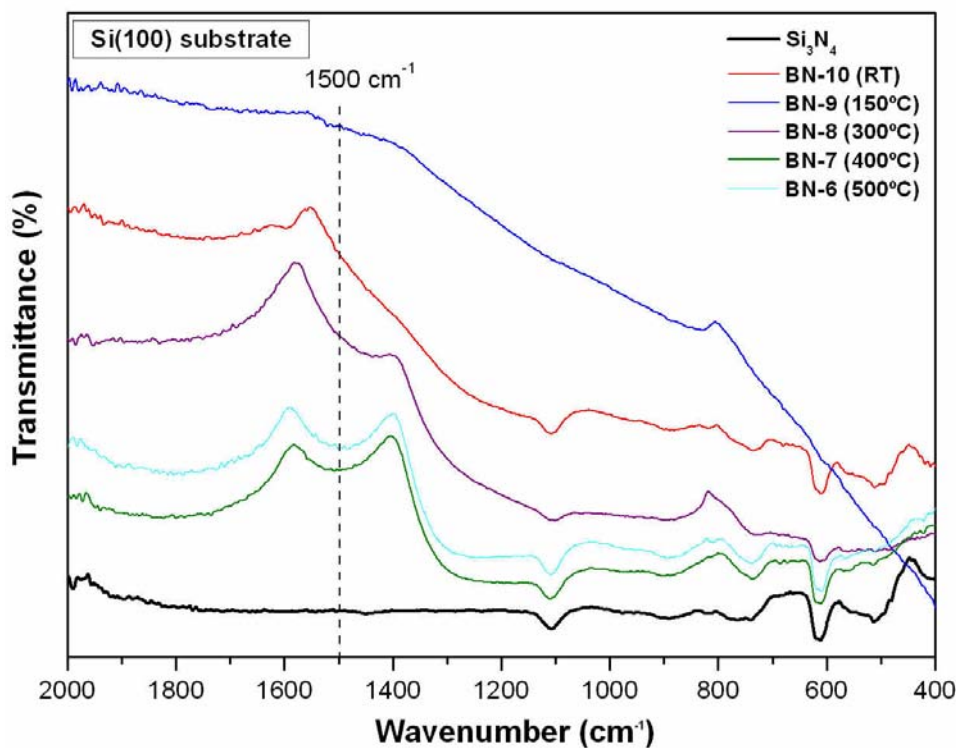

Fig. 4.16 – FT-IR absorption spectra in transmittance mode of BN films deposited on Si(100) substrates under different substrate temperatures.

X-ray Diffraction has been also performed on BN films grown over silicon. Fig. 4.17 shows the glancing-incidence XRD pattern under 2º incidence-angles and the XRD patterns were acquired in the range was 2*θ*=5–80º

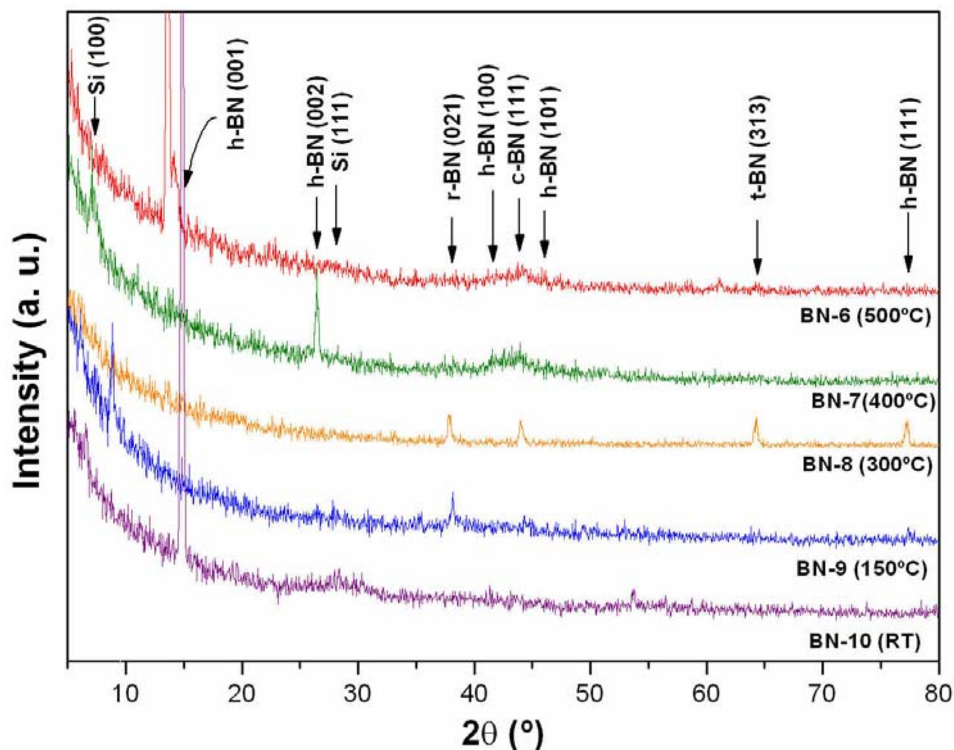

Fig. 4.17 - Glancing-angle X-ray Diffraction patterns of the BN film on Si(100) wafer substrates deposited at different substrate temperatures.

The X-ray reflection planes of the samples deposited on Si(100), in the substrate temperature studies, are resumed in the Table 4.3, with their relative intensities in each sample.

Table 4.3 – Identification of the X-ray reflection planes, taken from Fig. 4.17, of the BN coating deposited on Si(100), substrate temperature studies.

Sample	Ts (ºC)	XRD planes									
		Si (100)	Si (111)	h-BN (001)	h-BN (002)	h-BN (100)	h-BN (101)	h-BN (111)	c-BN (111)	r-BN (021)	t-BN (313)
BN-6	500	-	-	↑↑↑	↑	-	-	-	↑	-	↑
BN-7	400	↑↑↑	-	-	↑↑↑	-	-	-	↑	-	-
BN-8	300	-	-	-	-	-	-	↑↑↑	↑↑↑	↑↑↑	↑↑↑
BN-9	150	↑↑↑	↑	-	↑	-	-	-	↑	↑	-
BN-10	RT	-	↑	↑↑↑	↑	-	-	-	-	-	-

Intensity: high ↑↑↑ and low ↑

The Table 4.3 and the Fig.4.17 show that the h-BN is the main phase grown, appearing in different reflection planes. In addition, traces of r-BN and t-BN were found. The c-BN was also found, however, it appears in a broad band composed by other reflection planes, namely h-BN.

Generally, a large broad band occur between the diffraction peaks of c-BN and h-BN because the atomic numbers of nitride and boron elements are very low and the signals of various phases are greatly widened and weakened by the arbitrary orientation of various crystal particles in the film [118]. Moreover, growing of the cubic phase requires high energies, without that, the BN films will stabilize in the hexagonal structure [116, 117].

The morphologies of BN films deposited at different substrate temperatures were investigated by SEM in plain and cross-sectional views, as depicted in Fig. 4.15 and Fig. 4.16, respectively.

Fig. 4.18 shows the surface morphologies of the films deposited on Si_3N_4 samples with a surface finishing of 6 μm at the substrate temperature in the range of RT-500ºC. It were used Si_3N_4 the samples with a surface finishing of 6 μm because the surface finishing of 15 μm presents a rougher surface comparing to 6 μm, turning more difficult the SEM observation.

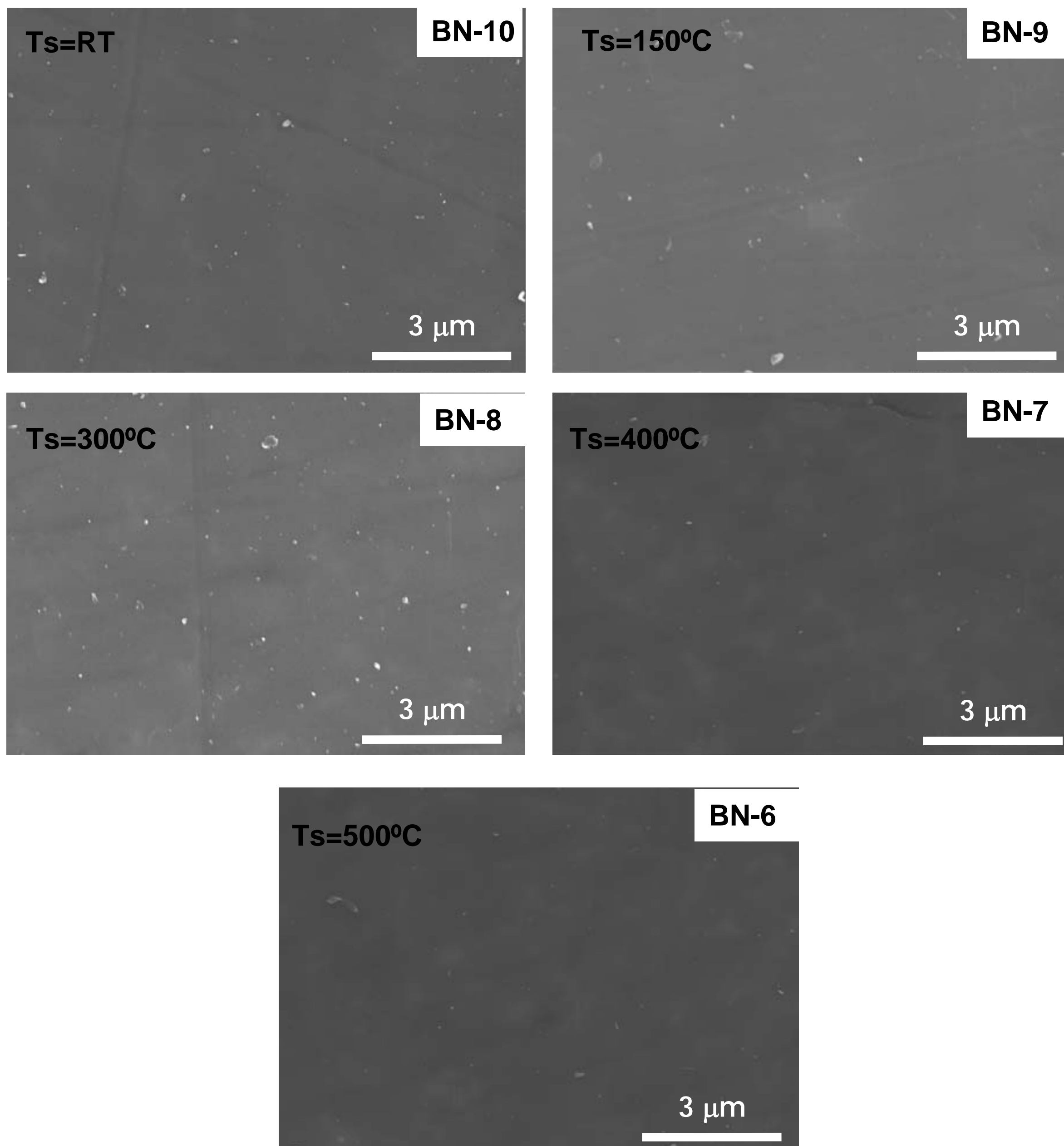

Fig. 4.18 - SEM micrographs of the surface of BN films on Si_3N_4 (surface finishing of 6 μm) substrates deposited at different substrate temperatures.

It is visible in all samples, that the film surface is very smooth and no crystal facets are grown. From Fig. 4.18, it is also possible to observe the microstructure of intergranular glassy phase of the substrate. Comparing with Fig. 4.1 the microstructure of this phase is out-of-focus, due to the transparent behaviour of the BN films. The white dots in some microstructures are due to the impurities during the SEM sample preparation.

Fig. 4.19 shows SEM micrographs in cross-section of the deposition of BN over Si_3N_4 samples (surface finishing at 6μm) at different substrate temperatures. The images were taken by tilting the surface at 45º.

The existence of a BN thin film is evident in all cases. The BN films are dense and homogeneous in all their extension. It can be observed that the film thickness of the samples slightly increases with the increasing of the substrate temperature, as well as, the deposition rate, as shown in the Fig. 4.20. However, it is not valid for a substrate temperature of 500ºC (see Fig.4.19 – BN-7), since at this temperature a net decrease of the film thickness was observed.

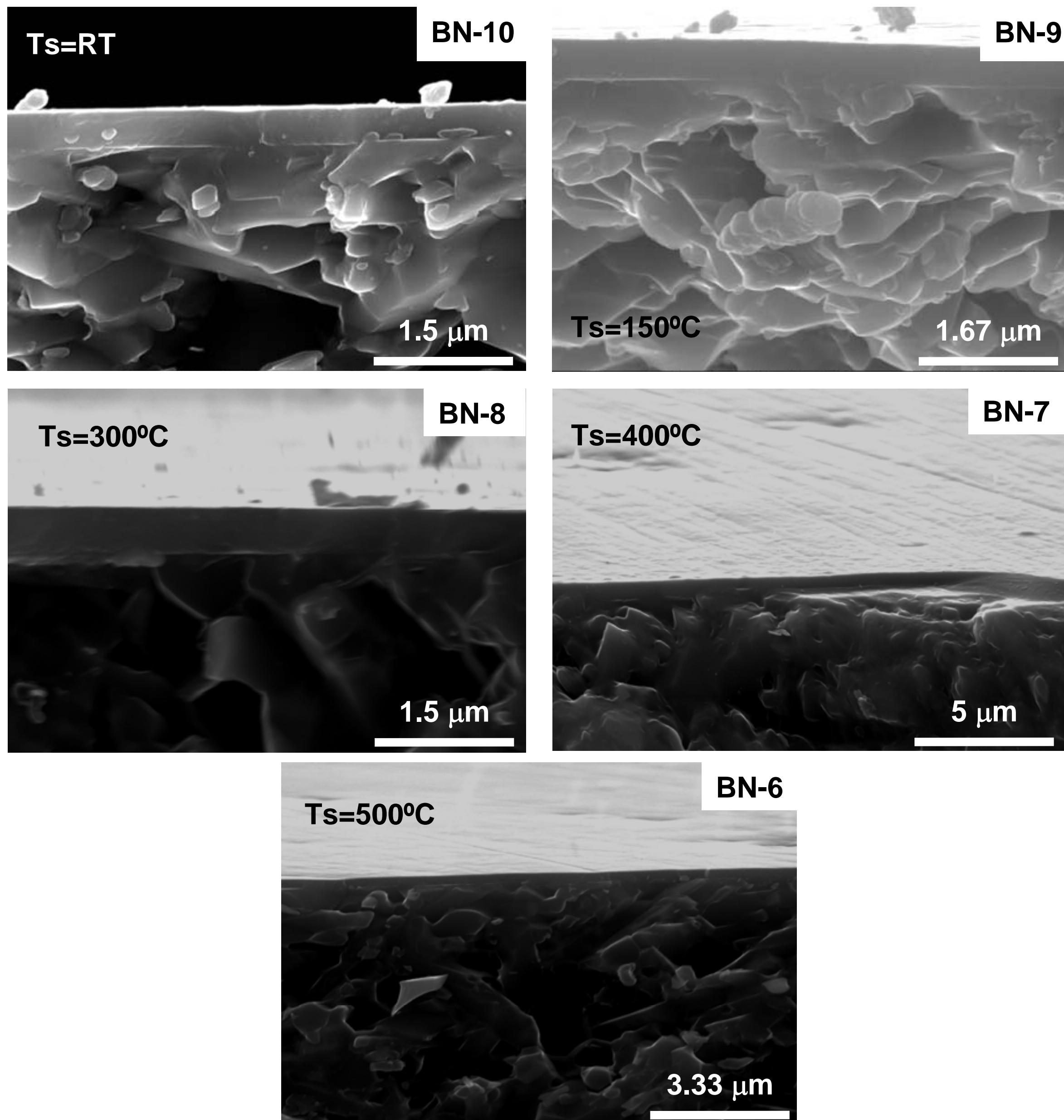

Fig. 4.19 - SEM cross-sectional images of BN layer system on Si_3N_4 (surface finishing of 6 μm) substrates deposited at different substrate temperatures.

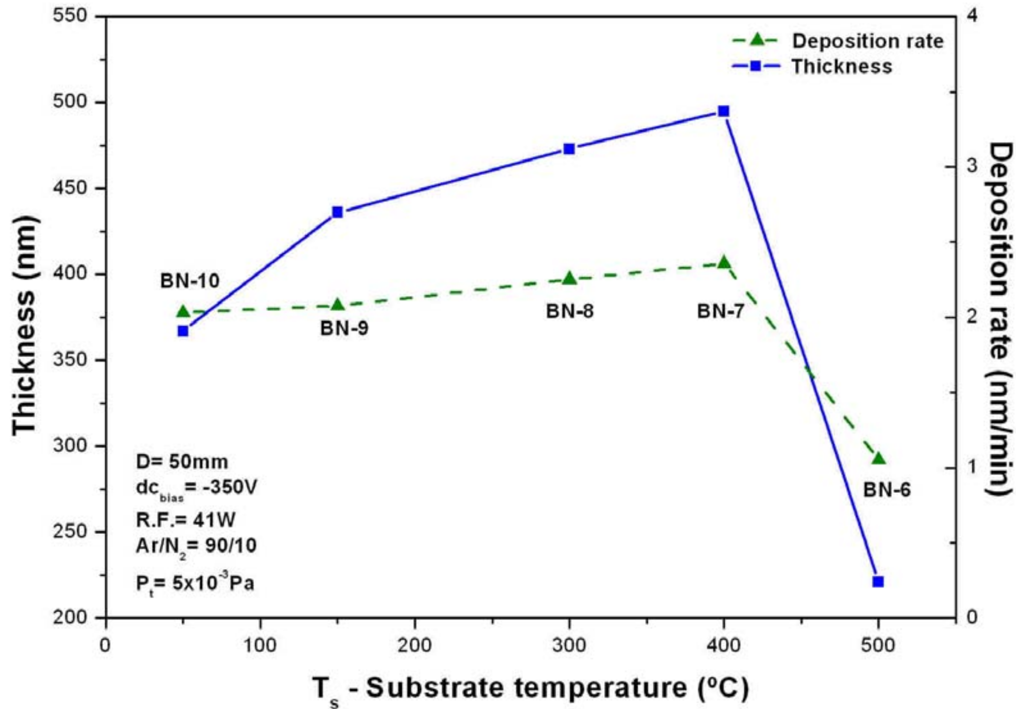

Fig. 4.20 – Dependence of the thickness and deposition rate of BN thin films with substrate temperature (Ts).

It can be concluded that a substrate temperature of 400ºC leads to an optimal grown of the BN films. The substrate temperature is an important parameter, since it controls the nitrogen incorporation into the growing film [112]. The deposition rate, the ratio between thickness and deposition time, increases when the substrate temperature increases, until a maximum of 400ºC (Fig. 4.20).

The hardness values of the BN coatings are presented in Table 4.4. In addition, Fig. 4.21 shows the dependence of the hardness as function of substrate temperature.

Table 4.4 - The physical and mechanical properties of BN thin films prepared by R.F magnetron sputtering using different substrate temperatures.

Material	*Substrate temperature (ºC)*	*Thickness (μm)*	*Nanohardness 1mN (GPa) and Err*
BN-6	500	0.22	8.1 ± 0.3
BN-7	400	0.50	9.4 ± 0.7
BN-8	300	0.47	9.2 ± 0.6
BN-9	150	0.44	10.1 ± 0.5
BN-10	RT	0.37	6.1 ± 0.6

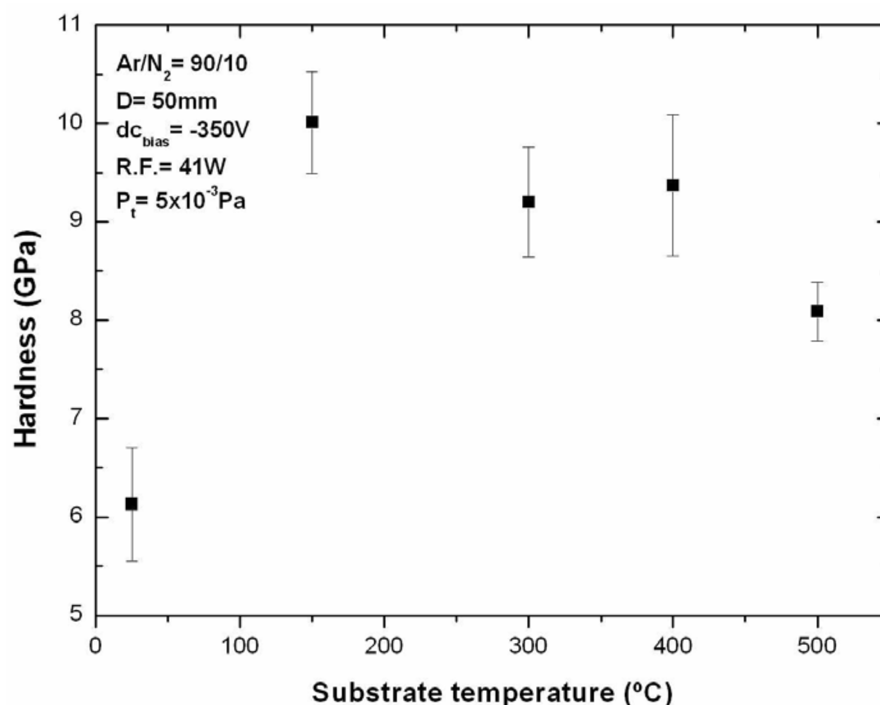

Fig. 4.21 – Hardness and errors associate with the measurement as function of substrate temperature.

The sample grown at room temperature (BN-10) is the softest coating; with a hardness around 6 GPa. For this sample only h-BN was detected in the X-ray Diffraction pattern, Fig. 4.17 and Table 4.3.

The following samples, BN-6, BN-7, BN-8 and BN-9, present values of hardness somewhat higher than observed in the samples BN-10 [113-115]. The hardness increasing is related to the fact that in these samples small traces of the cubic and metastable phases appear which is confirmed by X-ray Diffraction pattern (Fig. 4.17 and Table 4.3).

4.2.3.2. Working gas composition studies

The effect of working gases ratio (mixture of Ar and N_2) on the growth of the BN thin films was also studied. The acquired FT-IR spectra for samples deposited under different working atmospheres Ar/N_2 (%vol.) ratio of 100/0, 90/10, 70/30 and 50/50, keeping the other parameters constant, are presented in Fig. 4.22, Fig. 4.23 and Fig. 4.25.

As it is shown in Fig. 4.22, samples grown over Si_3N_4 substrates with a 6 μm surface finishing present a broad band composed by the two bands at 1350 cm^{-1} and 1500 cm$^{-1,}$ which are related to the h-BN phase, as before explained.

As can be observed from Fig. 4.22 and Fig. 4.23, the main peak at 1350 cm^{-1} is strongly shifted as a function of the gas composition in the sputtering atmosphere, additionally to the stress contribution of the surface finishing of the Si_3N_4 substrates. It is important to study the shape of the two-peak-composition. This change, from broad to narrow shape, is related to the fact that the order of h-BN is increasing with the increasing of ratio of $N_{2.}$

As it has been mentioned before, usually, peak shift is related to stress or to different stoichiometries. In this case, as the gas composition is directly related with the future composition of the films a careful analysis should be done. Spectra in Fig.4.22 shows a narrowing of the peak perfectly positioned in 1350cm^{-1} related to the h-BN phase for the samples grown with the biggest amount of nitrogen (50% and 30%). These narrow peaks are a sign of the increase of order in the h-BN phase. As soon as the nitrogen content in the atmosphere lowers down, for the 10% of nitrogen sample, the peak shifts downwards and also broadens with 0% of nitrogen the peak is the broader and also the less intense. This means that the h-BN phase is decreasing.

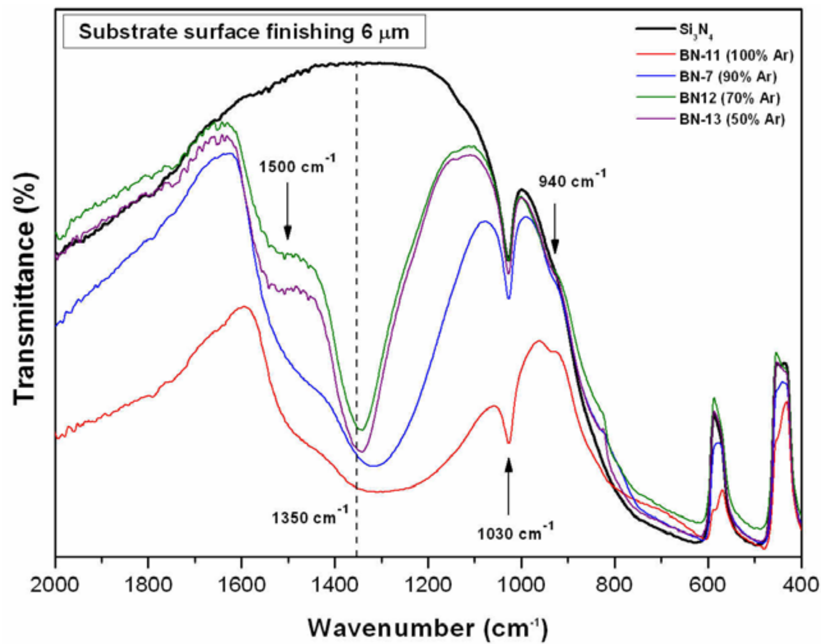

Fig. 4.22 – FT-IR absorption spectra in transmittance mode of BN films deposited on Si_3N_4 substrates (surface finishing of 6 μm) at 400ºC, using different working gas composition Ar/N_2 (%vol.).

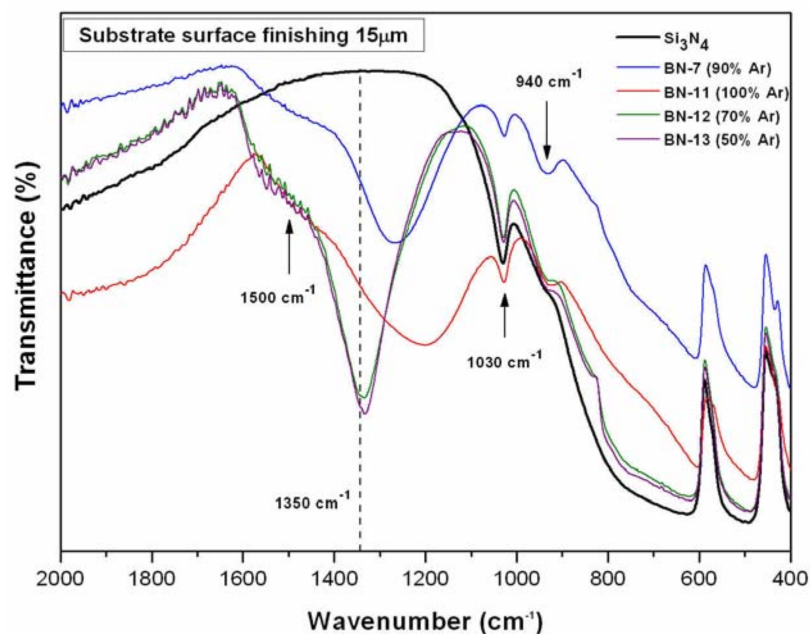

Fig. 4.23 – FT-IR absorption spectra in transmittance mode of BN films deposited on Si_3N_4 substrates (surface finishing of 15μm) at 400ºC, using different working gas composition Ar/N_2 (%vol.).

However, by making a comparison between Fig. 4.22 and Fig. 4.23, where the only difference between them is the substrate surface finishing, it can be observed that the mean peak position at 1350 cm^{-1} for Si_3N_4 15 μm is strongly shifted with respect to the ones grown over 6 μm substrates. In this case, an introduction of residual stress also is clearly demonstrated as a function of the surface finishing the surface finishing of 15 μm, like in the temperature difference studies.

The peak shift, for both Si_3N_4 substrate surface finishing, can be seen in Fig. 4.24. The peak shifts for 15 μm surface finishing and the possible related stress is higher than for the 6 μm surface finishing ones. Additionally, the peak shift and the residual stress are activated by the working gas ratio, namely by the increasing of the argon content, that means, the peak shift and the compressive stress is higher in the BN films with 15 μm substrate surface finishing. This occurs because of the compressive stress have at the same time two contributions, one from surface roughness and other from the sputtering atmosphere (stoichiometry) of the films. It is clearly observed, from Fig. 4.24, that the compressive stress of the BN films increasing with the increasing of the argon content.

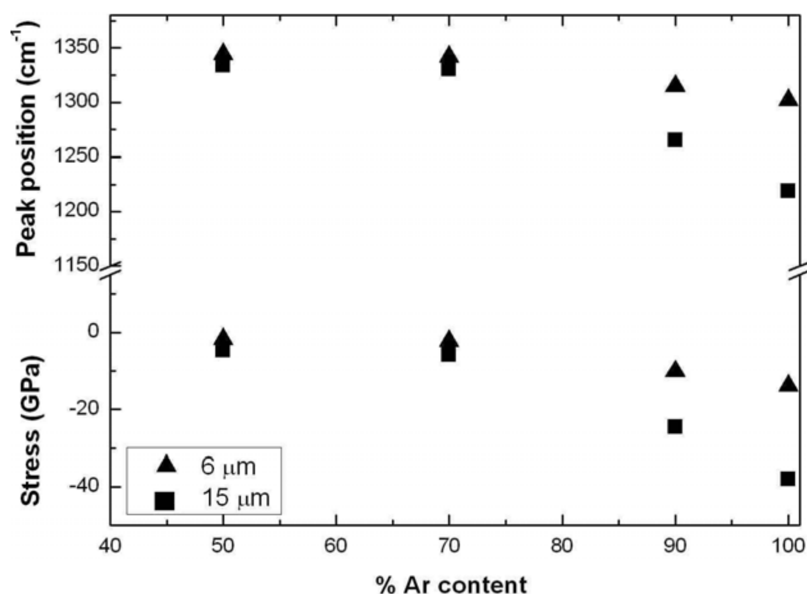

Fig. 4.24 – Stress and peak position of the BN films deposited on Si_3N_4 substrates (surface finishing of 6 μm and 15 μm) under working atmospheres ratio (Ar/N_2).

In the working gas studies, samples also were grown simultaneously over Si(100) substrates. However, FT-IR spectra shown in Fig. 4.25, present the same feature as observed in the substrate temperature studies.

Nevertheless, it is evident that the characterisation of BN films is non-trivial and requires the use of several complementary techniques. For this reason, the samples grown on Si(100) were used in the X-Ray Diffraction measurements in order to confirm the existence

of BN phases within the coatings and also the Si(100) substrates were used to determine the hardness of the BN coatings.

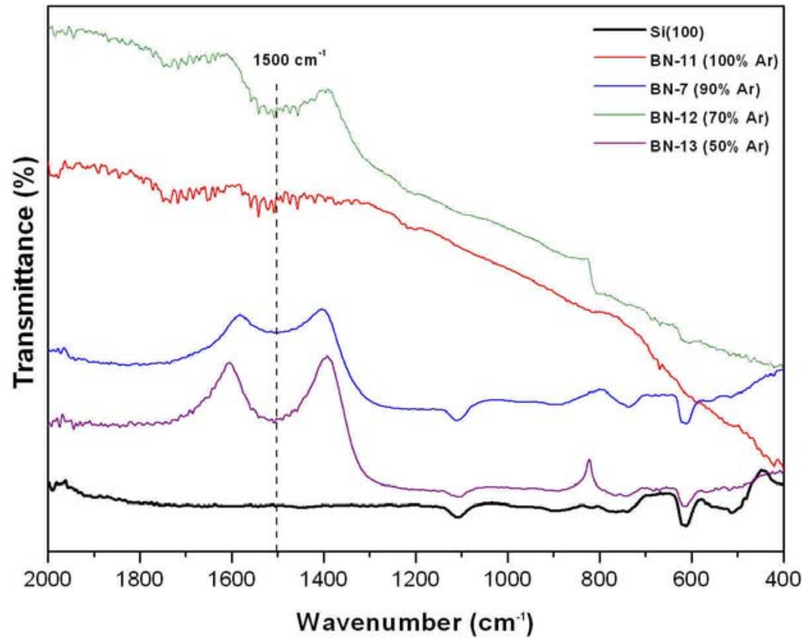

Fig. 4.25 – FT-IR absorption spectra in transmittance mode of BN films deposited on Si(100) substrates at 400ºC, using different working gas composition Ar/N_2 (%Vol.).

Fig. 4.26 shows the glancing-incidence XRD pattern for all samples deposited at 400ºC, using different working gas mixture (Ar/N_2). The XRD patterns were collected in the 2θ=5–80º range. The X-ray reflection planes of the samples deposited on Si(100), in the working gas studies, are summary shown in the Table 4.5 with their relative intensities for each sample.

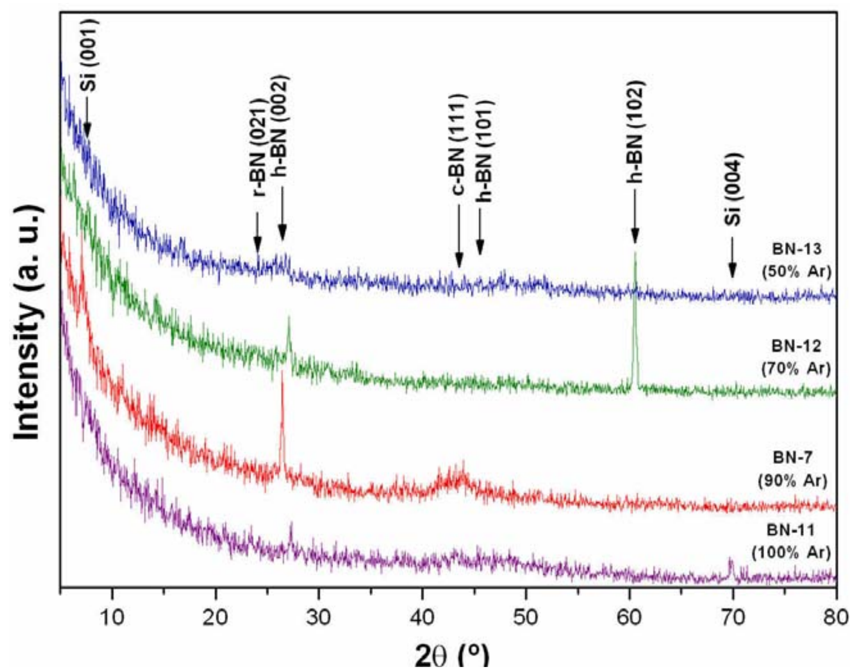

Fig. 4.26 - Glancing-angle (2º) X-ray diffraction patterns of the BN film on Si(100) wafer substrates deposited at 400ºC, using different ratios of Ar/N_2 (vol.%).

Table 4.5 – Identification of the X-ray reflection planes, taken from Fig. 4. 26, of the BN coating deposited on Si(100), during the working gas (Ar/N_2) ratio study.

Sample	Ar/N_2 (vol %)	XRD planes							
		Si (001)	Si (004)	h-BN (002)	h-BN (102)	h-BN (101)	c-BN (111)	c-BN (220)	r-BN (012)
BN-11	100/0	-	↑↑↑	↑↑↑	-	↑	↑	-	↑
BN-7	90/10	↑↑↑	-	↑↑↑	-	-	↑	-	-
BN-12	70/30	-	-	↑	↑↑↑	-	-	↑	-
BN-13	50/50	-	-	↑	-	↑	↑	↑	-

Signal: high ↑↑↑ and low ↑

From the analysis of Table 4.5 and Fig.4.26, it is possible to observe that the h-BN is the main crystalline peaks, appearing in different reflection planes of X-Ray Diffraction patterns. Besides, a small trace of r-BN (metastable phase of h-BN) was detected in the sample grown in a 100% of argon atmosphere. In addition, a low signal of cubic phase was also detected in the samples grown using 100% and 70% of Ar, which appear in a broad band composed by h-BN.

Fig. 4.27 shows the surface morphologies of the films deposited on Si_3N_4 samples (surface finishing at 6μm) at the substrate temperature of 400ºC, using different ratios of Ar/N_2 (%Vol.). From these analyses, it is possible to verify that all samples presented the same characteristics as in the previous study (substrate temperature studies). This means that is possible to observe the microstructure of intergranular glassy phase of the substrate, but the intergranular glassy phase is out-of-focus, due to the transparent behaviour of the BN films.

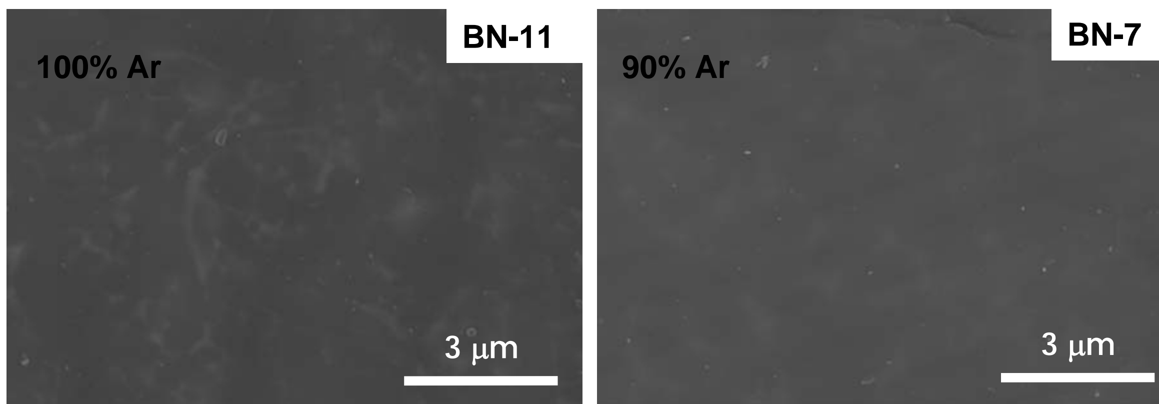

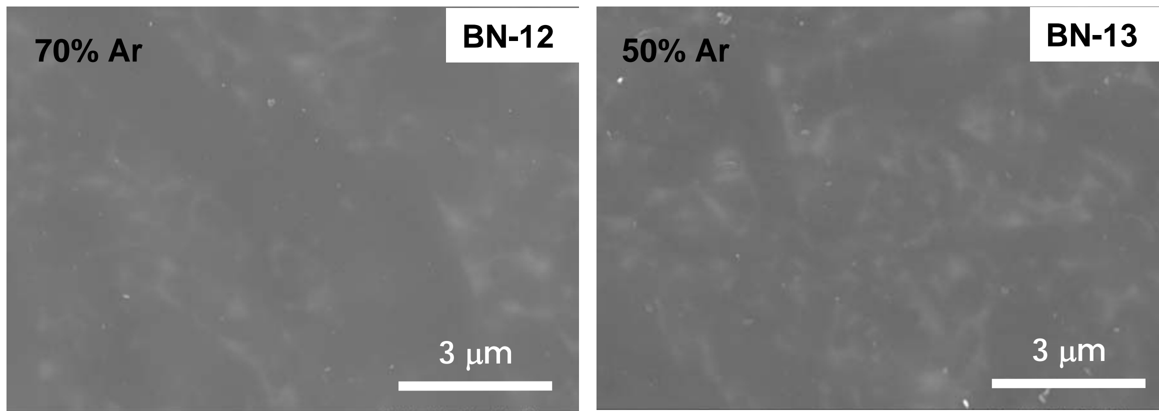

Fig. 4.27 - SEM micrographs of the surface of BN films on Si_3N_4 (surface finishing of 6 μm) substrates deposited at 400ºC using gas mixtures of Ar/N_2 (%Vol.) as working gas.

Fig. 4.28 shows SEM micrographs in cross-section of the coated Si_3N_4 sample (surface finishing at 6μm) at 400ºC, using different ratios of Ar/N_2 (%Vol.). The images of the cross section were taken by tilting the surface at 45º.

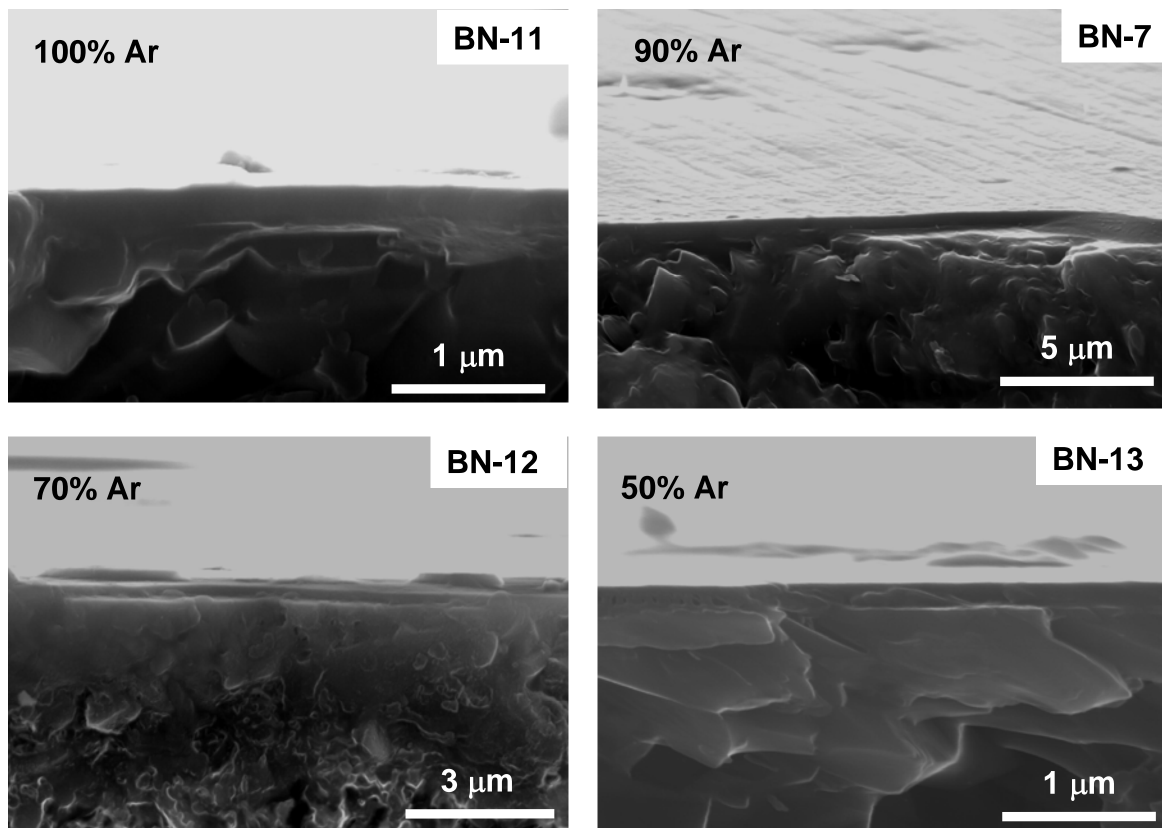

Fig. 4.28 - SEM cross-sectional images of BN layer system on Si_3N_4 (surface finishing of 6 μm) substrates deposited at 400ºC using gas mixtures of Ar/N_2 (%Vol.) as working gas.

The presence of a film is observable all samples (Fig. 4.28). The BN films apparently are dense and homogeneous in all their extension. As seen in Fig. 4.29, the film thickness of the samples decreases when the N_2 ratio increases. However, this behaviour was not

observed for the sample deposited using 10% of N_2 (see sample BN-7, Fig.4.28). Using this working gas mixture a maximum thickness of the BN film was obtained.

In that way, there exists an optimum working gas composition of Ar to N_2 ratio and RF target power to achieve the highest deposition thickness. In the deposition conditions range that was tested, the highest thickness was obtained in the film deposited using a working atmosphere of Ar to N_2 ratio of 90/10 with a RF target power of 41 W at 400 ºC.

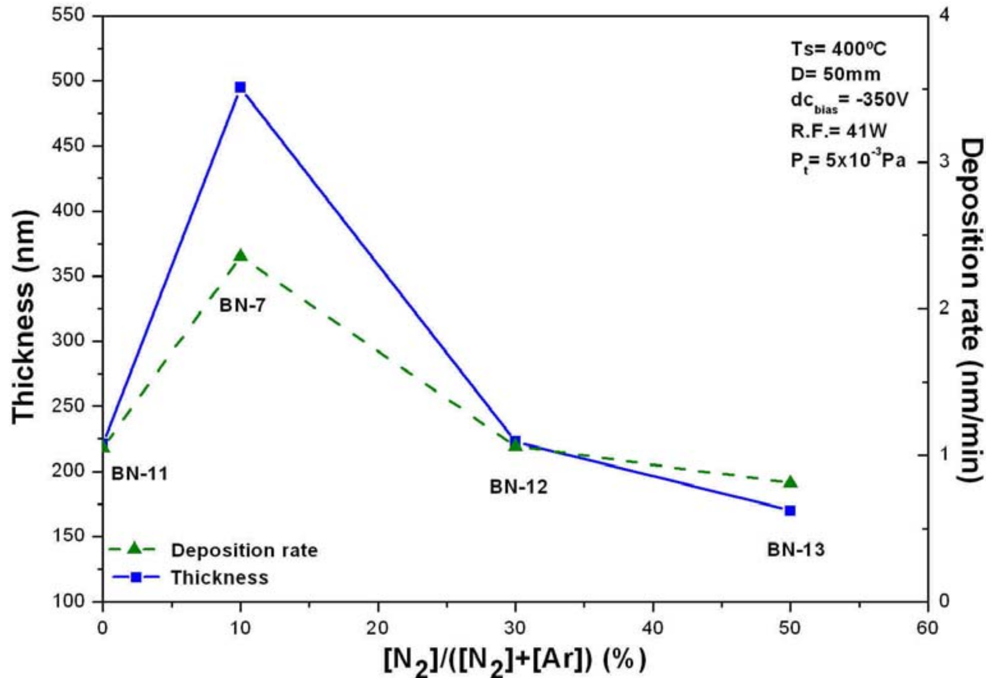

Fig. 4.29 - Dependence of the thickness and deposition rate of BN thin films with the N_2 working gas content.

Nanoindentation was also used in the samples grown with different atmosphere ratio (Ar/N_2) to measure the hardness of the BN coatings. It was used a high nominal load of 1mN, as studied before.

The average experimental hardness values for each sample as well as its errors are listed in the Table 4.6. In addition, Fig. 4.30 shows the hardness as a function of the atmosphere gas composition.

Table 4.6 - The physical and mechanical properties of BN thin films prepared by R.F magnetron sputtering using different working gas ratio (Ar/N_2).

Material	*Ar content (%)*	*Thickness (μm)*	*Nanohardness 1mN (GPa)* (Err)
BN-11	100	0.22	15.9 ± 1.3
BN - 7	90	0.50	9.4 ± 0.7
BN-12	70	0.22	8.6 ± 0.5
BN-13	50	0.17	7.6 ± 0.4

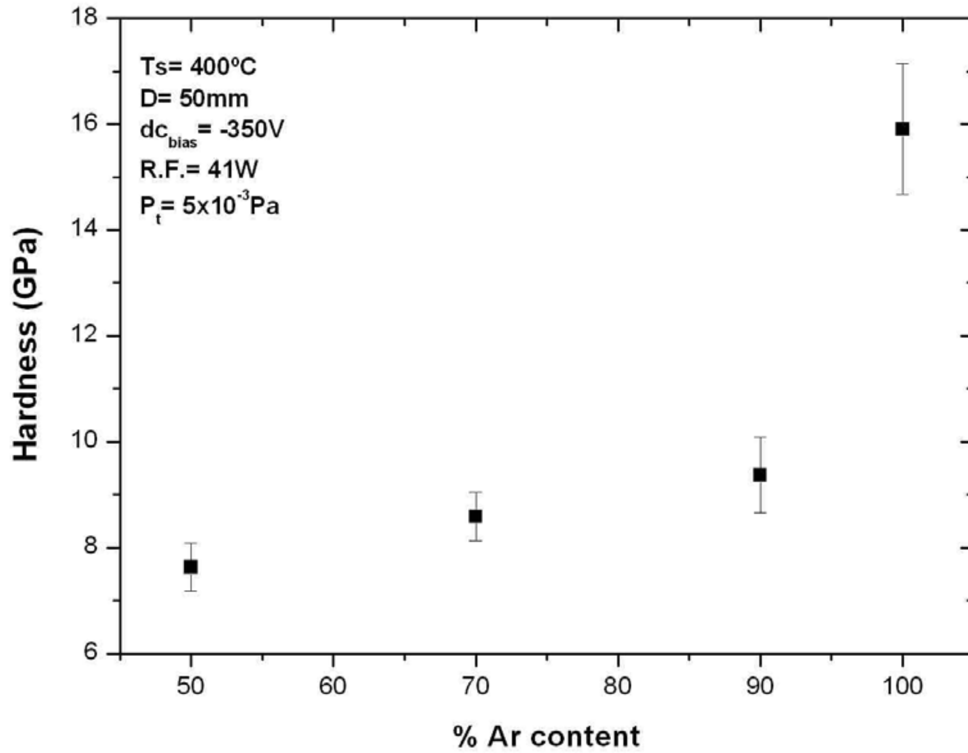

Fig. 4.30 – Hardness and errors associate with the measurement as function of working gas composition.

As is shown in Fig. 4.30, where the hardness is plotted vs. the argon content, there is a hardness increase with the reduction of nitrogen gas from 7 to 16 GPa (the value of the Si substrate is around 9 GPa). These values vary between those of a very soft h-BN (1 GPa [113-115]) film to values approaching the limit of the range reported for films containing a fraction of cubic phase (12 GPa [115]).

In fact, the hardest sample (BN-11) presents the lowest h-BN intensity in the X-ray Diffraction pattern (Fig. 4.26), while the softest ones (BN-13), where presents a predominance of h-BN phase. The following samples (BN-7 and BN-12) present intermediate hardness values comparing to the soft h-BN films.

Chapter 5

Conclusions

BN thin films synthesis using DC and RF magnetron sputtering deposition methods has been performed.

Based on the analysis of the results from the different deposition sets, the following concluding remarks are drawn:

i. Silicon nitride ceramic substrates were produced by pressureless sintering. The final microstructure is composed mainly by hexagonal elongated β-Si_3N_4 grains which are embedded in a secondary phase, formed by sintering additives. The measured values of hardness and fracture toughness were around 15.5 GPa and 5.8 $MPa.m^{1/2}$, respectively;

ii. Ceramics targets were produced by hot isostatic pressing, one electrically conductor (B_4C) and one electrically insulator (h-BN). The production quality was confirmed by XRD and FT-IR;

iii. Boron nitride films have been first synthesised by DC magnetron sputtering onto Si_3N_4 substrates, using B_4C as target ceramic material. However, the result of this process was not the expected. The reason for these results was mainly due to some restrictions of the equipment;

iv. Boron nitride films have been also synthesised by RF magnetron sputtering on different substrates, using h-BN as target. The films surface is very smooth, and is possible to observe the glassy intergranular phase of the Si_3N_4 substrate though the film. Furthermore, the BN films thickness is in the range of 180-490 nm, and are dense and homogeneous;

v. Two deposition sets were systematically investigated, substrate temperature and working gas composition ratio, using several techniques, like FT-IR, glancing-angle X-ray diffraction, scanning electron microscopy and nanohardness;

vi. The substrate temperature study show that the deposition rate increases with an increasing of the substrate temperature. The softest BN coating in this case achieved for the lower temperature, because of h-BN being the main phase grown. The increase of temperature favours the formation of other phases, decreasing the contribution of h-BN phase, leading to an increasing of the hardness of the BN coatings;

vii. In the working gas composition studies, the main band observed in all FTIR spectra corresponds to the h-BN vibration modes, which can be confirmed by XRD. Moreover, it was found traces of other BN phases. The deposition rate of the samples decreases when the N_2 ratio increases.

viii. It was observed that the mean peak position (1350 cm^{-1}) is strongly shifted because of two factors: surface roughness of the substrate and the working gas composition. The peak shifts are related to the stress, thereby, the stress increases with the peak shift. The hardness increases with the reduction of nitrogen gas in the sputtering atmosphere, obtaining values from a soft h-BN (6 GPa) to values approaching the limit of the range reported for films containing a fraction of cubic phase (16 GPa) up to 40%.

Chapter 6

Recommendation of future work

Through the development of this project, a number of possible paths for future work have been identified.

Based on the experimental results presented in this work, numerous further investigations are conceivable. After this thesis, the work will continue towards the goal of attaining a better understanding of how thin films obtain their interesting properties. That is to gain knowledge about the growth mechanisms and the phase formation.

The present work demonstrated the feasibility of preparing BN films by the magnetron sputtering method. In order to this method be more widely utilised, further work must be done, primarily in the areas of further apparatus optimisation, and further sample characterisation. If completed, both areas would yield a wealth of further information about the process itself, as well as how to prepare BN films with specific properties.

Based on this, new deposition must be done in order to optimise the processes, doing it more trustworthy. Besides, it is necessary to include a new deposition parameter which is a dc bias on the substrates. According to many researchers these parameters along with the substrate temperature is important on the formation of hardest phases of BN films.

In order to have a full knowledge, mechanical and tribological properties must be determinate. We propose the following: scratch test may be used, in order to determine the adhesion and the stress of the BN films on the Si_3N_4 substrates. The resistance to abrasive wear can be determined with a ball cratering tester. Furthermore, a tribological property that can be determined in the future is the friction coefficient using a pin-on-disc device without lubrication. Finally, for an innovative approach, the deposition of the BN can be done directly on the cutting tools (Si_3N_4 cutting tools) or still, on the diamond coatings, providing a barrier to avoid the carbon diffusion during machining of ferrous materials. In addition, the cover tools can be tested in turning tests in cutting service.

Bibliography

[1] WTEC Panel Report, Trends in Nanoparticles, Nanostructured Materials, R. W. Siegel, E. H. Hu, M. C. Roco, 1997.

[2] Surface Engineering, Science and Technology I, Editors: A. Kumar, Y.-W. Chung, J. J. Moore, J. E. Smugeresky, The Minerals, Metals & Materials Society, Warrendale, 1999.

[3] Gommert E, Cerva H, Rucki A, von Helmolt R, Wecker J, Kuhrt C and Samwer K, Appl. Phys. Lett. 81 (1997) 5496.

[4] Materials synthesis and processing thin film science. T. Wagner, Max-Planck, Institut fur Metalforschung, Germany, p.196, 1999.

[5] K. M. Liang and G. Fantozzi, Evaluation by indentation of fracture toughness of ceramic materials, Jour. Mat. Sci. 25 (1990) 207-214.

[6] Jack, K. H. Nitrogen ceramics for engine applications. Materials Science Forum, (2000) 325-326.

[7] Maissel and Glang, ed., Handbook of thin film technology, 1970.

[8] Rossnagel SM. Sputter Deposition. In: Sproul WD, Legg KO, editors. Opportunities for Innovation: Advanced Surface Engineering. Switzerland: Technomic Publishing Co., 1995.

[9] Amaral M, Oliveira FJ, Belmonte M, Fernandes AJS, Costa FM, Silva RF. Surf Eng. 19 (2003) 410-416.

[10] CERAM Research - UK, http://www.azom.com/keyservices.asp?supplierID=188. Accessed 15/10/2006.

[11] E. Dow Whitney, Ceramic cutting tools – Materials, development and performance. Noyes Publications, 1994.

[12] Lewis, M. H. Sialons and silicon nitrides; microstructural design and performance. Materials Research Society Symposium Proceedings 287 (1993) 159-72.

[13] C. T. Kirk Jr., J. Appl. Phys. 50 (1979) 4190

[14] P. Morgan, in Nitrogen Ceramics, ed. F. Riley, Noordhoff, Leyden (p. 23), 1977.

[15] K. H. Jack, J. Mater. Sci. 11 (1976) 1135.

[16] A. Zerr, G. Miehe, G. Serghiou, *et al.,* Nature, 440 (1999) 340.

[17] Matovic, B., Low Temperature Sintering Additives for Silicon Nitride, Max-Planck-Institut für Metallforschung, Stuttgart, Bericht (137), 2003.

[18] F. Riley, J. Am. Ceram. Soc., 83 (2000) 245-65.

[19] S. Hampshire and K. H. Jack, in "Special Ceramics 7", edited by D. TayLor and P. Popper, British Ceramic Research Association, Stoke-on-Trent, 1981.

[20] A. H. Heuer and V. L. Lou, J. Am. Ceram. Soc., 73 (1990) 2785.

[21] T. Honma, Y. Ukyo, J. Mat. Sci.. Let. 18 (1999) 735-737.

[22] C. Galassi, V. Biasini and A. Bellos, Processing of Adv. Mater. 3, (1993) 153.

[23] F. Riley, Mat. Sci. Forum, 47 (1989) 70.

[24] H. M. Jennings, J. Mater. Sci., 18 (1983) 951.

[25] C. Greskovich, J. Rosolovski, J. Am. Ceram. Soc., 59 (1976) 336.

[26] G. Deeley, J. Herbert, Powder Metall., 8 (1961) 145.

[27] J. Rödel, J. Eur. Ceram. Soc., 10 (1992) 143.

[28] M. M. Schwartz, Handbook of structural ceramics, McGraw-Hill. p. 21, 1992.

[20] H. Mandel and M. J. Hoffmann, in Nitrides and Oxynitrides, ed. S. Hampshire, Trans. Tech. Publications Ltd., Zelene, (2000) p. 219),

[30] I. Peterson and T. Tien, J. Am. Ceram. Soc., 78 (1995) 2345.

[31] I. Tanaka, G. Pezzotti, K. Matsushita, Y. Miyamoto, and T. Okamoto, J. Am. Ceram. Soc., 74 (1992) 755.

[32] S. Haggerty and A. Lightfoor, Ceram. Eng. Sci. Proc., 16, (1995) 475.

[33] L. Vel, G. Demazeau and J. Etourneau, Mater. Sci. Eng. B, 10 (1991) 149.

[34] W. H. Balmain, J. Prakt. Chem. 27, (1989) 422.

[35] W. H. Balmain, J. Prakt. Chem. 32, (1994) 494.

[36] Carborundum Co., US Patent 2, (1958) 08-314.

[37] R. H. Wentorf Jr., J. Chem. Phys. 26, (1957) 956.

[38] J. Thomas Jr., N. E. Weston and T. E. O’Connor, J. Am. Chem. Soc. 84, (1963) 4619.

[39] P.B. Mirkarimi, K.F. McCarty, and D.L. Medlin, Mater. Sci. Eng. R 21 (1997) 47.

[40] E. Yamaguchi, Mater. Sci. Forum 329, (1990) 54-55.

[41] M. Bauccio, ASM Engineered Materials Reference Book, 2nd edition, ASM International, Materials Park, OH, 1994.

[42] F.P. Bundy, H.T. Hall, H.M. Strong, and R.H. Wentorf, Nature 176, (51), 1955.

[43] L. Vel, G. Demazeau, and J. Etourneau, Mater. Sci. Eng. B 10, (149), 1991.

[44] A. Bartl, S. Bohr, et. al., Int. J. of Refractory Metals and Hard Materials 14, (145), 1996.

[45] R.H. Wentorf, J. Chem. Phys. 36, (1962), 1990.

[46] O. Mishima, in: Synthesis and Properties of Boron Nitride, J.J. Pouch, S.A. Alterovitz, Materials Science Forum, Vol. 54/55, Trans Tech Publications, Brookfield, (p. 313), 1990.

[47] H. Hofsäs and C. Ronning, Conf. Beam Processing of Advanced Materials, J. Singh, S.M. Copley, and J. Mazumder (eds.), ASM Int., Materials Park, (p. 29), 1996

[48] Handbook on Deposition Technologies for Films and Coatings, 2nd Ed., (R. F. Bunshah, ed.), Noyes Publications, Park Ridge, NJ. 1994.

[49] Rointan F. Bunshah, Handbook of Hard Coatings, Edited by Bunshah, RF Noyes, 2001.

[50] K. Wasa, S. Hayakama.. “Handbook of sputter deposition technology”. Noyes Publication. New Jersey, USA, 1992.

[51] D. M. Mattox, Journal of Vacuum Science Technology, A7 (3), 1105, 1989.

[52] Ohring, M. The Materials Science of Thin Films. Academic Press, Inc. New York, 1992.

[53] Angstrom Sciences, World Leader in Magnetron Sputtering Technology, website accessed in 15/11/2006. http://www.angstromsciences.com/index.html.

[54] Angstrom Science, World leader in magnetron sputtering technology, website accessed in: 15/11/2006. <http:// www.angstromscience.com>.

[55] PHASIS 2006, Chemin des Aulx, CH-1228 Plan-les-Ouates, Geneva – Switzerland – website accessed in 10/08/2006, <http://www.phasis.ch/en/>.

[56] J. George. “Preparation of thin films” Ed. Dekker, New York USA 1992.

[57] S. P. S. Arya and A. D’Amico, Thin Solid Films 157, (1988) 267.

[58] M. Sokolowski, J. Cryst. Growth 46 (1979) 136.

[59] M. Okamato, H. Yokoyama, Y. Osaka, Jpn. J. Appl. Phys. 29, (1990) 930.

[60] A. Chayahara, H. Yokoyama, T. Imura, Y. Osaka, Jpn. J. Appl. Phys. 26 (1987) L1435.

[61] T. Ichiki, T. Momose, T. Yoshida, J. Appl. Phys. 75 (1994) 1330.

[62] H. Saitoh, W.A. Yarbrough, Appl. Phys. Lett. 58 (1991) 2482.

[63] D.J. Kester, K.S. Ailey, RF Davis, K.L. More, J. Mater. Res. 8, (1993) 1213.

[64] D.J. Kester, R. Messier, J. Appl. Phys. 72(1992) 504.

[65] T.A. Friedmann, P.B. Mirkarimi, D.L. Medlin et al., J. Appl. Phys. 76 (1994) 3088.

[66] K. Ballal, L. Salamanca-Riba, G. L. Doll, C. A. Taylor II, and R. Clarke, J. Mater. Res. 7 (1992) 1618.

[67] C.I. Chiang, G. Linker and O. Meyer. Mater. Chem. Phys. 48 (1997) 178–185.

[68] J. Ye, U. Rothhaar, H. Oechsner, Surf. Coat. Technol. 105 (1998) 159.

[69] S. Matsumoto, W.J. Zhang, Jpn. J. Appl. Phys. 39 (2000) L442.

[70] H. Hofsäss, C. Ronning, U. Griesmeier, M. Gross, S. Reinke, and M. Kuhr, Appl. Phys. Lett. 67 (1995) 46.

[71] S. Reinke, M. Kuhr and W. Kulisch, Proceedings of the 4th European Conference on Diamond, Diamond-Like and Related Coatings, Albufeira, Portugal, 1993.

[72] N. Tanabe, T. Hayashi and M. Iwaki, Diamond Rel. Mater., 1 (1993) 151.

[73] M. Mieno and Yoshida, Jpn. J. Appl. Phys., 29, (1990) L1175.

[74] K. Bewilogua, J. Buth, H. Hubsh and M. Grishke, Diamond Rel. Mater., 2 (1993) 1206.

[75] I. Konyashin, V. Khvostov and Babaev, Diamond Rel. Mater., 8 (1999) 2053.

[76] B. Bhattacharyya, B. Deb, D. Ganguli, et. al., Mater. Chem. Phys. (under publication).

[77] D. McKenzie, W. McFall, W. Sainty, C. Davis and R. Collins, Diamond Rel. Mater. 2 (1993) 970.

[78] Y. Lifshitz, S.R. Kasi, J.W. Rabalais, Phys. Rev. Lett. 62 (1989) 1290.

[79] J. Robertson, Diamond Relat. Mater. 5 (1996) 519.

[80] D.R. McKenzie, W.D. McFall, W.G. Sainty, et. al., Diamond Rel. Mater. 2 (1993) 9790.

[81] P.B. Mirkarimi, K.F. McCarty, D.L. Medlin, W.G. Wolfer, et al., J. Mater. Res. 9 (1994) 2925.

[82] W. Kulisch and S. Ulrich. Thin Solid Films 403 (2003) 183.

[83] R. Glang, Handbook of Thin Film Technology, McGraw-Hill, New York, 1970.

[84] K. Suzuki and Y. Kanno, J. Ceram. Soe. Jpn 92, (1984) 101.

[85] G.R. Anstis, P. Chantikul, B.R. Lawn and D.B. Marshall, J. Am. Ceram. Soc., 64 (1981) 533-538.

[86] R. Geick, C.H. Perry, and G. Rupprecht, Phys. Rev. 146 (1966) 543.

[87] J.T. Smith and C.L. Quakenbuch, J. Am. Ceram. Soc. Bull., 5 (1980) 529-537.

[88] H. Takata, et. al., J. Ceram. Soc. Jpn. Int. Edn, 96 (1988) 847-881.

[89] J.L. Bredas, in: T.A. Skotheim (Ed.), Handbook of Conducting Polymers, vol. 2, Marcel Dekker, New York, (p. 859), 1986.

[90] M. Belmonte, A.J.S. Fernandes, F.M. Costa, F.J. Oliveira and RF Silva; Diamond Rel. Mater., 12 (2003) 733-737.

[91] G. Petzow and M. Herrmann, Structure and Bonding, 102 (2001) 51.

[92] J. B. Wachtmann., Mechanical Properties of Ceramics, John Wiley & Sons Inc, New York, 1996.

[93] Xingwang Zhang, Jinshun Yue, Guanghua Chen, Hui Yan, Thin Solid Films, 315 (1998) 202–206.

[94] S. Acquaviva, G. Leggieri, A. Luches, A. Perrone, A. Zocco, N. Laidani, G. Speranza, M. Anderle, Appl. Phys. A 70 (2000)197–201.

[95] G. Arslan, F. Kara, S. Turan, J. Eur. Ceram. Soc. 23 (2003) 1243–1255.

[96] Q.C. Jiang, H.Y. Wang, B.X. Ma, Y. Wang, F. Zhao, J. of Alloys and Compounds, 386 (2005) 177–181.

[97] K. Shibata, T. Hagio and H. Yoshida. Jpn. J. Appl. Phys. Vol. 40 (2001) 1030-1034.

[98] S.H. Lin, D. Li, B.J. Feldman, in: M.D. Drory, D.B. Bogy, M.S. Donley, J.E. Field., Mat. Res. Soc., (1995) 127-132.

[99] K. Shirai and S. Emura, J. Phys. Condens. Matter. 8 (1996) 10919.

[100] U. Kuhlmann, H. Werheit and K.A. Schwetz, J. Alloys Compd. 189 (1992) 249.

[101] P.J Giellisse, S. S. Mitra, E. A. Pascoe et al. Phys. Rev. 3, 155 (1967) 1039-1046.

[102] J. Zhang, Q. Cui, X. Li, Z. He, et al., Chem. Phys. Lett., 399 (2004) 441-455.

[103] C. Fitz, A. Kolitsch and W. Fukarek Thin Solid Films 389 (2001) 173.

[104] R. Geick, C.H. Perry, G. Rupprecht, Phys. Rev. 146 (1966) 543.

[105] A. Olszyna, J. Konwerska-Hrabowaska, M. Lisicki, Diamond Relat. Mater. 6 (1997) 617.

[106] J.B. Wang, G.W. Yang, C.Y. Zang, X.L. Zhong, ZH.A. Ren., Chem. Phys. Lett. 367 (2003) 10-14.

[107] S.S. Batsanov, G.E. Blohina, A.A. Deribas, Zh. Strukt. Khim. 6 (1965) 227.

[108] J. A. Sanjurjo, E. López.Cruz, P. Vogl and M. Cardona, Phys. Rew. B. 28 (1983) 4579-4584.

[109] T. Klotzbucher, M. Mergens, D.A. Wesner, E.W. Kreutz, Surf. Coat. Techn. 100-1001 (1998) 388-392.

[110] J. Ye, U. Rothhaar, H. Oechsner, Surf. Coat. Technol. 105 (1998) 159.

[111] M.A. Djouadi, A. Vasin, C. Nouveau, B. Angleraud, P.Y. Tessier, Surf. Coat. Techn. 180-181 (2004) 174–177.

[112] H. Oechsner. Thin Solid Film, 515 (2006) 33-38.

[113] A.F. Jankowski, Thin solid Films, 343-344 (1999) 228-241.

[114] W. Gissler, J. Haupt, T.A. Crabb, P.N. Gibson, D.G. Rickerby, Mater. Sci. Eng. A, 139 (1991) 284.

[115] P.M. Ossi and A. Miotello, Appl. Organometal. Chem., 15 (2001) 430-434.

[116] S. Kidner, C.A. Taylor II, and R. Clarke, Appl. Phys. Lett., 64 (1994) 14.

[117] J.M. Caicedo, G. Bejarano, G. Zambrano, E. Baca, O. Morán and P. Prito, -hys. Stat. Sol. B, 242 (2005)1920-1923.

[118] C.Y. Zhang, X.L. Zhong, J.B. Wang, G.W. Yang, Chem. Phys. Lett., 370 (2003) 522–527.

[119] Po-Chih Huang, Tien-Syh Yang, Shou-Shu Chu, Ming-Show Wong, Thin Solid Films 515 (2006) 973–978